

January 2022 | VOL.3 | ISSUE 2

INTERNATIONAL JOURNAL OF CHEMICAL AND ENVIRONMENTAL SCIENCES



US ISSN Center at the Library of Congress

ISSN: 2689-6389 (Print)

ISSN: 2687-7939 (Online)

A Publication of



Society for Makers, Artists, Researchers and Technologists

6408 Elizabeth Avenue SE, Auburn, Washington 98092, USA

www.ijcaes.thesmartsociety.org

**INTERNATIONAL
JOURNAL OF
CHEMICAL AND
ENVIRONMENTAL
SCIENCES**

VOLUME 3, ISSUE 2

(January, 2022)



SOCIETY FOR MAKERS, ARTISTS, RESEARCHERS AND TECHNOLOGISTS

6408 ELIZABETH AVENUE SE, AUBURN, WA 98092, USA

SMART

SOCIETY FOR MAKERS, ARTISTS, RESEARCHERS AND TECHNOLOGISTS

SMART is a publishing organization which seeks to bring to light new and innovative research ventures and publish original works of study. All publications by SMART is undertaken with due authorization of the related author(s).

International Journal of Chemical and Environmental Sciences is a publication by SMART.

First Published in November, 2019

Auburn, USA

ISSN: 2689-6389 (Print)

ISSN 2687-7939 (Online)

Copyright © 2019 SMART

All rights reserved. No part of this publication may be reproduced, distributed, or transmitted in any form or by any means, including photocopying, recording, or other electronic or mechanical methods, without the prior written permission of the publisher, except in the case of brief quotations embodied in critical reviews and certain other non-commercial uses permitted by copyright law. For permission requests, write to the publisher, addressed "Attention: Permissions Coordinator," at the address below.

SMART

SOCIETY FOR MAKERS, ARTISTS, RESEARCHERS AND TECHNOLOGISTS

6408 ELIZABETH AVENUE SE, AUBURN, WA 98092, USA

Price: 200 USD

Editorial and Administrative Information

From Managing Editor's Desk

International Journal of Chemical and Environmental Sciences is an open access, peer reviewed journal that provides authoritative source of information for professionals in a wide range of chemical and environmental disciplines. It provides an international forum for the rapid communication of research that broadly embraces the interface consisting of new research opportunities and discoveries.

The journal publishes original papers, brief communications, reviews and letters related to every aspect of theory and practice of chemical, (bio) chemical, nano-sciences, environmental sciences and chemical engineering disciplines. Actually, interdisciplinary studies require an integration of many different scientific and professional disciplines. The Journal provides a platform for the exposure in advancement of interdisciplinary approaches related to every aspects of science. Manuscripts are initially reviewed by the editors and, if found appropriate are sent to scientists who assess the quality, originality, significance, and validity of the work before finally approving for publication. All rights are reserved with the publishers. A Reprint Service is available and copies might be obtained on prior permission for limited and specified reproduction sought on payment of prescribed charges.

We are taking this opportunity to announce the publication of the first volume of IJCAES, a journal published by SMART SOCIETY, USA. The contributions involve multi-disciplinary or trans-disciplinary aspects of science and identify the ways in which the work will be instrumental in present day research, education, or related activities. The editors are pinning their hopes that this present issue will be able to get across students, faculties and researchers. We are confident that IJCAES will act as a podium for its related scientific community it caters around the world and a trusted medium to interact and communicate.

Dr.Ruchira Mukherjee

Dr, Pratap Mukherjee

THE EDITORS:

1 Paromita Raha, Ph.D,
Senior Scientist Preclinical
Research Bold Therapeutics
Vancouver,
British Columbia, Canada

2. Neeladri Roy, Ph.D
Department of Chemistry,
Royal College of Surgeons
123 St. Stephens Green
Dublin 2, Ireland.

3. Koushik Roy, Ph.D
University of Utah, Health
Department of Pathology
15 North Medical Dr. East
Suite 2600C
Salt Lake City, Utah 84112,
USA.

4. Subrata Debnath, Ph.D
Howard University
College of Medicine
Department of Biochemistry and
Molecular Biology
Adams/4105
Washington, DC-20059, USA.

5. Sanchaita Das, Ph.D
Department of Chemistry &
Biochemistry
University of California, Los
Angeles
sanchaita06@gmail.com

6. Uddalak Bharadwaj, PhD
Faculty Member
Department of Infectious
Diseases Infection Control and
Employee Health MD
Anderson Cancer Center
Houston, Texas

PATRON

Prof. (Dr) Satyajit Chakrabarti
Director
Institute of Engineering & Management.
Salt Lake Electronics Complex, Kolkata-700091
India.

THE MANAGING EDITORS

Dr. Ruchira Mukherjee
Professor
Department of Basic Sciences and
Humanities
Institute of Engineering & Management.
Salt Lake Electronics Complex,
Kolkata-700091
India

Dr. Pratap Mukherjee
Associate Professor
Department of Basic Sciences and
Humanities
Institute of Engineering & Management.
Salt Lake Electronics Complex,
Kolkata-700091
India

THE ASSOCIATE EDITORS

Dr. Tina De

Assistant Professor
Department of Basic Science &
Humanities,
Institute of Engineering & Management.
Salt Lake Electronics Complex,
Kolkata-700091
India.

Dr. Kakoli Dutta

Associate Professor
Department of Basic Sciences and
Humanities
Institute of Engineering & Management.
Salt Lake Electronics Complex,
Kolkata-700091
India

Prof. Prabir Kumar Das

Assistant Professor
Department of Basic Science & Humanities,
Institute of Engineering & Management.
Salt Lake Electronics Complex, Kolkata-700091
India

Contact Us:

Society for Makers, Artist, Researchers and Technologists.
6408 Elizabeth Avenue SE, Auburn, WA 98092, USA.

Email: secretary@ijcaes.org

Phone- 1-425-605-0775

CONTENTS	Page No.
<p>Advancement of Biomimetic Nanoparticles for Targeted Drug Delivery</p> <p>Adnan Ahmed Sultan*, Aditya Pratap Singh, Abhipriya Rajan, Anupam Tiwary</p>	7
<p>‘Eutrophication’ is Malediction or Benediction in nature – An assessment</p> <p>Debaleena Ghosh, Amlan De, Phanibhusan Ghosh* and Tarun Kumar De</p>	42
<p>Posterior Parietal Cortex Dysfunction is Central to Working Memory Storage and Broad Cognitive Deficits in Schizophrenia</p> <p>Aniket Hazra*, Atri Panda , Priyanshu Sarkar</p>	50
<p>Synthesis, antibacterial activity study, molecular docking and molecular properties prediction of new organo phosphonate derivatives</p> <p>Jhonsee Rani Telu¹, Naveen Kuntala¹, Venkanna Banothu², Bala Divya Mallavarapu¹, Sarbani Pal^{3*} and Jaya Shree Anireddy^{1*}</p>	67
<p>Using Fly Ash Bricks as a Sustainable Building Material</p> <p>Priyanjana Saha^{1*} and Piyush Raj</p>	85

Advancement of Biomimetic Nanoparticles for Targeted Drug Delivery

Adnan Ahmed Sultan*, Aditya Pratap Singh, Abhipriya Rajan, Anupam Tiwary

Department of Information Technology, Institute of Engineering & Management, Kolkata – 700091

Abstract

There has been an increasing requirement for more efficient and less iatrogenic therapies for drug delivery, encouraging researches to develop new vectors that ensure targeted delivery of drugs and other therapeutic agents in medicine. Traditional synthetic drug vectors which include polymer and lipid particles are not preferred for clinical applications due to their high cytotoxicity, greater immunogenicity and low cell membrane penetrability. On the other hand, natural particulates ranging from pathogens to mammalian cells are specially optimized for *in vivo* functions and possess features desirable for drug delivery vectors. Biomimetics involves exploiting biological organisms, cells and molecules or deriving inspiration from them. The Biomimetic Nanoparticles have ushered a new generation of drug carriers, attracting researchers because of their excellent biocompatibility, biodistribution, low chances of recognition and removal by the immune system. Their ability to mimic the bio-structure and function of the biological system makes them reliable drug delivery vectors especially for disease targeting. The advanced biotechnology tools used for engineering synthetic and natural derived nano-systems along with better understanding of biological systems, have enabled researchers to apply these ideas to the delivery of drugs, small interfering RNA, proteins and other therapeutic agents. This review summarizes recent advances in biomimetic nanoparticles used for targeted drug delivery in medicine, obtained by processing synthetic materials using biomimetics. The challenges of biomimetic delivery systems and future directions are also discussed and proposed herein.

Keywords: Biomimetic, biomimetic nanoparticles, nano-systems, drug carriers, biomimetic vector

1. Introduction

The word 'biomimetic' was first used by Otto Schmitt in 1957, who explained it in relation with biophysics science. His expression was: "Biomimetics is not so much a subject matter as it is a point of view. It is an approach to problems of technology utilizing the theory and technology of the biological sciences" [1]. The application of biomimetics to resolve various problems in medicine and pharmaceuticals is a promising method for treatment of various diseases.

Understanding macromolecular structure and sophisticated processes at the cellular and subcellular level (such as protein structure and biological activities) allows scientists to be inspired by and mimic these natural processes for biomedical applications. The study of cell growth and division, metabolic regulation of cellular interactions and hormone signaling pathways [2] is all a part of biomimetics in cellular processes. The focus of today's drug delivery research is on targeted drug delivery which involves transferring medications into the cytoplasm of selected cells while avoiding detrimental, deleterious effects on healthy tissues and organs. Poor solubility, stability and unintended toxicity, and/or an inability to cross cell membranes are all inherent problems with drugs that have not been modified or processed to improve their physicochemical properties and pharmacokinetics profile. These concerns have prompted

Corresponding author
Email address: adnansultandr@gmail.com

the creation of novel drug delivery vector technologies with enhanced therapeutic activity and improved *in vivo* pharmacokinetics.

Despite the fact that many medicines have strong pharmacological action against certain diseases, their usage in their natural state is frequently restricted for practical reasons. The poor stability, limited biodistribution, low barrier penetrating abilities and lack of targeting features are all major problems related to drug delivery. With the development of nano-sized controlled drug delivery systems, the above mentioned limits have favoured the use of nanoscience in medicine. The research and development of drug delivery systems in the form of polymeric nano and/or micro particles, liposomes and micelles, among others [3-5], has seen significant expansion in recent decades fueled by many developments in nanotechnology and biotechnology. The success of these devices is primarily determined by the choice of proper design parameters to address the physicochemical limits of the drugs (i.e., solubility and stability) as well as biological barriers to reaching the target (i.e., the first-pass effect, immune clearance, cell entry and off-target deposition). The precise hurdle for drug delivery is determined by the nature of the medication (whether it is a peptide, antibody or siRNA) as well as the mode of administration (oral, injectable, transdermal or inhalation), each of which has its own set of advantages and disadvantages.

Nanoparticles for drug delivery efficiently lower the barriers to free drug administration encouraging the use of existing pharmaceuticals that have already been developed and studied but have not been utilized in free form due to their side effects. Nanoparticles are homing systems that hide and protect weakly stable active molecules from the physiological environment allowing the preservation of their pharmacological activity. Their customizability and functionalized ability which provide specialized features to overcome low bioavailability, solubility difficulties and off-target deposition in healthy tissues, are additional benefits connected with their use in drug administration.

Due to the enormous benefits that these vectors may give, the use of nanoparticles derived from synthetic, biological or biohybrid sources, has been increasingly popular in recent years. Initially, natural origin materials were treated to become vectors for drug delivery. Natural materials derived from plants (e.g., alginate) or animals (e.g., chitosan), were widely used due to their biocompatibility and degradability. Liposomes were also thought to be useful carriers for encasing and transporting medicines. By using well consolidated processes, liposomes can be made from amphiphilic natural substances. For a wide range of starting materials, preparation processes and designs for vectors from natural derivation were optimized. Natural carriers were successfully improved by adding chemical alterations and subsequently creating hybrid materials, as a result of which new and more performant synthetic polymers were discovered and tested as starting materials for carrier preparation. Artificial drug vectors made of biodegradable polymers or inorganic materials are constantly being researched, with promising results propelling a number of systems to market. Some synthetic nanoparticles can be manipulated and functionalized to improve stealth and targeting.

Natural nano-systems created from pathogens or cells have the potential to improve pharmacological therapy. Biological vectors have inherent properties that allow for extended circulation and district-specific targeting. Natural vectors have evolved over time to achieve the goals, homing their unique properties. Scientists have now developed precise processes for obtaining safe vectors from living cells as well as enhanced techniques to increase drug loading without sacrificing native carrier qualities, ghost and living cells are currently being investigated with promising findings. The functional qualities of natural and manufactured nanoparticles are well understood and have already been enhanced using consolidated techniques [6]. Furthermore, breakthroughs in cell biology now allow for the combination of advantageous traits from all classes, resulting in combined biohybrid structures with improved qualities.

This review summarizes the advances in the design of biomimetic nanoparticles used for targeted drug delivery, including an overview of their development status, clinical trial utilization, and commercial penetration during the last few years and also highlights the various applications and limitations of each approach.

2. Artificial Drug Vectors

Degradable or biodegradable artificial materials are employed as safe therapeutic carriers [7]. Synthetic polymer nanoparticles [8] are the most intriguing family of artificial nanoparticles for drug delivery. Soft polymer nanocarriers, such as dense spheres, hollow capsules, micelles, niosomes, interpenetrated networks, and dendrimers, can be built in a variety of designs. Different drug delivery kinetics can be achieved depending on the starting materials used, which can be rapid, sustained, pulsatile, or on-demand. Polymer carriers are currently being used to transport drugs, small molecules, proteins, and genes, with applications in cancer treatment [9], brain disease treatment [10,11], cardiovascular diseases [12], orthopedic applications [13], and as sensors to research the intracellular environment [14].

On-demand medication release is a basic biomimetic trait that allows a synthetic structure to become active only when it is required and when it reaches the targeted location. Using natural-inspired processes, biomimetic features can be successfully added during carrier synthesis [15,16]. Another way to improve biomimicry was to use bioresponsive materials [17], which are synthetic polymers that respond to biological signals or pathological circumstances such changes in pH, temperature, hypoxia, or redox conditions. As an example, according to the study of Guha *et al.* [18] responsive materials are useful in improving the administration of active molecules via the oral route. The scientists created a core/shell system for oral insulin administration made of mesoporous silica and coated with a pH-responsive substance in this study. The coating provided preferred release at a systemic pH of 7.4 in this system. T-responsive nanocarriers also allow for on-demand drug administration and can be initiated by an external stimulation or a rise in temperature caused by pathological lesions [19]. As illustrated by He *et al.*, who recently discovered the capacity of fluorescent tagged T-responsive nanoparticles to change shape in response to temperature change, temperature can alter nanoparticle characteristics [20]. The use of an external heat source significantly increased the diameter of nanoparticles, allowing for fluorescence and size-measurement experiments. This use was originally proposed for image-guided drug release, however the ability to change the size and shape of nanoparticles *in vivo* improves their important biomimetic features, such as cell contacts, intravascular transport, barrier penetration, and recognition qualities [21]. Mechanical stimuli can also be used to initiate medication delivery. Deformable nanoparticles are strong candidates to fulfil the role of mechanically activated drug vector, as it is now widely acknowledged that mechanical forces can modify drug delivery [22]. Along with their use as drug delivery systems, shape-adaptable nanoparticles have also been used to investigate intracellular mechanical forces, as described by Chen *et al.*, who found distinct distorted morphologies in soft synthetic particles incubated within different cell lines [23].

With a biomimetic system design, recognition properties can be obtained as well. The molecular imprinting (MI) technique is one of the most intriguing technologies for modifying synthetic materials in this regard. Functional cavities act as selective binding sites in particles generated using the MI technique, allowing for a unique lock and key mechanism for molecule recognition. The inherent recognition properties of MI materials allow therapeutic efficacy without the usage of drugs [24]. Despite its potential, the MI technique has yet to be widely used in the preparation of drug delivery systems [25], limiting its use as synthetic plastic antibodies to bind molecules of various sizes and properties, such as nonsteroidal anti-inflammatory drugs [26], intracellular protein sequestration [27], or imaging agents [28]. One of the

most significant drawbacks of molecularly imprinted nanoparticles is the requirement for the structure to be cross-linked and stiff in order to provide strong recognition capabilities.

Culver *et al.* offered a new application that partially addresses his constraint by crosslinking a non-degradable polymer around a non-MI degradable core to get surface recognition capabilities [29]. This treatment lowers non-degradable material while also decreasing the amount of polymer potential accumulated after delivery, although it is not a permanent solution. A completely degradable bulk-imprinted nanoparticle system was recently proposed [30], demonstrating efficient recognition properties toward the small biotin molecule and, with the same functionalization, also toward the large biotin-tagged albumin molecule, thus combining degradability and recognition properties for the first time.

2.1. Biomimetic hydrogels

Hydrogels are a class of hydrophilic polymeric materials that can be either natural or manufactured. Furthermore, hydrogels can absorb enormous volumes of water or biological fluids and remain in solution in an aqueous environment due to chemical or physical cross-linking of individual polymer chains [31]. Softness, flexibility, adjustable porosity, and biocompatibility are among important features of these biomaterials. The circumstances for gel production are relatively gentle, so they match natural living cells and tissues as closely as possible [32]. By modifying the hydrogel matrix, it is possible to achieve certain qualities in rapid and reversible responses to a variety of chemical and physical stimulation (such as pH, temperature, and ionic strength), which are suitable for long-term active drug release. This characteristic

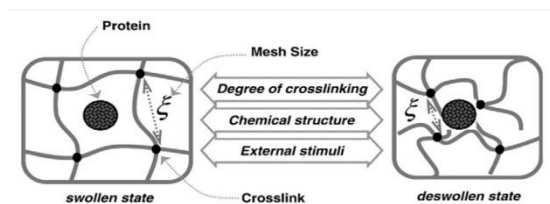


Fig 1. Schematic diagram of hydrogels at swollen or shrunken states for drug release [31].

also allows them to deliver biomolecules (such as protein and peptide therapeutics) [31]. Figure 1 shows how hydrogels can be swelled or shrunken for drug release. Biomimetic hydrogels have arisen as a result of the incorporation of biological recognition sites for covering cellular processes and synchronising responses to environmental stimulation. In addition, appropriate biological moieties should be added to the inert polymer chains of hydrogels to make them suitable for *in vivo* targeted drug delivery systems [31]. Furthermore, through spatiotemporal inclusion of biological cues such as peptides, growth factors, and proteins into hydrogel matrices, it is possible to construct a unique controlled drug delivery system to regenerate tissues [32]. The incorporation of growth factors in a biomimetic hydrogel matrix for regulated medication delivery is shown in Figure 2. A synopsis of works on biomimetic hydrogels in drug delivery applications is shown in Table 1.

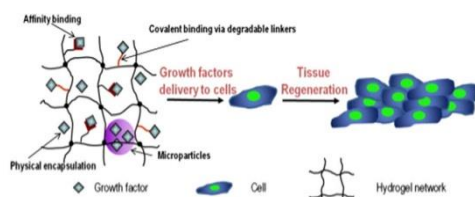


Fig 2. The incorporation of growth factors in biomimetic hydrogel matrix for tissue regeneration [33]

Table 1. Synopsis of works on biomimetic hydrogels in drug delivery applications [48].

Authors	Brief Title	Highlights	References
Liang et al.	Protein Diffusion Hydrogels	The diffusion of the biological molecules was optimized agarose hydrogel	[34]
Moschou et al.	Hydrogels Based Proteins	The stimuli-responsive Hydrogels were fabricated by binding protein and its low-affinity ligand.	[35]
Moon et al.	Hydrogels Therapeutic Angiogenesis	Biomimetic hydrogels were developed to be enabled to stimulate endothelial cell adhesion.	[36]
Fisher et al.	Tight Junction Disruption Hydrogel	Biomimetic peptide-base hydrogels were investigated for oral protein delivery.	[37]
Anderson et al.	Gelation Properties Peptide Amphiphiles	The mechanical properties of PAs hydrogels were moderated.	[38]
Orive et al.	Cell-hydrogel Drug Delivery	Biomimetic cell-hydrogel capsules were designed for the Long-term efficacy of immobilized cells.	[39]
Bozzini et al.	Cross-linking Human Recombinant Elastin (HELP)	The biomimetic HELP hydrogel was fabricated by enzymatic cross-linking.	[40]
Ravi et al.	Coupling Peptide Protein Polymer	The RGD-modified ELP hydrogels were utilized to mimic cellular microenvironment.	[41]
Xue et al.	Facile Green Fabrication Hydrogel	A simple Physically method of cross-linking was used to produce a biomimetic GT-S hydrogel	[42]
Zhao et al.	Polysaccharide Antibiotics Delivery	A biomimetic antibiotic-loaded hydrogel was fabricated for wound dressing.	[43]
Kim et al.	Hydrogel Tissue Regeneration	Biomimetic hybrid hydrogels were biomineralized of for binding calcium ions.	[44]
Huh et al.	Biomineralized Biomimetic Hydrogels	Biomimetic hybrid hydrogels were biomineralized of for binding calcium ions.	[45]
Boffito et al.	Novel Thermosensitive Hydrogels	A thermoresponsive hydrogel was fabricated for in situ injectable drug delivery systems.	[46]
Sawicki et al.	Formation Patterning Hydrogels	Click chemistries methods of the fabrication of biomimetic hydrogels were studied.	[47]

2.2. Biomimetic micelles

Micelle is a common term in chemistry that refers to a structure in aqueous solutions that has one hydrophobic core and one hydrophilic end. The utilisation of these supermolecules in drug delivery systems results in the development of innovative drug carriers in the treatment of diseases such as cancer.

Polymeric micelles are the most popular colloidal delivery technology because of their superior performance in drug modification [49]. Polymeric micelles are tiny spheres that are produced by the self-assembly of amphiphilic di or tri block copolymers in an aqueous environment [49,50]. The hydrophobic (lipophilic) core is used to encapsulate and solubilize hydrophobic medicines, proteins, and DNA, while the hydrophilic shell interacts with the biological environment and provides stealth. The chemical structure of block copolymers in micelles can be used to design or adjust physicochemical properties of

encapsulated pharmaceuticals, disease pathophysiology, and the release mechanism of individual drugs in specific areas. Additionally, the chemical structure of the core might be changed to improve drug encapsulation, increase micelle stability, and control the amount of medication released from the micelles. Biomimetic micelles might also be created by using biological moieties or biomimetic base-block copolymers via self-assembly of innovative biomimetic amphiphiles in a micellar structure to give more controlled localised Drug delivery systems [49,51–53]. A biomimetic micelle containing medicinal medicines is shown in Figure 3. A synopsis of works on biomimetic micelles in drug delivery applications is shown in Table 2.



Fig 3. A biomimetic micelle in which drug is encapsulated [54].

Table 2. Synopsis of works on biomimetic micelles in drug delivery applications [48].

Authors	Brief Title	Highlights	References
Xu et al.	Biomimetic Amphiphiles	A sustained release of ADR was obtained by Chol-PEO micelles.	[51]
Xu et al.	Biomimetic Polymersomes	A sustained release of ADR was obtained by CMPC micelles.	[52]
Sallach et al.	Micelle Protein Structure	Protein polymer-based micelles were fabricated by means of recombinant DNA procedure.	[55]
Xiong et al.	Virus-Mimetic Micelles siRNA	PEO-block-PCL micelles as siRNA carriers were modified by viral vectors to provide dual peptide functionality (RGD/TAT) micelles.	[53]
Tang et al.	Stability Acid Sensitivity Micelles UV	A biomimetic method by means of UV irradiation was utilized to form stable micelles.	[56]
Jang et al.	Cell-Penetrating Paclitaxel siRNA Tumor Suppression	Dual-functional drug-loaded micelles were fabricated For the suppression of tumor cells.	[57]
Wang et al.	Zwitterionic Polymers Targeting Carriers	A hyperbranched polymer was utilized as cores of biomimetic DOX loaded micelles.	[58]
Jiang et al.	Hyperbranched Polyether Zwitterionic Polymers	A hyperbranched polymer was utilized as cores of biomimetic IND loaded micelles.	[59]
Wu et al.	Drug Release Micelles Chitosan Conjugate	Proper drug release profile was obtained from biomimetic DCA-PCC micelles as quercetin carrier.	[60]

2.3. Biomimetic liposomes

Liposomes are spherical vesicles with phospholipids forming a double layer (bilayer). Because the lipid bilayer of liposomes is analogous to the cell membrane in the human body or animals, they can be used as medication delivery vehicles.

In an aqueous solution, liposomes could be self-assembled from cholesterol and natural phospholipids. Liposomes have both hydrophobic and hydrophilic properties due to their concentric phospholipid bilayer around an aqueous centre portion. They are also non-toxic, biocompatible, and biodegradable, with the ability to transport both hydrophobic and hydrophilic medicines in phospholipids and the interior aqueous section, respectively. Liposomes are classified according to their lipid composition, surface charge, size, and manufacturing method. They were further divided into two types based on their size and number of bilayers: unilamellar vesicles (UV) and multilamellar vesicles (MLV) [61,62]. Liposomes can be divided into two categories, as seen in Figure 4.

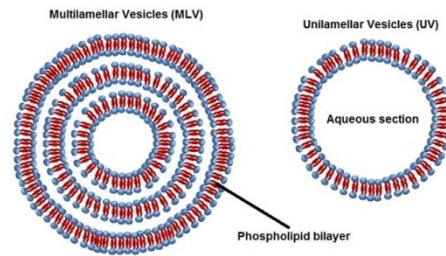


Fig 4. Unilamellar vesicles (UV) and multilamellar vesicles (MLV) which are two main types of liposomes [63].

Liposomes can be made using biomimetic techniques, which replicate the biological behaviour of cells. Biomimetic liposomes could also be targeted with specific moieties or ligands to deliver medications or biomolecules intracellularly. Biomimetic liposomes could also allow the controlled release of loaded cargo in response to a specific stimulation in the cell microenvironment [64,65]. Figure 5 depicts a biomimetic liposome containing two types of medicines. A synopsis of works on biomimetic liposomes in drug delivery applications is shown in Table 3.

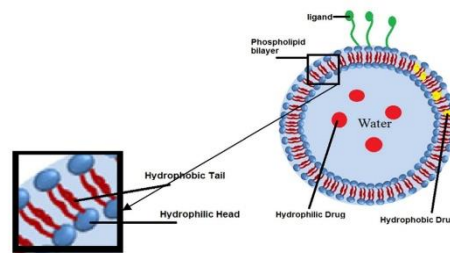


Fig 5. One biomimetic liposome with the capability of carrying hydrophilic and hydrophobic drugs within target cells, simultaneously [48].

Table 3. Synopsis of works on biomimetic liposomes in drug delivery applications [48].

Authors	Brief Title	Highlights	References
Westhaus et al.	Lipid Vesicles Polysaccharide Protein	Thermal-responsive CaCl ₂ -loaded liposomes were fabricated as in situ injectable drugs.	[66]
Sakai et al.	Metabolism Hemoglobin-Vesicles	Hemoglobin-loaded liposomes were fabricated to be able to transfer O ₂ artificially.	[67]
Boyer et al.	Multiple Lipid Vesicle	The stability and the EPR effects were promoted in multi lipid layer liposomes	[68]
Zhu et al.	Glycoliposomes Targeting P-Selectin Activated Platelets	Biomimetic SuLea-PEG-liposomes were fabricated to be able to target activated platelets.	[69]
Gao et al.	Biofunctionalization Microcapsules Liposomes	Biofunctionalization Microcapsules Liposomes	[70]

2.4. Biomimetic dendrimers

Dendrimers are tree-shaped synthetic polymers that can be modified for a specific purpose as drug carriers in drug delivery systems by a sequence of processes. Dendrimers are highly branched three-dimensional macromolecular cubes with a compact spherical form and internal repeating units (generations) that emerge from a focal core [71,72]. These macromolecules have several functional groups on their surface (exterior reactive terminal groups) that make them excellent carriers in drug delivery systems, in addition to a specified shape, size, molecular weight, and monodispersity. Drugs can

be physically encapsulated inside the dendritic structure or electrostatically or covalently attached to the surface via end functional groups [72,73].

Dendrimers may also improve medicinal compounds' water solubility, bioavailability, and biocompatibility [74]. The number of generations, composition, and charge of the surface are three aspects in dendrimer structure that induce toxicity and should be resolved before biological applications. Furthermore, cationic dendrimers have higher harmful effects than anionic or neutral dendrimers via inducing apoptosis via cell and organelle membrane [61]. The structure of a dendrimer from generation four is shown in Figure 6.

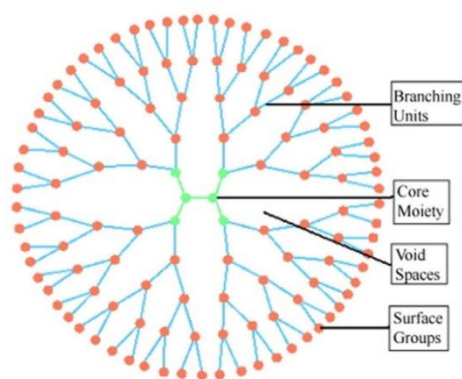


Fig 6. The structure of dendrimer of generation four and their different parts [75].

To produce biomimetic drug carriers for targeted drug delivery, significant moieties can be coupled to reactive terminal groups on the surface of dendrimers. Furthermore, due to dendrimers' unique monodispersity, these macromolecules could be self-assembled into structures that are similar to natural proteins, with the capacity to replicate a variety of natural materials [76]. A synopsis of works on biomimetic dendrimers in drug delivery applications is shown in Table 4.

Table 4. Synopsis of works on biomimetic dendrimers in drug delivery applications [48].

Authors	Brief Title	Highlights	References
Paleos et al.	Acid Salt Dendrimer Drug Delivery	PEG and guanidinium ligand were attached on dendrimers to enhance the stability and drug release.	[77]
Huang et al.	Biomimetic Amphiphiles Multi-Armed Nanoparticles	Biomimetic multi-armed dendrimers were synthesized to be enabled to mimic protein structure.	[78]
Singh et al.	Folate Folate-PEG-PAMAM Dendrimers	FA-PEG-PAMAM dendrimers were synthesized to release 5-fluorouracil within target cells.	[79]
Kurtoglu et al.	Dendrimer-Drug Intracellular	The stability of PAMAM dendrimer-NAC was enhanced due to the existence of a disulfide linkage.	[80]
Yuan et al.	Novel Dendrimer pH-Sensitive Targeting	DOX and biotin were immobilized on poly(L-glutamic acid) dendrimers to create pH-sensitive targeting	[81]

2.5. Biomimetic polymeric carriers

Polymeric carriers have special properties for drug delivery applications, including as facile nanoscale production, high drug loading capacity, regulated drug release, and surface alteration due to active functional groups [57]. Cell attachment, cytokine signalling, and endocytosis are all examples of biomimetic polymers, which are new biomaterial carriers that replicate physiological interactions with the environment. Furthermore, the physiologically active components of these polymers enable medication delivery through cell barriers within sick cells. Furthermore, the ideal biomimetic polymeric carrier is one that may limit unspecific interactions on surface cells while extracting the necessary cellular response, resulting in the achievement of its goal [82]. Surface coating and modification on biomimetic polymers are critical for controlling the interactions of specific cells via endocytosis, as shown in Figure 7 [83]. The optimization of stoichiometry in polymerization processes, as well as the creation of biomimetic structures, are the foundation issues for determining the specific drug release mechanism and diffusion model for these polymeric carriers [84]. A synopsis of works on biomimetic polymeric carriers in drug delivery applications is shown in Table 5.

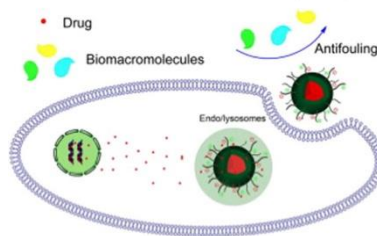


Fig 7. The special ligands on the surface of biomimetic polymeric drug carriers could facilitate the endocytosis and intercellular drug release [83].

Table 5. Synopsis of works on biomimetic polymeric carriers in drug delivery applications [48].

Authors	Brief Title	Highlights	References
Zhang et al.	Biomimetic Poly (carboxybetaine)	A PolyCBMA with a dual-functional property in adsorption or desorption proteins was fabricated	[85]
Duncan	Polymer Conjugates Lysosomotropic Nanomedicines	Two HPMa copolymers were modified by aminogluthimide and DOX to improve intercellular drug release.	[86]
Oliveria et al.	Ca-P Coating Starch-Based Biomaterials	CaP coating on starch was utilized to regulate osteoblastic/osteoclastic cell line activity.	[87]
Ho et al.	Endosomolytic Pseudo-Peptides Spheroids Tumor	One biomimetic endosomolytic polymer was synthesized to improve intercellular drug release.	[88]
Ekkelenkamp et al.	Poly(amido amine) Minimal Cytotoxicity	The comparison between two kinds of PAA nanoels was made.	[89]

2.6. Biomimetic nanostructures

Therapeutic nanoparticles are drug carriers with a size range of 10 to 1000 nm, which is similar to the size of proteins or DNA [90]. By rolling up inorganic materials (such as graphene) or self-assembling biomaterials (such as peptides), hollow cylindrical nanotubes can be made [91,92]. Phase separation, self-assembly, and electrospinning are the three major methods for producing nanofibers with the shape of a fibre from natural or manufactured polymers. Furthermore, because these nanoparticles are biodegradable and biocompatible, they have a high capacity for drug loading and cellular uptake [93]. Inorganic nanoparticles made of materials such as gold, silica, fullerene, and grapheme are also suitable drug

carriers [61]. A synopsis of works on biomimetic nanostructures such as nanotubes, nanofibers and nanoparticles in drug delivery applications is shown in Table 6.

Table 6. Synopsis of works on biomimetic nanostructures in drug delivery applications [48].

Authors	Brief Title	Highlights	References
Biomimetic Nanotubes			
He et al.	Layer-by-Layer Nanotubes Calcium Carbonate Deposition	Polyelectrolyte multilayer nanotubes were used to produce calcium carbonate into their cavities.	[94]
Chen et al.	Rosette Nanotubes Dexamethasone	Rosette Dex-loaded nanotubes were fabricated to improve osteoblast proliferation.	[95]
Shang et al.	Rosette Nanotubes hydrophobic drugs	Two kinds of RNTs were comprised as TAM carrier in targeting drug delivery.	[96]
Biomimetic Nanofibers			
Freshwater et al.	Electrospun Dendrimer-Gelatin Nanofiber Drug Delivery	Electrospun dendrimer-gelatin nanofiber was fabricated to improve the rate of wound healing.	[97]
Anderson et al.	Modulating Gelation Peptide Amphiphiles	The nanofibrous networks properties of PAs were modulated to be enabled to mimic ECM.	[98]
Kim et al.	Peptide Amphiphile Nanofiber Gel Cisplatin Delivery	The CDDP-PA nanofiber Gel matrix was synthesized to provide spatially and temporally intercellular drug release.	[99]
Biomimetic Nanoparticles			
Palazzo et al.	Hydroxyapatite–Nanocrystals Antitumor	Cisplatin, alendronate, and DPM on the drug affinity for HA nanocrystal were studied.	[100]
Sheikh et al.	Biomimetic Matrix Nano-Hydroxyapatite	The comparison between BSA, CL and PVA matrices for HA nanocrystal production as drug carriers was done.	[101]
Byun et al.	Efficiency Sustained Composite Hydrogels Mussel-Inspired	The loading capacity and drug release profile of DOX were promoted by means of HA/GO nanocomposites.	[102]

3. Bacteria based drug delivery vectors

Bacteria and viruses have the natural ability to enter the host body, eluding the immune system and causing powerful connections with their target cells. Pathogens have developed over time to optimise properties that are similar to those sought by medication delivery vehicles. As a result, scientists have attempted to get drug-delivery systems from infections in a number of ways.

Some infections have unique bioavailability properties, including the capacity to reach organs that are often difficult to access, such as the CNS. Pathogen biodistribution is governed by complex but well-documented molecular mechanisms that entail several interactions with host receptors [103]. Several bacteria-based treatments have previously been proven to be effective. Plasmids were inserted into the sacculus of recombinant bacteria (Figure 8a) to create a system that can generate and release these proteins in situ at the target region [104].

Advances in genetic engineering have made it possible to modify living bacteria to create vaccines for diseases like Type 1 diabetes [105] and anti-inflammatory medicines for bowel ailments [106]. The capacity of ghost, nonliving bacteria (Figure 8c) to target particular cells with their chemical surface features was also studied as a vaccine carrier. A recent application [107] demonstrated the ability of bacteria-based drug carriers to transport drugs to the brain. Recently, a biohybrid drug-delivery system based on the *Escherichia coli* bacteria envelope encasing elliptical disk-shaped polymeric microparticles was presented [108]. The chemotactic response of hybrid bacteria particles, which present the native bacterium's tropism, was found to outweigh the effect of body shape on extravascular movement.

Using an attenuated form of the intracellular bacteria *Listeria monocytogenes*, Akin *et al.* [109] developed bacteria-based nanoparticle delivery systems known as 'microbots' (Figure 8b). Without any genetic manipulation, nanoparticles containing plasmid DNA were conjugated to the surface of bacteria)via

biotin–streptavidin interactions, and the microbots successfully entered tumour cells and released nanoparticles, resulting in subsequent transcription and translation of the target proteins.

Although the bacteria utilised in these applications are typically deemed safe, their immunogenicity is not always favourable, and various human safety concerns should be evaluated before clinical use. Table 7 shows the current development status of bacteria based drug delivery vectors.

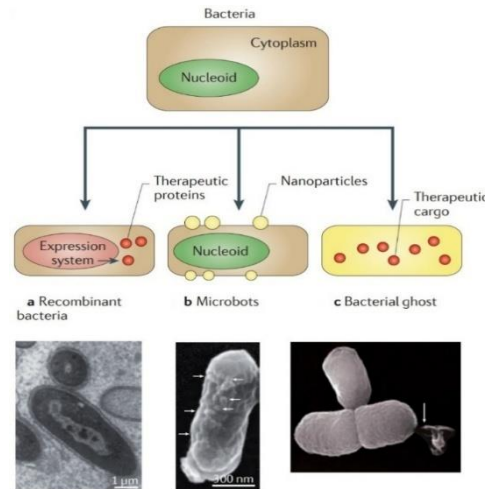


Fig 8. **Biomimetic engineering strategies for bacteria.** a) **Recombinant bacteria** - image in the panel shows recombinant *Salmonella typhimurium* internalized in macrophages. b) **Microbots** - image in the bottom panel shows *Listeria monocytogenes* bacteria carrying polystyrene particles. c) **Bacterial ghosts** - image in the bottom panel shows protein E-lysed *Mannheimia haemolytica* bacterial ghosts. [110].

Table 7. Current development status of biomimetic bacteria based vectors [110].

Strategies	Key attributes/capabilities	Applications	Current status	Challenges and/or limitations	References
Recombinant bacteria	<ul style="list-style-type: none"> •Full set of RNA polymerases that enable expression of various substances, including antigens, therapeutic proteins and siRNAs •Tumour tropism •No pathogenicity of GRAS bacteria 	<ul style="list-style-type: none"> •Vaccine delivery •<i>In vivo</i> factory for therapeutic proteins at disease sites •RNA interference-based cancer therapy 	Clinical trials (Phase I)	<ul style="list-style-type: none"> •Safety concerns associated with attenuated bacteria (reversion to virulence) 	36-39
Microbots	<ul style="list-style-type: none"> •Carry nanoparticles on the surface of bacteria •Neither bacterial disruption nor genetic manipulation is required •Take advantage of the invasive property of bacteria 	<ul style="list-style-type: none"> •Gene or protein delivery 	Preclinical	<ul style="list-style-type: none"> •Safety concerns associated with attenuated bacteria (reversion to virulence) •Applicability in actual disease models •Feasibility with biocompatible nanoparticles 	40
Bacterial ghosts	<ul style="list-style-type: none"> •No cytoplasmic contents •Intact surface properties •Large drug-loading capacity •Natural tropism to various tissues, including tumours •Considerable safety and low production cost 	<ul style="list-style-type: none"> •Drug or DNA delivery •Vaccine delivery 	Preclinical	<ul style="list-style-type: none"> •Potential immunogenicity owing to lipopolysaccharide •Limited <i>in vivo</i> data 	41,42

4. Virus based nanoparticles

The self-assembly of capsid or envelope proteins produced from viruses produces virus-based particles. These carriers are safe since they do not contain natural virus genetic material, and they can be enhanced by adding peptides and antibodies to the surface [111]. Furthermore, they are capable of demonstrating the natural tropism of living parent viruses [112]. Their manufacture is simple and inexpensive. Because the antigenicity of virus-based particles is similar to that of the parent virus, this family of carriers was designed to deliver vaccines [113]. The human papillomavirus is one of the most misunderstood viruses (HPV). HPV-like nanoparticles are very comparable to genuine virion and can thus be employed as a vaccine because they are both safe and immunogenic [114]. HPV-like nanoparticles are utilised in clinical practise, and the US FDA has approved two commercial treatments (Gardasil, from Merck, and Cervarix from GlaxoSmithKline).

Virus-based nanoparticles can carry a therapeutic payload within their capsular structure, in addition to vaccine uses. This type of particle effectively enclosed genes [115], proteins [116], and medicines [117]. Recently, exciting results were reported in research involving virus-like nanoparticles generated from plants [118,119], which constitute a viable alternative to synthetic particles due to their biodegradability and biocompatibility.

5. Pathogen based biomimetic strategies

5.1. Pathogen mimicking vaccines

Since soluble antigens have poor immunogenicity, antigen-carrying synthetic particles that imitate the structure and/or content of microorganisms in a reductionist approach have been developed [120]. Professional antigen-presenting cells (APCs) that internalise particle-associated proteins process these antigens up to 1,000-fold more efficiently for presentation to CD8+ T lymphocytes (a process known as cross-presentation) than if the identical extracellular proteins are internalised in a soluble form [121,122]. Antigen presentation to CD4+ T cells is also enhanced, resulting in better T cell support for CD8+ T cell and antibody responses [123, 124]. As a result, polymer particles such as poly(lactic-co-glycolic acid) (PLGA) micro- and nanoparticles have been designed to allow for the continual release of antigens within APCs, which could help to maintain T cell priming *in vivo* [125].

The size of pathogen influences their spread *in vivo* in part; virus particles small enough to move freely through the extracellular matrix are swiftly drained from peripheral tissue locations to lymph nodes, where main immune responses are generated [126]. Synthetic polymer particles that carry antigens and are less than 100 nm in size have been found to efficiently reach lymph nodes following injection into the skin, resulting in more efficient immune responses, by replicating this size-dependent transport mechanism [127,128].

Internalization of antigens in a particulate form is simply one of many aspects that influence natural infections' ability to elicit powerful immune responses. Unmethylated cytosine–guanosine DNA (CpG DNA), double-stranded RNA, LPS, flagellin, and other conserved molecular motifs in the structure of microorganisms are recognised by immune cells as danger signals, and they engage receptors such as Toll-like receptors (TLRs). Incorporating defined TLR agonists or other molecular danger signals into antigen-carrying particles mimics infections' coexistence of antigens and stimulatory signals, promoting both antibody and cellular immune responses.

Antigen-carrying vesicles have been proposed as a crucial method by which APCs discriminate safe environmental antigens from true pathogenic threats by delivering danger signals and antigens to a

common phagosomal compartment [129]. Encapsulation or surface immobilisation has been used to include pathogen-derived warning signals into synthetic particle vaccinations [130,131, 138]. Components of the host response, such as complement, can also be triggered by antigen-carrying particles. Pathogens can be detected by intracellular sensors of cellular damage and/or stress, in addition to stimulating the activation of pattern recognition receptors. It has also been revealed that pathogens disrupting phagosomes and/or endosomes create a complex intracellular signalling network known as the inflammasome [132]. Synthetic particles, such as adjuvant alum [133,134] and degradable PLGA particles [135], have the potential to trigger this system, revealing a hitherto unknown route for the development of effective vaccination carriers.

Pathogen-mimicking vaccines have shown proven advantages over traditional vaccines in preclinical investigations, including increased antibody titres and cytotoxic T cell responses [136]. However, this field is still in its early stages, with only a few investigations in non-human primates and Phase I clinical trials to yet; future research will decide whether these techniques are useful for therapeutic or preventative vaccination.

Antigen presentation from a surface and simultaneous presentation of danger signals are two of the most basic principles of pathogens used in current designs. For these engineered materials to become extensively employed, the development of easily translatable synthetic and/or manufacturing techniques, as well as demonstration of enhanced efficacy in patients (as opposed to equivalent performance to existing adjuvants such as alum), will be required. However, other aspects of pathogen-mimicking vaccines need to be investigated, especially as more details about host–pathogen interactions emerge. Future research aimed at gaining a deeper grasp of this landscape will be critical for the field's growth.

5.2. Virus-mimicking particles, including effects of shape

Researchers are adapting viral shapes and functionalities to the construction of synthetic medicine carriers as their understanding of viral infection mechanisms grows. As tumor-targeted gene delivery carriers, self-assembled liposomes that mirror viral structures have been produced. Liposomes made of lipids, transferrin, and DNA have been shown to produce highly compact nanostructures with a uniform size distribution (50–90 nm); these nanostructures have a multicentre lamellar core structure and a transferrin-coated membrane, resembling the architecture of envelope viruses like influenza and herpesvirus. The efficacy of delivering the gene encoding the cellular tumour antigen p53 into human prostate cancer tumours *in vivo* [137] was improved by these virus-like transferrin nanostructures.

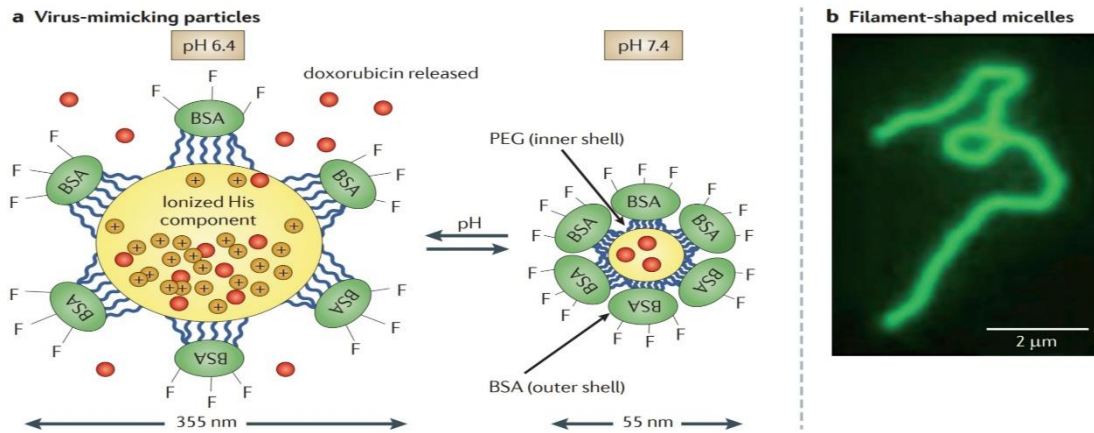


Fig 9. **Virus-mimicking synthetic drug carriers.** a) Virus mimicking nanogels. b) Filomicelles [110].

A pH-sensitive nanogel system with structural and functional characteristics similar to those of a virus has also been produced [139]. A hydrophobic core and two layers of hydrophilic shells with tumor-targeting ligands make up this virus-mimetic nanogel. Doxorubicin, an anticancer medication, was put into the hydrophobic core. PEG was attached to the core polymer (which served as the inner shell) and bovine serum albumin was bound to the other end of PEG to replicate the capsid-like structure (this functioned as the outer shell). These virus-like particles were pH-sensitive, so lowering the pH from physiological (pH 7.4) to endosomal (pH 6.4) produced reversible swelling of the nanogel and a size increase from 55 nm to 340 nm, which allowed endosomal escape and doxorubicin release into the cytosol. After the cells were killed and dissolved by doxorubicin, the nanogels migrated to nearby cells and continued the cycle, reproducing the virus infection (Figure 9a).

Filomicelles - wormlike filamentous micelles — have been created to take use of the morphological properties of viruses, as several viruses are filamentous [140] (Figure 9b). The reticuloendothelial system (RES) is efficiently evaded by the long and flexible filomicelles made of self-assembling amphiphilic block copolymers, resulting in unusually lengthy blood circulation periods (approximately 1 week). Filomicelles shrunk tumours more effectively than either the free drug or spherical nanocarriers when loaded with the widely prescribed anticancer medication paclitaxel. In the coming years, the *in vivo* effectiveness of such carriers with nonspherical forms is likely to be investigated further. However, these techniques are still in the early stages of development, and their clinical value has yet to be established.

In comparison to simple particle carriers, strategies based on emulating the structure of viruses have proven substantial advantages. The impact of form and flexibility on filomicelle circulation and targeting is highly promising. The capacity of pH-sensitive nanogels to escape endosomes and infect neighbouring cells on a continual basis is also encouraging. Overall, these methodologies support the advanced engineering of viruses into synthetic drug delivery carriers, which goes beyond basic surface alteration, and they expand the applications of these virus-mimicking particles in targeted drug delivery. However, these techniques are still in the early stages of development, and their clinical value has yet to be established. Table 8 illustrates some of the recent advances in this domain.

Table 8. Current development status of biomimetic pathogen based vectors [110].

Strategies	Key attributes/capabilities	Applications	Current status	Challenges and/or limitations	References
<i>Pathogen-mimetic vaccines</i>					
Pattern recognition mechanisms	<ul style="list-style-type: none"> •Ability to stimulate immune cells using danger signals from pathogens via pattern recognition mechanisms •Co-packaging of danger signals as adjuvants and antigens for improved immunization 	•Vaccine delivery	Preclinical	•Limited to vaccine delivery	[138]
<i>Virus mimetics</i>					
pH-sensitive nanogels	<ul style="list-style-type: none"> •Capsid-like structure •pH-sensitive reversible swelling is followed by drug release and endosomal escape •Ability to migrate to neighbouring cells 	•Targeting tumours	<i>in vitro</i>	<ul style="list-style-type: none"> •Vulnerable to immune recognition •<i>In vivo</i> validation needed 	[139]
Filomicelles	<ul style="list-style-type: none"> •Flexible and filament-shaped micelles •Prolonged circulation time in blood (over one week) 	•Targeting tumours	Preclinical	•Thorough investigation into PK/PD needed	[140]

6. Cell based drug delivery vectors

Despite extensive research into innovative synthetic materials, interest in cell-based medication delivery systems continues to grow. For this use, natural cells and extracellular vesicles made up of endogenous components appear to be safe and reliable [141]. Circulating cells, such as erythrocytes (RBCs), leukocytes (WBCs), and stem cells (SCs), have inherent disease-targeting capabilities and can house active chemicals within their structure. These unusual qualities have prompted researchers to create and test cell-mediated drug delivery systems in recent years, with promising results.

RBC-mediated drug delivery systems (Figure 10a) have been extensively researched among cell-based drug carriers [142] because they are easy to extract and load with medicines, both *ex vivo* and *in vivo* [143], and they are stable to store. RBCs are useful for trapping large amounts of medicines because they have a lengthy circulation duration in the bloodstream (up to 120 days) and a big internal capacity volume of 185–191 m³ [144]. As a result, as revealed in recent clinical studies [145], RBCs seem particularly promising, and numerous ways to increase drug encapsulation, such as utilising cell-penetrating peptides [146] and their surface functionalization, are now being investigated [147–149]. Natural RBCs' excellent tailorability enables for a wide range of uses, including diagnostic imaging [150] and therapeutic action. One intriguing use of surface-modified RBCs in this field is homeostasis. Erythrocytes have been shown to speed up thrombus breakdown and allow for thromboprophylaxis in patients at high risk of thrombosis [151]. RBCs' potential, on the other hand, is mostly expressed as a carrier for therapies, with the goal of improving the pharmacokinetics and activity of active compounds. Free administration in humans fails in autoimmune illnesses in several applications, such as antigen delivery, and erythrocytes bypass this constraint to develop effective and long-lasting immunological tolerance [152]. Erythrocytes do not extravasate because of their physiological purpose, hence their use in cancer treatment is confined to situations involving one of the mononuclear phagocyte system (MPS) organs [153] or the elimination of circulating cancer cells [154].

WBCs (Figure 10b) are immune system cells that play a key role in inflammatory processes, infections, and a variety of local illnesses. WBCs have a shorter circulation duration than RBCs (up to 20 days), but their specific functions, which allow for high cellular contacts and considerable tissue penetration, particularly over physiological barriers, make them appealing for drug delivery applications. Leukocytes have many activities associated to transport, migration toward inflammatory regions, and attachment to endothelium wall tissues with tumour cells [155], making them ideal drug carriers for cancer treatment. Their use in this field is currently confined to the production of biohybrid nanoparticles (which is discussed in a later section).

Stem Cells (Figure 10c) can also deliver therapeutic substances to specific regions, taking advantage of their inherent targeting abilities. Due to their innate tumour tropism [156] and ability to restrict specific types of metastatic processes [157], SC-based treatments have been successfully employed in the treatment of cancer. This method offers promise in the treatment of ovarian [158], brain [159–161], and breast [162] cancers. Oncolytic viruses infecting cells that can transport a therapeutic chemical payload have been effectively administered using SCs [163]. The employment of cells as a homing system is particularly important in this scenario for improving virus-based therapeutics. Viruses that target cancer are highly effective and particular, but their spread is hindered by the immune system. The combination of oncolytic viruses and SCs is a successful technique for increasing oncolytic viral bioavailability and, as a result, overall efficiency. Previous studies have revealed some intriguing *in vivo* results, underlining SCs' innate proclivity for invasive malignancies [164,165]. Table 9 shows some biomimetic drug delivery strategies based on eukaryotic cells.

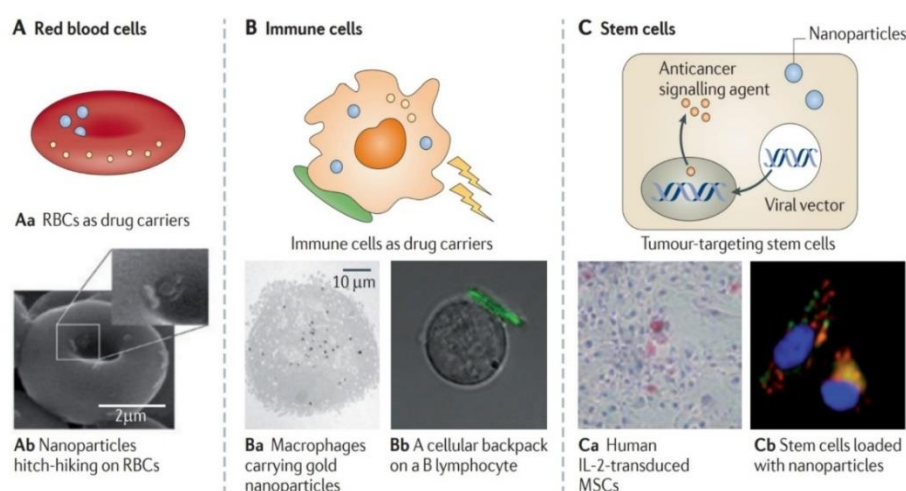


Fig 10. Bioengineered **eukaryotic cells** for drug delivery [110].

Table 9. Current development status of biomimetic eukaryotic cell based drug delivery vectors [110].

Strategies	Key attributes/capabilities	Applications	Current status	Challenges and/or limitations	References
RBCs	<ul style="list-style-type: none"> •Prolonged circulation (~120 days) •Large volume for drug encapsulation •Ability to carry nanoparticles and thrombolytics 	<ul style="list-style-type: none"> •Drug delivery •Targeting the RES 	Preclinical	<ul style="list-style-type: none"> •Difficult to maintain integrity •Limited targeting ability 	[166,167]
Macrophages	<ul style="list-style-type: none"> •Natural homing tendency to disease sites •Ability to move through the BBB •Ability to phagocytize nanoparticles 	<ul style="list-style-type: none"> •‘Trojan horse’ delivery carriers 	Preclinical	<ul style="list-style-type: none"> •Difficult to collect •Difficult to maintain integrity 	[168,169]
Lymphocytes	<ul style="list-style-type: none"> •Ability to carry various sizes of particles •No damage to intrinsic functionality of the cells 	<ul style="list-style-type: none"> •‘Cellular backpack’ •Adoptive T cell therapy of cancer 	Preclinical	<ul style="list-style-type: none"> •Difficult to collect •Difficult to maintain integrity 	[170,171]
Stem cells	<ul style="list-style-type: none"> •Gene delivery by genetic engineering •Natural homing tendency to solid tumours •Ability to internalize nanoparticles 	<ul style="list-style-type: none"> •Cancer therapy 	Preclinical	<ul style="list-style-type: none"> •Difficult to collect •Difficult to maintain integrity 	[172,173]

7. Cell-based bioinspired and biomimetic strategies

7.1. Biomimetic particles that mimic cell morphology and functions

Biocompatible polymeric particles that mimic RBCs have been investigated (Figure 11A). Layer-by-layer construction onto a PLGA template was used to create some of these particles, which were designed to match natural RBCs in size, shape, mechanical flexibility, and oxygen-carrying capabilities [174]. These polymeric particles could also encapsulate a variety of chemicals, such as medications and imaging agents. Haghgoie *et al.* [179] created PEG particles that were able to flow through narrow capillary channels and mimicked certain elements of the size, shape, and flexibility of RBC. Cell-based bio-inspired and -mimetic strategies. Merkel *et al.* [175] created RBC-like hydrogel microparticles with tunable elasticity and discovered that when the modulus of these particles was tuned to that of RBCs (26 kPa) or lower, circulation time in the blood was greatly increased

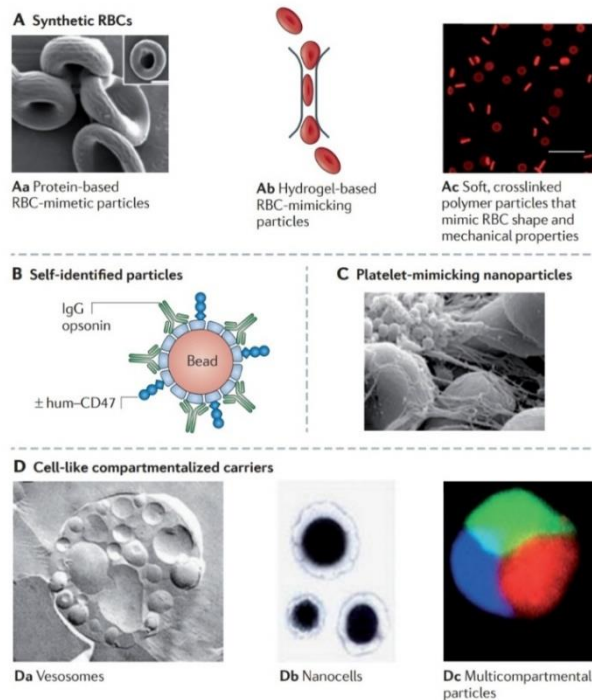


Fig11. Cell-mimicking synthetic drug particles [110].

A 'marker of self' identification system, in addition to the size, shape, and mechanical flexibility of RBCs, has been deemed a crucial element that contributes to RBCs' extraordinarily long circulation time (120 days). CD47, a membrane protein found on all cells, has been shown to communicate macrophage phagocytic activity suppression [180]. In normal mice, CD47-knockout RBCs were promptly removed from the bloodstream. This 'marker of self' is now being added to polymer particles in order to prolong the circulation of nanoparticles in the blood for nanomedicine applications [181,182]. Tsai *et al.*, [176] for example, used a recombinant form of CD47's immunoglobulin-like domain to modulate *in vitro* phagocytosis (Figure 11B) by attaching it to polystyrene particles. CD47 decrease 7d phagocytosis by human macrophages and monocytes in a dose-dependent manner, according to particle uptake tests. The incorporation of such a "self-marker" into RBC-mimicking systems and a variety of other particles is predicted to increase immunocompatibility *in vivo*. For encouraging haemostasis [183], platelet-mimicking nanoparticles have also been produced. Synthetic platelets were made from poly-L-lysine attached to PLGA (PLGA-PLL) block copolymers and functionalized with RGD (Arg-Gly-Asp) peptides,

which have a specific binding affinity for active platelets (Figure 11C). Synthetic platelets have been shown to bind to active platelets at the bleeding site and successfully stop bleeding *in vitro* and *in vivo* investigations.

7.2. Particles that mimic compartmental cellular architecture:

The structuring of the cellular machinery inside spatially defined compartments aids the complicated chemistry and function of live cells. The purpose of early studies of hierarchical drug carrier architectures that mirror, at a basic level, the compartmental organisation of eukaryotic cells was to develop improved drug delivery systems capable of sequestering several chemicals within a single particle carrier [184].

Kisak *et al.* [185] used the reversible vesicle-to-bolster sheet transition to create several internal bilayer-enclosed compartments, dubbed 'vesosomes' (Figure 11D). Because vesosomes have multiple non-nested internal compartments with different membrane compositions that encapsulate drugs, drug cargos must first diffuse through the internal vesicle wall into the cytosol of the vesosome before passing through the external bilayer, resulting in a sustained release profile (nearly over 10 hours) [177].

Hybrid lipid and/or polymer 'nano-cells,' which are based on the encapsulation of biodegradable polymer nanoparticles within lipid vesicles [178], have been designed to co-deliver two antitumour medicines with different release kinetics. A doxorubicin–PLGA combination was used to make the nanoparticles, while combrestatin, an anti-angiogenesis drug, was contained within the surrounding lipid bilayer compartment. As these intravenously injected particles collected in tumours and induced the collapse of blood arteries within the tumours, this design aimed for quick release of the anti-angiogenesis agent from the outside compartment, irrevocably trapping the nanocells within the tumour environment. The remaining tumour cells were then eliminated by a constant discharge of the cytotoxic doxorubicin cargo from the nanocell's nuclear compartment. This two-pronged approach significantly slowed tumour growth in comparison to single drug treatment controls. As a result, this method might be used to a variety of chemotherapeutic drug combinations with known or prospective treatment synergy.

Micellar structures and multicompartamental solid particles have also been developed. Block copolymers with numerous different block chemistries that assemble to form stable structures in water are used to create multicompartamental micelles [186,187]. Multiple therapeutic cargos with different physical properties can be sequestered within discrete nanoscale zones of individual micelles using these structures. Microfluidic reactors [188,189] and emulsion spray-drying methods [190] have been used to create particles with well-defined 'core-shell' architectures on the micrometre scale which offers concentric compartments for loading of drugs.

Electrohydrodynamic spray-dying techniques [191,192], in which controlled phase separation in polymer solutions is employed to build complex multicompartamental particle formations, can access more complicated morphologies. Using techniques such as continuous- and stop-flow lithography [193,194], methods for fabricating hydrogel particles with defined internal compartments of varying composition and chemistry have been demonstrated; these methods allow for the synthesis of monodispersed microparticles with well-defined internal structures. Although efforts utilising tailored micelle and polymer particle architectures are less progressed in terms of medical applications than lipid vesicle-based strategies (described above), they may provide unique features not available in simple phospholipid-based materials.

Engineering methods have advanced and more sophisticated particles have been constructed as the importance of carrier features (such as size, shape, mechanical flexibility, surface property, and internal architecture) in particle–cell interactions for drug delivery has been revealed. As a result, scientists have begun to mimic the morphologies and functions of cells in order to benefit from them. As a result, particles capable of partially imitating known cell features have been produced. RBCs' size, shape, and

mechanical characteristics, for example, have been merged into biocompatible particles, but their internal structure and CD47 — a critical maker for surface recognition — have yet to be mixed. To build and enhance specialised drug delivery carriers for specific applications, key desirable features of multiple cells or pathogens can be integrated into a single synthetic particle. Synthetic particle systems that imitate cells will offer enormous potential for future drug vector delivery systems as our knowledge of known critical cellular features expands. Table 10 summarizes recent advances in cell based biomimetic and bioinspired strategies.

Table 10. Current development status of cell based biomimetic and bioinspired strategies [110].

Strategies	Key attributes/capabilities	Applications	Current status	Challenges and/or limitations	References
<i>Cell mimetics</i>					
Synthetic RBCs	<ul style="list-style-type: none"> •Ability to mimic shape and mechanical property of RBCs •Drug-loading ability •Oxygen-carrying ability 	<ul style="list-style-type: none"> •Drug delivery •Component of artificial blood 	Preclinical	<ul style="list-style-type: none"> •Vulnerable to immune recognition •Detailed <i>in vivo</i> validation needed 	[174,175]
Self marker CD47	<ul style="list-style-type: none"> •Membrane protein that is derived from RBCs •Contributes to self-recognition of RBCs by RES, thus enabling prolonged circulation time 	<ul style="list-style-type: none"> •Evasion of RES 	<i>in vitro</i>	<ul style="list-style-type: none"> •Limited resource 	[176]
<i>Compartmentalization</i>					
Vesosomes	<ul style="list-style-type: none"> •Liposomes within a liposome: distinct inner compartments separated from the external membrane •Sustained release profile 	<ul style="list-style-type: none"> •Drug delivery 	Preclinical	<ul style="list-style-type: none"> •Vulnerable to immune recognition •<i>In vivo</i> validation needed 	[177]
Nanocells	<ul style="list-style-type: none"> •Polymer nanoparticles within lipid vesicles •Dual drug release system: rapid release of one drug from the lipid layer and sustained release of the other drug from polymer nanoparticles 	<ul style="list-style-type: none"> •Cancer therapy 	Preclinical	<ul style="list-style-type: none"> •Vulnerable to immune recognition 	[178]

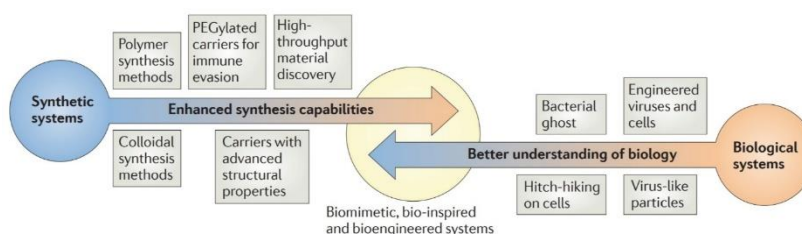


Fig 12. Bioengineered, bio-inspired and biomimetic systems. Recent advances in the synthesis of novel materials and understanding of biological systems have paved the way towards bridging the gap between synthetic and biological systems [195].

8. Biomimetic hybrid nanoparticles

Natural cells have obvious capabilities, but disadvantages in terms of safety, stability, and preparation methods effectively limit their usage as drug carriers. Biomimetic hybrid nanoparticles have attracted a lot of attention in recent years. Developing innovative therapeutic nanocarriers for targeted delivery by mimicking unique properties of natural cells or organisms is a strong strategy (Figure 12). Iatrogenic effects are limited when good biomimetic nanoparticles are delivered without eliciting strong responses in the host body. Host responses cause MPS activation, complement activation, and immunological

hypersensitivity reactions after injection. The usage of biomimetic hybrid nanoparticles has the advantage of limiting the activation of mechanisms that produce side effects in patients and resulting in rapid exogenous nanoparticle clearance. A drug-based immune suppression decreases the host response in non-biomimetic nanoparticles. Traditional nanocarrier-mediated targeted drug delivery techniques relied mostly on synthetic nanoparticles encasing the medication. In the last ten years, a new technique that mixes artificial and biological materials has gained traction, resulting in greater biocompatibility and functional properties [196]. The unique qualities of the final structures are created by combining the peculiar characteristics of artificial (e.g., tailorability of chemico-physical properties of nanoparticle bulk

and surface) and biological (e.g., functions, target-specific recognition) materials. Several techniques to drug administration and diagnostics yielded promising outcomes.

By constructing a protein cage around the synthetic structure, biohybrid nanoparticles can be created. Liu *et al.* [197] created a core/shell system consisting of gold nanoparticles that were trapped within a virus protein shell from the cowpea chlorotic mottle virus with great effectiveness (up to 97%, depending on the working conditions).

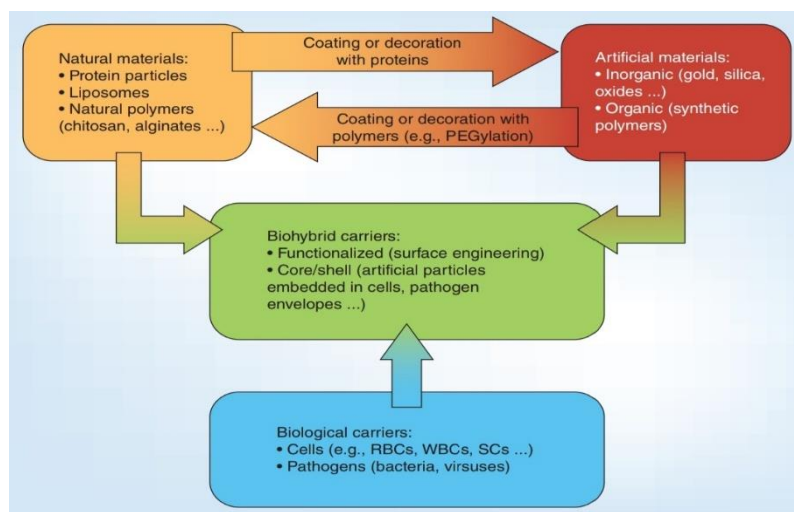


Fig 13. Schematic depiction of the contribution of several groups of materials and carriers to the creation of biohybrid carriers [195].

Nanoparticle encapsulation within natural cell membranes [198], resulting in cell membrane wrapped nanoparticles, is another technique to disguise particles using biological materials. Cloaked nanoparticles (Figure 14) made of inorganic or polymeric materials are encapsulated within intact cell membranes, resulting in a core/shell biohybrid structure. Copp *et al.* [199] described the use of biodegradable PEGylated nanoparticles made of poly(lactide-co-glycolide) and encapsulated within intact RBC membranes for the selective clearance of disease-causing antibodies while minimising therapy-related side effects. The significant affinity between RBC membrane decoys and pathogenic antibodies was exploited by core/shell nanoparticles, which halted the pathological process. This strategy is effective in customised medicine because of the nonspecific absorption process, which is useful when the trigger differs from patient to patient (e.g., in antibody-mediated autoimmune diseases). Interesting studies on RBC membrane-cloaked drug carriers have been reported in the literature, with potential uses as

nanovaccines [200], on-demand targeted drug delivery systems activated by an external stimulus [201], or in cancer treatment to improve the pharmacokinetics of routinely used drugs [202].

This method has lately sparked research into functionalizing cell membrane surfaces in order to improve carrier qualities beyond those of natural cells. Synthetic functionalization procedures have been shown to be effective in achieving this goal [203,204]. This approach effectively slows carrier clearance in systemic circulation, minimising immunological response and increasing targeting qualities, despite the fact that it has not yet been consolidated due to some safety concerns.

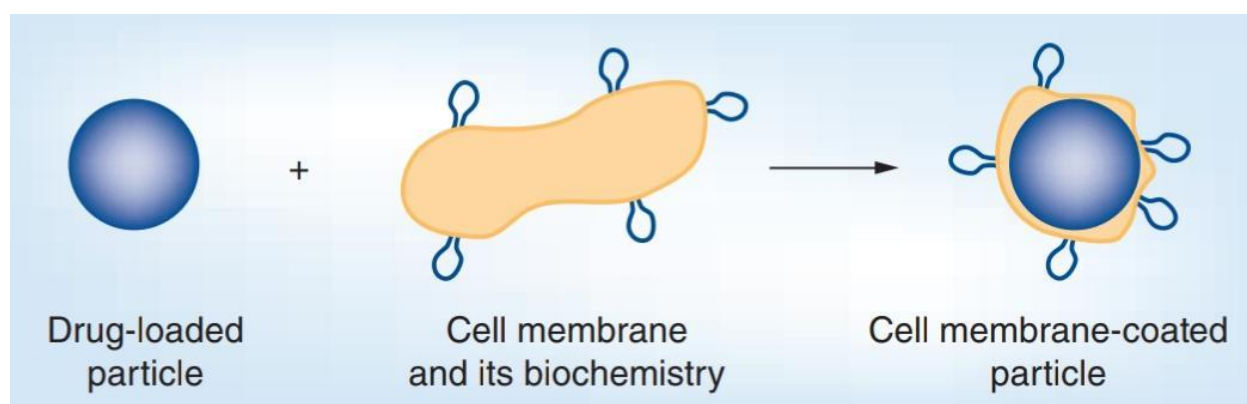


Fig 14. **Preparation of cell membrane cloaked artificial nanoparticles:** drug-loaded nanoparticles are immersed in intact cell membranes during the method, resulting in a system with biochemical surface properties of the cell membrane as well as drug delivery capabilities of the polymer platform [195].

8.1. Increasing circulation time and reducing immunological response

PEGylation is the most widely used technique for extending the half-life of pharmacological carriers. Polyethyleneglycol (PEG) is chemically or physically conjugated to the surface of nanoparticles [205]. This functionalization has been shown to inhibit opsonization and limit MPS clearance in numerous studies. PEGylation was effectively introduced in clinical goods [206], with positive results in the first dose but significant downsides in subsequent administrations [207], prompting researchers to investigate other options. Different hydrophilic synthetic compounds, such as zwitterionic units, (such as poly(carboxybetaine) [208], poly(sulfobetaine) [209]) hydroxyl groups [210], dendritic polyglycerol sulfate [211], polyoxazolines [212] and other additional natural polymers [213,214] are viable alternatives to PEGylation. Chemical functionalization or coatings are achieved using the cited functional units.

Cell biology has revealed some viable approaches to artificial functionalization for increasing carrier half-life. The most common cells in human blood are red blood cells (RBCs). They have their own geometry, size, mechanical qualities, and molecular composition, all of which have been tailored to achieve their specialised biological performance. RBCs are long-circulating cells, which is why they were chosen as a model for developing better delivery platforms. Synthetic approaches proved useful in the creation of polymeric particles that replicated the size, shape, and mechanical stiffness of RBCs [214], as well as

mechanical thin film stretching [215], electrospraying [216], and particle replication in non-wetting templates [217, 218]. Although RBC-shaped drug carriers have the potential to improve bioavailability, reproducing the complex surface features of RBCs *in vitro* is a significant barrier to overcome in the development of fully RBC-mimicking drug vectors. The core/shell particle preparation method, in which the shell is the natural RBC cell membrane, appears to be the most promising. The complicated biochemical RBC structure is completely translocated to nanoparticles in this manner. Hu *et al.* [219] confirmed this by finding the same CD47 density in biohybrid particles as natural RBCs (the surface protein that determines their long half-life in the bloodstream [220]). In iron oxide-based nanoparticulate systems, the camouflage with RBC cell membranes efficiently decreases MPS activation, resulting in superior *in vivo* biodistribution than PEGylated nanoparticles [221] and much decreased nonspecific macrophage uptake in mice [222]. The topological influence of the nanoparticle core on cell membrane

protein distribution is an additional benefit. As a result of interface interactions [223], cell membrane proteins are induced to position themselves out of the RBC membrane after encapsulation in the presence of hydrophobic core particles. It keeps the biological features of the cell envelope.

WBC-based particles also have a longer circulation period. Parodi *et al.* [224] created and tested leukocyte-like nanoparticles with a nanoporous silicon core and a leukocyte cell membrane-derived exterior shell. The obtained results revealed that the orientation of leukocyte transmembrane proteins was unaffected by core encapsulation. In compared to uncloaked particles, prepared leukocyte-like nanoparticles had a tenfold slower opsonization and delayed MPS absorption. The end result was a significantly longer half-life and more accumulation at the target spot. Platelet-cloaked nanoparticles, like erythrocyte- and leukocyte-coated nanoparticles, can decrease the immune response and limit phagocytosis after injection [225].

8.2. Improving targeting properties

Biohybrid nanoparticles with biological components boost their ability to target different illnesses. Biohybrid nanoparticles functionalized with WBC cell membrane show great promise in cancer treatment. Due to inherent propensity of immune cells to target inflamed vasculature and extravasate across the endothelium, Palomba *et al.* recently demonstrated that nanoporous silica nanoparticles encapsulated in a leukocyte cell wrap improved tumour vascular permeability [226]. He *et al.* [227] found that Janus nanoparticles half-coated with leukocyte membrane had a higher absorption in cancer cells, indicating that they can distinguish between different types of cancer cells. A similar approach has shown to be effective in the photothermal treatment of cancer [228]. The use of macrophage cell membrane coated gold nanoparticles for cancer photothermal therapy was recently reported by Xuan *et al.* Using the camouflage of macrophages [229], coated particles accumulated in cancer cells *in vivo*. When compared to RBC-coated nanoparticles, this method provided active drug targeting and more efficient accumulation due to the unique identification of tumour endothelium by nanoparticle envelopes. Similarly, macrophage cell membranes were employed to wrap mesoporous silica nanoparticles, resulting in increased circulation time and tumour accumulation, as well as active drug targeting in cancer cells for doxorubicin delivery [230].

Cancer cell membrane coated nanoparticles are another difficult strategy for cancer targeting. The homologous binding adhesion molecules in this cell membrane have been functionalized in a way that makes them appropriate for the creation of theranostic nanoparticles for photothermal cancer therapy [231]. Although the impressive results of Chen *et al.* should be applied to this type of nanoparticle, this strategy has not yet been completely explored in drug-delivery systems. Fang *et al.* [232] recently published a key study in this sector, proposing an anticancer vaccine based on poly(lactide-co-glycolide) degradable nanoparticles coated with mouse melanoma cells. The same cell adhesion of source cells was seen in prepared nanoparticles, with better cell-specific targeting. While most instances focus on targeting

cancer cells in specific districts, Li *et al.* reported a biomimetic technique that uses platelet membrane functionalized particles [233,234] to inhibit metastatic activities. This is a novel method based on the discovery that activated platelets are physically connected with blood-borne cancer cells in the blood flow, where cancer cells circulate. A tumor-specific apoptosis-inducing ligand cytokine was conjugated to activated platelet-coated silica particles. When the particles attached to circulating tumour cells, they overactivated platelets, which in turn stimulated immune cells that kill cancer cells in the bloodstream. Platelet membrane coated polymer particles have also been produced for drug co-delivery in the treatment of myeloma and thrombus formation reduction [235]. A targeting ligand (alendronate) was used in this example to allow for the precise accumulation of drug-loaded vectors at the diseased region, reducing off-target deposition.

9. Clinical trials and market

The translation of drug-delivery nanoparticles from bench to bedside is expanding as manufacturing techniques improve, with a growing number of clinical and preclinical investigations. In humans, research is necessary to understand particle/cell interactions and the efficacy of built systems. Since the mid-1990s, there have been roughly 13 nanoparticle drug delivery systems approved, including 51 new pharmaceuticals. Liposomal and first-generation polymer nanoparticles are commonly used in approved clinical trial systems [236].

The therapeutic development of long-circulating nanoparticles is well progressed. Open clinical studies of long-circulating nanoparticles, mostly PEGylated compounds, were evaluated in a recent report. Clinically tested systems are mostly employed in the treatment of cancer and contain chemotherapeutic drugs that are already in use in clinical practice (e.g., paclitaxel, docetaxel and doxorubicin). Renagel (Sanofi S.A., Gentilly, France), a non-PEGylated stealth nanoparticle system made of poly(allylamine hydrochloride), is the only example of a non-PEGylated stealth nanoparticle system for the treatment of chronic kidney disorders [237].

Only a few biological carriers, on the other hand, have been approved for clinical studies, and they only account for bacteria-derived nanocells. The TargomiRs [238] are a fascinating biomimetic technology that is currently undergoing a clinical Phase I trial. This technology consists of tailored bacterial minicells that release miRNA for use as a replacement therapy in patients with thoracic cancer. This study (trial ID: NCT02369198) uses EnGeneIC Ltd's EDVTM nanocells technology, which has already been tested *in vivo* for the delivery of chemotherapeutic drugs [239], siRNAs [240], and miRNAs [241] in preclinical investigations. The same delivery system, loaded with doxorubicin and targeting EGFR, is currently being tested in a Phase I clinical trial for the treatment of recurrent glioblastoma multiforme (trial ID: NCT02766699), while EDV loaded with mitoxantrone is being tested in a Phase I trial for the treatment of refractory solid and CNS tumours in children (trial ID: NCT02687386).

10. Conclusion

Targeted drug delivery has undeniably grown in relevance over the years. Overcoming physiological obstacles and reducing off-target drug deposition are two goals that biomimetic nanoparticle vectors can help with. Biomimetic nanoparticles, whether natural, synthetic, or biological in origin, offer a number of advantages for improving the pharmacological action of active compounds, including increased biodistribution, extended circulation time, and greater biocompatibility. Preclinical studies have been focusing on artificial, hybrid, and cell-based systems, and the combination of biological materials with synthetic nanoparticles appears to have a synergistic influence on numerous carrier characteristics. Preclinical findings are promising, indicating that the method has the potential to improve medication pharmacokinetics. With the discovery of new materials and cellular systems, materials science and cell

biology are helping to improve biomimetic features. The development of biomimetic hydrogels with cellular microenvironments that approximated the ECM proved to be extremely beneficial in terms of localised drug delivery. The physicochemical features of biomimetic micellar carriers have been improved. The stable micellar structure provided total protection for loaded pharmaceuticals until they reached their target sites, as well as facilitating cellular absorption to sustainably release medications.

The biomimetic alteration of liposome surfaces and biomimetic liposome fabrication methods improved therapeutic liposomes' ability to target drug administration by improving the EPR effect. Intercellular drug uptakes for targeted drug transfer have been promoted in biomimetic PAMAM dendrimers.

Biomimetic polymeric carriers have made it easier to endocytose for intercellular drug release. Other biomimetic nanostructures based on organic and inorganic materials (nanocomposite drug carriers) have dramatically improved drug loading capacity, cellular uptake, and drug release profile. The obtained results were primarily proved *in vitro* and in animal experiments, and their widespread translation into clinical trials requires additional research.

Challenges

The field of biologically inspired drug carriers is still in its early stages, and there are a number of obstacles to overcome. First, the techniques required for the production of such carriers, such as genetic engineering or *ex vivo* therapies to manufacture or include therapeutic substances, make maintaining the integrity of natural particles, particularly eukaryotic cells, challenging. For example, during *ex vivo* engineering, the surface integrity of RBCs, which is necessary for their sustained circulation, may be damaged, resulting in a more rapid removal of the drug from the blood. As a result, more optimization is needed to reduce structural changes and improve delivery.

Second, delivery vectors based on pathogens like bacteria and viruses have the potential to be immunogenic. Due to their adjuvant capabilities, pathogen-based carriers with a certain level of immunogenicity can be excellent for vaccine administration. However, in uses other than vaccine delivery, pathogen-based carriers' immunogenicity always raises safety issues. The immunogenic components of pathogens must consequently be eliminated or rendered inactive, and their *in vivo* safety must be thoroughly addressed. However, there are certain GRAS bacteria, such as food-grade and commensal bacteria, that are devoid of safety difficulties and hence have the potential to move forward with clinical applications until other pathogen-based systems' potential safety issues are resolved.

Future prospects

Some of the most recent attempts to improve drug delivery have focused on simulating key characteristics of biological carriers in synthetic systems, such as physical morphologies (such as shape, structure, and cellular compartments), self-markers (such as CD47), and molecular danger signals (such as TLRs). To satisfy the complexity of the requirements, a better understanding of the delivery mechanisms utilised by biological carriers is required, as well as improved synthesis techniques that will allow this understanding to be applied to synthetic systems. Combining the advantages of synthetic systems — such as controllability and mass manufacturing — with the exceptional delivery functions of biological systems, on the other hand, has a lot of promise for the advancement of successful targeted drug delivery methods.

The following points are suggested for development in clinical applications of biomimetic nanoparticles for targeted drug delivery:

1. A thorough grasp of drug release kinetics from biomimetic drug carriers, as well as ways to optimise them.

2. In-depth knowledge of particular and non-specific interactions in the microenvironment of cells.
3. Simulating real-world imbalances in a biological environment to explore how these biomimetic carriers react to challenges.
4. Concentration on *in vivo* investigations of materials whose benefits outweigh their drawbacks.

References

- [1] J.F.V. Vincent, Biomimetics – a review, Proc. Inst. Mech. Eng. H J. Eng. Med. 223 (2009) 919–939.
- [2] S. Venkatesh, M.E. Byrne, N.A. Peppas, J.Z. Hilt, Applications of biomimetic systems in drug delivery, Expert Opin. Drug Deliv. 2 (2005) 1085–1096.
- [3] Farokhzad, O. C. & Langer, R. Impact of nanotechnology on drug delivery. ACS Nano 3, 16–20 (2009).
- [4] Langer, R. New methods of drug delivery. Science 249, 1527–1533 (1990).
- [5] Moghimi, S. M. & Kissel, T. Particulate nanomedicines. Adv. Drug Deliv. Rev. 58, 1451–1455 (2006).
- [6] Blanco E, Shen H, Ferrari M. Principles of nanoparticle design for overcoming biological barriers to drug delivery. Nat. Biotechnol. 33(9), 941–951 (2015).
- [7] Gagliardi M. Novel biodegradable nanocarriers for enhanced drug delivery. Ther. Deliv. 7(12), 809–826 (2016).
- [8] Banik BL, Fattahi P, Brown JL. Polymeric nanoparticles: the future of nanomedicine. Wiley Interdiscip. Rev. Nanomed. Nanobiotechnol. 8(2), 271–299 (2015).
- [9] Mishra B, Chaurasia S. Design of novel chemotherapeutic delivery systems for colon cancer therapy based on oral polymeric nanoparticles. Ther. Deliv. 8(1), 29–47 (2017).
- [10] Gagliardi M, Borri C. Polymer nanoparticles as smart carriers for the enhanced release of therapeutic agents to the CNS. Curr. Pharm. Des. 23(3), 393–410 (2017).
- [11] Gagliardi M, Bardi G, Bifone A. Polymeric nanocarriers for controlled and enhanced delivery of therapeutic agents to the CNS. Ther. Deliv. 3(7), 875–887 (2012).
- [12] Morales JO, Sepulveda-Rivas S, Oyarzun-Ampuero F, Lavandero S, Kogan MJ. Novel nanostructured polymeric carriers to enable drug delivery for cardiovascular diseases. Curr. Pharm. Des. 21(29), 4276–4284 (2015).
- [13] Pullan JE, Pullan AT, Taylor VB, Brooks BD, Ewert D, Brooks AE. Energy-triggered drug release from polymer nanoparticles for orthopedic applications. Ther. Deliv. 8(1), 5–14 (2017).
- [14] Troustil J, Filippov SK, Hrubý M et al. System with embedded drug release and nanoparticle degradation sensor showing efficient rifampicin delivery into macrophages. Nanomedicine 13(1), 307–315 (2016).
- [15] Lima AC, Custódio CA, Alvarez-Lorenzo C, Mano JF. Biomimetic methodology to produce polymeric multilayered particles for biotechnological and biomedical applications. Small 9(15), 2487–2492 (2013).
- [16] Alvarez-Lorenzo C, Concheiro A. Bioinspired drug delivery systems. Curr. Opin. Biotechnol. 24(6), 1167–1173 (2013).
- [17] Lu Y, Aimetti AA, Langer R, Gu Z. Bioresponsive materials. Nat. Rev. Mater. 2(1), 16075 (2016).
- [18] Guha A, Biswas N, Bhattacharjee K, Sahoo N, Kuotsu K. pH responsive cylindrical MSN for oral delivery of insulin-design, fabrication and evaluation. Drug Deliv. 23(9), 3552–3561 (2016).
- [19] Karimi M, Sahandi Zangabad P, Ghasemi A et al. Temperature-responsive smart nanocarriers for delivery of therapeutic agents: applications and recent advances. ACS Appl. Mater. Interfaces 8(33), 21107–21133 (2016).
- [20] He S, Tourkakis G, Berezin O et al. Temperature-dependent shape-responsive fluorescent nanospheres for image-guided drug delivery. J. Mater. Chem. 4(14), 3028–3035 (2016).
- [21] Kozlovskaya V, Xue B, Kharlampieva E. Shape-adaptable polymeric particles for controlled delivery. Macromolecules 49(22), 8373–8386 (2016).

- [22] Zhang Y, Yu J, Bomba HN, Zhu Y, Gu Z. Mechanical force-triggered drug delivery. *Chem. Rev.* 116(19), 12536–12563 (2016).
- [23] Chen X, Cui J, Sun H et al. Analysing intracellular deformation of polymer capsules using structured illumination microscopy. *Nanoscale* 8(23), 11924–11931 (2016).
- [24] Cristallini C, Gagliardi M, Barbani N, Giannessi D, Guerra GD. Novel biodegradable, biomimetic and functionalised polymer scaffolds to prevent expansion of post-infarct left ventricular remodelling. *J. Mater. Sci. Mater. Med.* 23(1), 205–216 (2012).
- [25] Gagliardi M, Mazzolai B. Molecularly imprinted polymeric micro- and nano-particles for the targeted delivery of active molecules. *Future Med. Chem.* 7(2), 123–138 (2015).
- [26] Awino JK, Zhao Y. Polymeric nanoparticle receptors as synthetic antibodies for nonsteroidal anti-inflammatory drugs (NSAIDs). *ACS Biomater. Sci. Eng.* 1(6), 425–430 (2015).
- [27] Liu Y, Fang S, Zhai J, Zhao M. Construction of antibody-like nanoparticles for selective protein sequestration in living cells. *Nanoscale* 7(16), 7162–7167 (2015).
- [28] Kunath S, Panagiotopoulou M, Maximilien J, Marchyk N, Sanger J, Haupt K. Cell and tissue imaging with molecularly imprinted polymers as plastic antibody mimics. *Adv. Healthc. Mater.* 4(9), 1322–1326 (2015).
- [29] Culver HR, Steichen SD, Peppas NA. A Closer look at the impact of molecular imprinting on adsorption capacity and selectivity for protein templates. *Biomacromolecules* 17(12), 4045–4053 (2016).
- [30] Gagliardi M, Bertero A, Bifone A. Molecularly imprinted biodegradable nanoparticles. *Sci. Rep.* 7, 40046 (2017).
- [31] C.-C. Lin, A.T. Metters, Hydrogels in controlled release formulations: network de-sign and mathematical modeling, *Adv. Drug Deliv. Rev.* 58 (2006) 1379–1408.
- [32] E. Calo, V.V. Khutoryanskiy, Biomedical applications of hydrogels: a review of patents and commercial products, *Eur. Polym. J.* 65 (2015) 252–267.
- [33] R. Censi, P. Di Martino, T. Vermonden, W.E. Hennink, Hydrogels for protein delivery in tissue engineering, *J. Control. Release* 161 (2012) 680–692.
- [34] S. Liang, J. Xu, L. Weng, H. Dai, X. Zhang, L. Zhang, Protein diffusion in agarose hydrogel in situ measured by improved refractive index method, *J. Control. Release* 115 (2006) 189–196.
- [35] E.A. Moschou, N. Chopra, S.L. Khatwani, J.D. Ehrick, S.K. Deo, L.G. Bachas, S. Daunert, Stimuli-responsive Hydrogels Based on the Genetically Engineered Proteins: Actuation, Drug Delivery and Mechanical Characterization, *MRS Proceedings*, 952, 2011.
- [36] J.J. Moon, S.-H. Lee, J.L. West, Synthetic biomimetic hydrogels incorporated with Ephrin-A1 for therapeutic angiogenesis, *Biomacromolecules* 8 (2007) 42–49.
- [37] O.Z. Fisher, N.A. Peppas, Quantifying tight junction disruption caused by biomimetic pH-sensitive hydrogel drug carriers, *J. Drug Deliv. Sci. Technol.* 18 (2008) 47–50.
- [38] J.M. Anderson, A. Andukuri, D.J. Lim, H.-W. Jun, Modulating the gelation properties of self-assembling peptide amphiphiles, *ACS Nano* 3 (2009) 3447–3454.
- [39] G. Orive, M. De Castro, H.-J. Kong, R.M. Hernandez, S. Ponce, D.J. Mooney, J.L. Pedraz, Bioactive cell-hydrogel microcapsules for cell-based drug delivery, *J. Control. Release* 135 (2009) 203–210.
- [40] S. Bozzini, L. Giuliano, L. Altomare, P. Petrini, A. Bandiera, M.T. Conconi, S. Fare, M.C. Tanzi, Enzymatic cross-linking of human recombinant elastin (HELP) as biomimetic approach in vascular tissue engineering, *J. Mater. Sci. Mater. Med.* 22 (2011) 2641–2650.
- [41] S. Ravi, V.R. Krishnamurthy, J.M. Caves, C.A. Haller, E.L. Chaikof, Maleimide–thiol coupling of a bioactive peptide to an elastin-like protein polymer, *Acta Biomater.* 8 (2012) 627–635.
- [42] Y. Xue, L. Wang, Y. Shao, J. Yan, X. Chen, B. Lei, Facile and green fabrication of biomimetic gelatin–siloxane hybrid hydrogel with highly elastic properties for biomedical applications, *Chem. Eng. J.* 251 (2014) 158–164.
- [43] Y. Zhao, X. Zhang, Y. Wang, Z. Wu, J. An, Z. Lu, L. Mei, C. Li, In situ cross-linked polysaccharide hydrogel as extracellular matrix mimics for antibiotics delivery, *Carbohydr. Polym.* 105 (2014) 63–69.
- [44] S.Y. Kim, J.-S. Park, Biom mineralized hyaluronic acid/poly(vinylphosphonic acid) hydrogel for bone tissue regeneration, *J. Appl. Polym. Sci.* 131 (2014).

- [45] H.W. Huh, L. Zhao, S.Y. Kim, Biomaterialized biomimetic organic/inorganic hybrid hydrogels based on hyaluronic acid and poloxamer, *Carbohydr. Polym.* 126 (2015) 130–140.
- [46] M. Boffito, E. Gioffredi, V. Chiono, S. Calzone, E. Ranzato, S. Martinotti, G. Ciardelli, Novel polyurethane-based thermosensitive hydrogels as drug release and tissue engineering platforms: design and in vitro characterization, *Polym. Int.* 65 (2016) 756–769.
- [47] L.A. Sawicki, A.M. Kloxin, Light-mediated formation and patterning of hydrogels for cell culture applications, *J. Vis. Exp.* 115 (2016), <http://dx.doi.org/10.3791/54462>.
- [48] Sheikhpour M, Barani L, Kasaeian A. Biomimetics in drug delivery systems: A critical review. *J Control Release.* 2017 May 10;253:97-109.
- [49] H.M. Aliabadi, A. Lavasanifar, Polymeric micelles for drug delivery, *Exp. Opin. Drug Deliv.* 3 (2005) 139–162.
- [50] Z.S. Haidar, Bio-inspired/-functional colloidal core-shell polymeric-based nanosystems: technology promise in tissue engineering, *Bioimag. NanoMed. Polym.* 2 (2010) 323–352.
- [51] J.P. Xu, J. Ji, W.-D. Chen, J.C. Shen, Biomimetic Amphiphiles for Polymeric Micellar Carrier System, *Key Eng. Mater.* 288–289 (2005) 465–468.
- [52] J.-P. Xu, J. Ji, W.-D. Chen, J.-C. Shen, Novel biomimetic polymersomes as polymer therapeutics for drug delivery, *J. Control. Release* 107 (2005) 502–512.
- [53] X.-B. Xiong, H. Uludağ, A. Lavasanifar, Virus-mimetic polymeric micelles for targeted siRNA delivery, *Biomaterials* 31 (2010) 5886–5893.
- [54] G. Liu, W. Zhuang, X. Chen, A. Yin, Y. Nie, Y. Wang, Drug carrier system self-assembled from biomimetic polyphosphorycholine and biodegradable polypeptide based diblock copolymers, *Polymer* 100 (2016) 45–55.
- [55] R.E. Sallach, M. Wei, N. Biswas, V.P. Conticello, S. Lecommandoux, R.A. Dluhy, E.L. Chaikof, Micelle density regulated by a reversible switch of protein secondary structure, *J. Am. Chem. Soc.* 128 (2006) 12014–12019.
- [56] Y. Tang, Z. Liu, X. Wu, G. Liu, K. Yang, Y. Li, L. Lu, Y. Cai, Modulating structural stability and acid sensitivity of photosensitive polymer micelles simply via one-batch UV irradiation, *J. Polym. Sci. A Polym. Chem.* 50 (2012) 2878–2888.
- [57] Y.L. Jang, U.J. Yun, M.S. Lee, M.G. Kim, S. Son, K. Lee, S.Y. Chae, D.W. Lim, H.T. Kim, S.H. Kim, J.H. Jeong, Cell-penetrating peptide mimicking polymer-based combined delivery of paclitaxel and siRNA for enhanced tumor growth suppression, *Int. J. Pharm.* 434 (2012) 488–493.
- [58] X. Wang, X. Sun, G. Jiang, R. Wang, R. Hu, X. Xi, Y. Zhou, S. Wang, T. Wang, Synthesis of biomimetic hyperbranched zwitterionic polymers as targeting drug delivery carriers, *J. Appl. Polym. Sci.* 128 (2013) 3289–3294.
- [59] G. Jiang, X. Sun, Y. Ma, J. Cao, Y. Wang, R. Wang, X. Wang, S. Wang, Hyperbranched polyether surface functionalized with biomimetic zwitterionic polymers as potential drug Release carriers, *Soft Matter* 150527100759009 (2013).
- [60] M. Wu, K. Guo, H. Dong, R. Zeng, M. Tu, J. Zhao, In vitro drug release and biological evaluation of biomimetic polymeric micelles self-assembled from amphiphilic deoxycholic acid–phosphorylcholine–chitosan conjugate, *Mater. Sci. Eng. C* 45 (2014) 162–169.
- [61] C. Cordon, M. Piva, C. Melo, M. Pinhal, E. Suarez, Nanoparticles as platforms of molecular delivery in diagnosis and therapy, *OA Cancer* 1 (2) (2013 Dec 01) 15.
- [62] A. Akbarzadeh, R. Rezaei-Sadabady, S. Davaran, S.W. Joo, N. Zarghami, Y. Hanifehpour, M. Samiei, M. Kouhi, K. Nejati-Koshki, Liposome: classification, preparation, and applications, *Nanoscale Res. Lett.* 8 (2013) 102.
- [63] Y.P. Patil, S. Jadhav, Novel methods for liposome preparation, *Chem. Phys. Lipids* 177 (2014) 8–18.
- [64] R. Chandrawati, F. Caruso, Biomimetic liposome- and polymersome-based multicompartmentalized assemblies, *Langmuir* 28 (2012) 13798–13,807.
- [65] T.M. Allen, P.R. Cullis, Liposomal drug delivery systems: from concept to clinical applications, *Adv. Drug Deliv. Rev.* 65 (2013) 36–48.

- [66] E. Westhaus, P.B. Messersmith, Triggered release of calcium from lipid vesicles: a bioinspired strategy for rapid gelation of polysaccharide and protein hydrogels, *Biomaterials* 22 (2001) 453–462.
- [67] H. Sakai, H. Horinouchi, Y. Masada, S. Takeoka, E. Ikeda, M. Takaori, K. Kobayashi, E. Tsuchida, Metabolism of hemoglobin-vesicles (artificial oxygen carriers) and their influence on organ functions in a rat model, *Biomaterials* 25 (2004) 4317–4325.
- [68] J. Zhu, J. Xue, Z. Guo, R.E. Marchant, Vesicle size and stability of biomimetic liposomes from 3'-sulfo-Lewis a (SuLea) containing glycolipids, *Colloids Surf. B: Biointerfaces* 58 (2007) 242–249.
- [69] J. Zhu, J. Xue, Z. Guo, L. Zhang, R.E. Marchant, Biomimetic glycoliposomes as nanocarriers for targeting P-selectin on activated platelets, *Bioconjug. Chem.* 18 (2007) 1366–1369.
- [70] J. Gao, U. Reibetanz, S. Venkatraman, B. Neu, Biofunctionalization of polyelectrolyte microcapsules with biotinylated polyethylene glycol-grafted liposomes, *Macromol. Biosci.* 11 (2011) 1079–1087.
- [71] M. Liu, J.M.J. Fréchet, Designing dendrimers for drug delivery, *Pharm. Sci. Technol. Today* 2 (1999) 393–401.
- [72] T. Garg, O. Singh, S. Arora, R. Murthy, Dendrimer—a novel scaffold for drug delivery, *Int. J. Pharm. Sci. Rev. Res.* 7 (2011) 211–220.
- [73] S. Tripathy, M.K. Das, Dendrimers and their applications as novel drug delivery carriers, *J. Appl. Pharm. Sci.* 3 (2013) 142–149.
- [74] Y. Cheng, J. Wang, T. Rao, X. He, T. Xu, Pharmaceutical applications of dendrimers: promising nanocarriers for drug delivery, *Front. Biosci.* 13 (2007) 1447–1471.
- [75] B.K. Nanjwade, H.M. Bechra, G.K. Derkar, F.V. Manvi, V.K. Nanjwade, Dendrimers: emerging polymers for drug-delivery systems, *Eur. J. Pharm. Sci.* 38 (2009) 185–196.
- [76] W.-D. Jang, K.M. Kamruzzaman Selim, C.-H. Lee, I.-K. Kang, Bioinspired application of dendrimers: from bio-mimicry to biomedical applications, *Prog. Polym. Sci.* 34 (2009) 1–23.
- [77] C.M. Paleos, D. Tsiourvas, Z. Sideratou, L. Tziveleka, Acid- and salt-triggered multifunctional poly(propylene imine) dendrimer as a prospective drug delivery system, *Biomacromolecules* 5 (2004) 524–529.
- [78] H. Huang, C.-M. Dong, Y. Wei, Biomimetic PAMAM-poly (benzyl l-glutamate) amphiphiles with multi-armed architecture: synthesis, physical properties and self-assembled nanoparticles, *Comb. Chem. High Throughput Screen.* 10 (2007) 368–376.
- [79] P. Singh, U. Gupta, A. Asthana, N.K. Jain, Folate and folate-peg-pamamdendrimers: synthesis, characterization, and targeted anticancer drug delivery potential in tumor bearing mice, *Bioconjug. Chem.* 19 (2008) 2239–2252.
- [80] Y.E. Kurtoglu, R.S. Navath, B. Wang, S. Kannan, R. Romero, R.M. Kannan, Poly(amidoamine) dendrimer–drug conjugates with disulfide linkages for intracellular drug delivery, *Biomaterials* 30 (2009) 2112–2121.
- [81] H. Yuan, K. Luo, Y. Lai, Y. Pu, B. He, G. Wang, Y. Wu, Z. Gu, A novel poly(l-glutamic acid) dendrimer based drug delivery system with both pH-sensitive and targeting functions, *Mol. Pharm.* 7 (2010) 953–962.
- [82] S. Drotleff, U. Lungwitz, M. Breunig, A. Dennis, T. Blunk, J. Tessmar, A. Göpferich, Biomimetic polymers in pharmaceutical and biomedical sciences, *Eur. J. Pharm. Biopharm.* 58 (2004) 385–407.
- [83] Q. Jin, Y. Chen, Y. Wang, J. Ji, Zwitterionic drug nanocarriers: a biomimetic strategy for drug delivery, *Colloids Surf. B: Biointerfaces* 124 (2014) 80–86.
- [84] A.C. Lima, C.A. Custódio, C. Alvarez-Lorenzo, J.F. Mano, Biomimetic methodology to produce polymeric multilayered particles for biotechnological and biomedical applications, *Small* 9 (2013) 2487–2492.
- [85] Z. Zhang, S. Chen, S. Jiang, Dual-functional biomimetic materials: nonfouling poly(carboxybetaine) with active functional groups for protein immobilization, *Biomacromolecules* 7 (2006) 3311–3315.
- [86] R. Duncan, Designing polymer conjugates as lysosomotropic nanomedicines, *Biochem. Soc. Trans.* 35 (2007) 56–60.
- [87] A.L. Oliveira, A.J. Pedro, C.S. Arroyo, J.F. Mano, G. Rodriguez, J.S. Roman, R.L. Reis, Biomimetic Ca-P coatings incorporating bisphosphonates produced on starch-based degradable biomaterials, *J. Biomed. Mater. Res. B Appl. Biomater.* 92B (2010) 55–67.
- [88] V.H.B. Ho, N.K.H. Slater, R. Chen, pH-responsive endosomolytic pseudo-peptides for drug delivery to multicellular spheroids tumour models, *Biomaterials* 32 (2011) 2953–2958.

- [89] A.E. Ekkelenkamp, M.M.T. Jansman, K. Roelofs, J.F.J. Engbersen, J.M.J. Paulusse, Surfactant-free preparation of highly stable zwitterionic poly(amido amine) nanogels with minimal cytotoxicity, *Acta Biomater.* 30 (2016) 126–134.
- [90] A.M. Carmona-Ribeiro, Biomimetic nanoparticles: preparation, characterization and biomedical applications, *Int. J. Nanomedicine* 5 (2010) 249.
- [91] A. Bianco, K. Kostarelos, M. Prato, Applications of carbon nanotubes in drug delivery, *Curr. Opin. Chem. Biol.* 9 (2005) 674–679.
- [92] S. Kimura, Molecular assemblies as biomimetic systems and their applications, *Macromol. Biosci.* 8 (2008) 979–980.
- [93] A. Babu, A.K. Templeton, A. Munshi, R. Ramesh, Nanodrug delivery systems: a promising technology for detection, diagnosis, and treatment of cancer, *AAPS PharmSciTech* 15 (2014) 709–721.
- [94] Q. He, H. Möhwald, J. Li, Layer-by-layer assembled nanotubes as biomimetic nanoreactors for calcium carbonate deposition, *Macromol. Rapid Commun.* 30 (2009) 1538–1542.
- [95] Y. Chen, S. Song, Z. Yan, H. Fenniri, T.J. Webster, Self-assembled rosette nanotubes encapsulate and slowly release dexamethasone, *Int. J. Nanomedicine* 6 (2011) 1035–1044.
- [96] S. Song, Y. Chen, Z. Yan, H. Fenniri, T.J. Webster, Self-assembled rosette nanotubes for incorporating hydrophobic drugs in physiological environments, *Int. J. Nanomedicine* 6 (2011) 101–107.
- [97] A.P. Smith-Freshwater, G.L. Bowlin, H. Yang, A novel electrospun dendrimer-gelatin hybrid nanofiber scaffold for tissue regeneration and drug delivery, *MRS Proceedings*, Cambridge Univ Press, 2008 (1094-DD1009-1007).
- [98] J.M. Anderson, A. Andukuri, D.J. Lim, H.-W. Jun, Modulating the gelation properties of self-assembling peptide amphiphiles, *ACS Nano* 3 (2009) 3447–3454.
- [99] J.-K. Kim, J. Anderson, H.-W. Jun, M.A. Repka, S. Jo, Self-assembling peptide amphiphile-based nanofiber gel for bioresponsive cisplatin delivery, *Mol. Pharm.* 6 (2009) 978–985.
- [100] B. Palazzo, M. Iafisco, M. Laforgia, N. Margiotta, G. Natile, C.L. Bianchi, D. Walsh, S. Mann, N. Roveri, Biomimetic hydroxyapatite–drug nanocrystals as potential bone substitutes with antitumor drug delivery properties, *Adv. Funct. Mater.* 17 (2007) 2180–2188.
- [101] L. Sheikh, S. Tripathy, S. Nayar, Biomimetic matrix mediated room temperature synthesis and characterization of nano-hydroxyapatite towards targeted drug delivery, *RSC Adv.* 6 (2016) 62556–62571.
- [102] E. Byun, H. Lee, Enhanced loading efficiency and sustained release of doxorubicin from hyaluronic acid/graphene oxide composite hydrogels by a mussel-inspired catecholamine, *J. Nanosci. Nanotechnol.* 14 (2014) 7395–7401.
- [103] van Sorge NM, Doran KS. Defense at the border: the blood-brain barrier versus bacterial foreigners. *Future Microbiol.* 7(3), 383–394 (2012).
- [104] Zhang L, Gao L, Zhao L et al. Intratumoral delivery and suppression of prostate tumor growth by attenuated *Salmonella enterica* serovar typhimurium carrying plasmid-based small interfering RNAs. *Cancer Res.* 67(12), 5859–5864 (2007).
- [105] Husseiny MI, Rawson J, Kaye A et al. An oral vaccine for type 1 diabetes based on live attenuated *Salmonella*. *Vaccine* 32(20), 2300–2307 (2014).
- [106] Lautenschläger C, Schmidt C, Fischer D, Stallmach A. Drug delivery strategies in the therapy of inflammatory bowel disease. *Adv. Drug Deliv. Rev.* 71, 58–76 (2014).
- [107] Whittle JR, Lickliter JD, Gan HK et al. First in human nanotechnology doxorubicin delivery system to target epidermal growth factor receptors in recurrent glioblastoma. *J. Clin. Neurosci.* 22(12), 1889–1894 (2015).
- [108] Sahari A, Traore MA, Scharf BE, Behkam B. Directed transport of bacteria-based drug delivery vehicles: bacterial chemotaxis dominates particle shape. *Biomed. Microdevices* 16(5), 717–725 (2014).
- [109] Akin, D. et al. Bacteria-mediated delivery of nanoparticles and cargo into cells. *Nature Nanotechnol.* 2, 441–449 (2007). This was a report on a novel technique for delivering nanoparticles, which are carried on the bacterial surface.
- [110] Yoo, JW., Irvine, D., Discher, D. et al. Bio-inspired, bioengineered and biomimetic drug delivery carriers. *Nat. Rev. Drug Discov.* 10, 521–535 (2011).

- [111] Strable E, Finn MG. Chemical modification of viruses and virus-like particles. *Curr. Top. Microbiol. Immunol.* 327, 1–21 (2009).
- [112] Seow Y, Wood MJ. Biological gene delivery vehicles: beyond viral vectors. *Mol. Ther.* 17(5), 767–777 (2009).
- [113] Lee KL, Twyman RM, Fiering S, Steinmetz NF. Virus-based nanoparticles as platform technologies for modern vaccines. *Wiley Interdiscip. Rev. Nanomed. Nanobiotechnol.* 8(4), 554–578 (2016).
- [114] Garland SM, Hernandez-Avila M, Wheeler CM et al. Quadrivalent vaccine against human papillomavirus to prevent anogenital diseases. *N. Engl. J. Med.* 356(19), 1928–1943 (2007).
- [115] Wang M, Tsou T-H, Chen L-S et al. Inhibition of simian virus 40 large tumor antigen expression in human fetal glial cells by an antisense oligodeoxynucleotide delivered by the JC virus-like particle. *Hum. Gene Ther.* 15(11), 1077–1090 (2004).
- [116] Pattenden LK, Middelberg APJ, Niebert M, Lipin DI. Towards the preparative and large-scale precision manufacture of virus-like particles. *Trends Biotechnol.* 23(10), 523–529 (2005).
- [117] Wu W, Hsiao SC, Carrico ZM, Francis MB. Genome-free viral capsids as multivalent carriers for taxol delivery. *Angew. Chem. Int. Ed Engl.* 48(50), 9493–9497 (2009).
- [118] Chariou PL, Lee KL, Wen AM, Gulati NM, Stewart PL, Steinmetz NF. Detection and imaging of aggressive cancer cells using an epidermal growth factor receptor (EGFR)-targeted filamentous plant virus-based nanoparticle. *Bioconjug. Chem.* 26(2), 262–269 (2015).
- [119] Pitek AS, Jameson SA, Veliz FA, Shukla S, Steinmetz NF. Serum albumin ‘camouflage’ of plant virus based nanoparticles prevents their antibody recognition and enhances pharmacokinetics. *Biomaterials* 89, 89–97 (2016).
- [120] Hubbell, J. A., Thomas, S. N. & Swartz, M. A. Materials engineering for immunomodulation. *Nature* 462, 449–460 (2009).
- [121] Kovacsovics-Bankowski, M., Clark, K., Benacerraf, B. & Rock, K. L. Efficient major histocompatibility complex class I presentation of exogenous antigen upon phagocytosis by macrophages. *Proc. Natl Acad. Sci. USA* 90, 4942–4946 (1993).
- [122] Reis e Sousa, C. & Germain, R. N. Major histocompatibility complex class I presentation of peptides derived from soluble exogenous antigen by a subset of cells engaged in phagocytosis. *J. Exp. Med.* 182, 841–851 (1995).
- [123] Serre, K., Giraudo, L., Siret, C., Leserman, L. & Machy, P. CD4 T cell help is required for primary CD8 T cell responses to vesicular antigen delivered to dendritic cells in vivo. *Eur. J. Immunol.* 36, 1386–1397 (2006).
- [124] Harding, C. V., Collins, D. S., Slot, J. W., Geuze, H. J. & Unanue, E. R. Liposome-encapsulated antigens are processed in lysosomes, recycled, and presented to T cells. *Cell* 64, 393–401 (1991).
- [125] Shen, H. et al. Enhanced and prolonged cross-presentation following endosomal escape of exogenous antigens encapsulated in biodegradable nanoparticles. *Immunology* 117, 78–88 (2006).
- [126] Junt, T. et al. Subcapsular sinus macrophages in lymph nodes clear lymph-borne viruses and present them to antiviral B cells. *Nature* 450, 110–114 (2007).
- [127] Manolova, V. et al. Nanoparticles target distinct dendritic cell populations according to their size. *Eur. J. Immunol.* 38, 1404–1413 (2008).
- [128] Reddy, S. T. et al. Exploiting lymphatic transport and complement activation in nanoparticle vaccines. *Nature Biotech.* 25, 1159–1164 (2007).
- [129] Blander, J. M. & Medzhitov, R. Toll-dependent selection of microbial antigens for presentation by dendritic cells. *Nature* 440, 808–812 (2006).
- [130] Demento, S. L. et al. TLR9-targeted biodegradable nanoparticles as immunization vectors protect against West Nile encephalitis. *J. Immunol.* 185, 2989–2997 (2010).
- [131] Alving, C. R. & Rao, M. Lipid A and liposomes containing lipid A as antigens and adjuvants. *Vaccine* 26, 3036–3045 (2008).
- [132] Brodsky, I. E. & Monack, D. NLR-mediated control of inflammasome assembly in the host response against bacterial pathogens. *Semin. Immunol.* 21, 199–207 (2009).
- [133] Hornung, V. et al. Silica crystals and aluminum salts activate the NALP3 inflammasome through phagosomal destabilization. *Nature Immunol.* 9, 847–856 (2008).

- [134] Eisenbarth, S. C., Colegio, O. R., O'Connor, W., Sutterwala, F. S. & Flavell, R. A. Crucial role for the Nalp3 inflammasome in the immunostimulatory properties of aluminium adjuvants. *Nature* 453, 1122–1126 (2008).
- [135] Sharp, F. A. et al. Uptake of particulate vaccine adjuvants by dendritic cells activates the NALP3 inflammasome. *Proc. Natl Acad. Sci. USA* 106, 870–875 (2009).
- [136] Malyala, P., O'Hagan, D. T. & Singh, M. Enhancing the therapeutic efficacy of CpG oligonucleotides using biodegradable microparticles. *Adv. Drug Deliv. Rev.* 61, 218–225 (2009).
- [137] Xu, L. et al. Self-assembly of a virus-mimicking nanostructure system for efficient tumor-targeted gene delivery. *Hum. Gene Ther.* 13, 469–481 (2002). This study described a virus-mimetic synthetic system that resembles the structural and functional traits of a virus.
- [138] Heit, A., Schmitz, F., Haas, T., Busch, D. H. & Wagner, H. Antigen co-encapsulated with adjuvants efficiently drive protective T cell immunity. *Eur. J. Immunol.* 37, 2063–2074 (2007).
- [139] Lee, E. S., Kim, D., Youn, Y. S., Oh, K. T. & Bae, Y. H. A virus-mimetic nanogel vehicle. *Angew. Chem. Int. Ed. Engl.* 47, 2418–2421 (2008).
- [140] Geng, Y. et al. Shape effects of filaments versus spherical particles in flow and drug delivery. *Nature Nanotechnol.* 2, 249–255 (2007).
- [141] Tan S, Wu T, Zhang D, Zhang Z. Cell or Cell Membrane-Based Drug Delivery Systems. *Theranostics* 5(8), 863–881 (2015).
- [142] Magnani M, Rossi L. Approaches to erythrocyte-mediated drug delivery. *Expert Opin. Drug Deliv.* 11(5), 677–687 (2014).
- [143] Villa CH, Cines DB, Siegel DL, Muzykantov V. Erythrocytes as Carriers for Drug Delivery in Blood Transfusion and Beyond. *Transfus. Med. Rev.* 31(1), 26–35 (2017).
- [144] Su Y, Xie Z, Kim GB, Dong C, Yang J. Design strategies and applications of circulating cell-mediated drug delivery systems. *ACS Biomater. Sci. Eng.* 1(4), 201–217 (2015).
- [145] Chessa L, Leuzzi V, Plebani A et al. Intra-erythrocyte infusion of dexamethasone reduces neurological symptoms in ataxia teleangiectasia patients: results of a phase 2 trial. *Orphanet J. Rare Dis.* 9, 5 (2014).
- [146] He H, Ye J, Wang Y et al. Cell-penetrating peptides mediated encapsulation of protein therapeutics into intact red blood cells and its application. *J. Control. Release* 176, 123–132 (2014).
- [147] Muzykantov VR. Drug delivery by red blood cells: vascular carriers designed by mother nature. *Expert Opin. Drug Deliv.* 7(4), 403–427 (2010).
- [148] Villa CH, Pan DC, Zaitsev S, Cines DB, Siegel DL, Muzykantov VR. Delivery of drugs bound to erythrocytes: new avenues for an old intravascular carrier. *Ther. Deliv.* 6(7), 795–826 (2015).
- [149] Shi G, Mukthavaram R, Kesari S, Simberg D. Distearoyl anchor-painted erythrocytes with prolonged ligand retention and circulation properties in vivo. *Adv. Healthc. Mater.* 3(1), 142–148 (2014).
- [150] Shi J, Kundrat L, Pishesha N et al. Engineered red blood cells as carriers for systemic delivery of a wide array of functional probes. *Proc. Natl Acad. Sci. USA* 111(28), 10131–10136 (2014).
- [151] Villa CH, Muzykantov VR, Cines DB. The emerging role for red blood cells in haemostasis: opportunity for intervention. *ISBT Sci. Ser.* 11(Suppl. 1), 158–164 (2016).
- [152] Cremel M, Guérin N, Horand F, Banz A, Godfrin Y. Red blood cells as innovative antigen carrier to induce specific immune tolerance. *Int. J. Pharm.* 443(1–2), 39–49 (2013).
- [153] Lynch WE, Sartiano GP, Ghaffar A. Erythrocytes as carriers of chemotherapeutic agents for targeting the reticuloendothelial system. *Am. J. Hematol.* 9(3), 249–259 (1980).
- [154] Mukthavaram R, Shi G, Kesari S, Simberg D. Targeting and depletion of circulating leukocytes and cancer cells by lipophilic antibody-modified erythrocytes. *J. Control. Release* 183, 146–153 (2014).
- [155] Mitchell MJ, King MR. Leukocytes as carriers for targeted cancer drug delivery. *Expert Opin. Drug Deliv.* 12(3), 375–392 (2015).
- [156] Stuckey DW, Shah K. Stem cell-based therapies for cancer treatment: separating hope from hype. *Nat. Rev. Cancer* 14(10), 683–691 (2014).
- [157] Bagci-Onder T, Du W, Figueiredo J-L, Martinez-Quintanilla J, Shah K. Targeting breast to brain metastatic tumours with death receptor ligand expressing therapeutic stem cells. *Brain* 138(6), 1710–1721 (2015).

- [158] Li L, Wang D, Zhou J, Cheng Y, Liang T, Zhang G. Characteristics of human amniotic fluid mesenchymal stem cells and their tropism to human ovarian cancer. *PLoS One* 10(4), e0123350 (2015).
- [159] Mapara KY, Stevenson CB, Thompson RC, Ehtesham M. Stem Cells as Vehicles for the Treatment of Brain Cancer. *Neurosurg. Clin. N. Am.* 18(1), 71–80 (2007).
- [160] Young JS, Morshed RA, Kim JW, Balyasnikova IV, Ahmed AU, Lesniak MS. Advances in stem cells, induced pluripotent stem cells, and engineered cells: delivery vehicles for anti-glioma therapy. *Expert Opin. Drug Deliv.* 11(11), 1733–1746 (2014).
- [161] Shah K. Stem cell-based therapies for tumors in the brain: are we there yet? *Neuro Oncol.* 18(8), 1066–1078 (2016).
- [162] Chiotaki R, Polioudaki H, Theodoropoulos PA. Stem cell technology in breast cancer: current status and potential applications. *Stem Cells Cloning* 9, 17–29 (2016).
- [163] Kim J, Hall RR, Lesniak MS, Ahmed AU. Stem cell-based cell carrier for targeted oncolytic virotherapy: translational opportunity and open questions. *Viruses* 7(12), 6200–6217 (2015).
- [164] Aboody KS, Brown A, Rainov NG et al. Neural stem cells display extensive tropism for pathology in adult brain: evidence from intracranial gliomas. *Proc. Natl Acad. Sci. USA* 97(23), 12846–12851 (2000).
- [165] Studeny M, Marini FC, Dembinski JL et al. Mesenchymal stem cells: potential precursors for tumor stroma and targeted-delivery vehicles for anticancer agents. *J. Natl. Cancer Inst.* 96(21), 1593–1603 (2004).
- [166] Muzykantov, V. R. Drug delivery by red blood cells: vascular carriers designed by mother nature. *Expert Opin. Drug Deliv.* 7, 403–427 (2010).
- [167] Murciano, J. C. et al. Prophylactic fibrinolysis through selective dissolution of nascent clots by tPA-carrying erythrocytes. *Nature Biotech.* 21, 891–896 (2003).
- [168] Choi, M. R. et al. A cellular Trojan Horse for delivery of therapeutic nanoparticles into tumors. *Nano Lett.* 7, 3759–3765 (2007). This was the first study of photothermal therapy that used TAMs as delivery carriers of gold nanoshells.
- [169] Alizadeh, D., Zhang, L., Hwang, J., Schlupe, T. & Badie, B. Tumor-associated macrophages are predominant carriers of cyclodextrin-based nanoparticles into gliomas. *Nanomedicine* 6, 382–390 (2009).
- [170] Swiston, A. J., Gilbert, J. B., Irvine, D. J., Cohen, R. E. & Rubner, M. F. Freely suspended cellular “backpacks” lead to cell aggregate self-assembly. *Biomacromolecules* 11, 1826–1832 (2010).
- [171] Stephan, M. T., Moon, J. J., Um, S. H., Bershteyn, A. & Irvine, D. J. Therapeutic cell engineering with surface-conjugated synthetic nanoparticles. *Nature Med.* 16, 1035–1041 (2010).
- [172] Danks, M. K. et al. Tumor-targeted enzyme/prodrug therapy mediates long-term disease-free survival of mice bearing disseminated neuroblastoma. *Cancer Res.* 67, 22–25 (2007).
- [173] Roger, M. et al. Mesenchymal stem cells as cellular vehicles for delivery of nanoparticles to brain tumors. *Biomaterials* 31, 8393–8401 (2010).
- [174] Doshi, N., Zahr, A. S., Bhaskar, S., Lahann, J. & Mitragotri, S. Red blood cell-mimicking synthetic biomaterial particles. *Proc. Natl Acad. Sci. USA* 106, 21495–21499 (2009). This study described RBC-mimetic synthetic polymer particles that resemble natural RBCs in size, shape, mechanical flexibility as well as oxygen-carrying ability.
- [175] Merkel, T. J. et al. Using mechanobiological mimicry of red blood cells to extend circulation times of hydrogel microparticles. *Proc. Natl Acad. Sci. USA* 108, 586–591 (2011). This paper demonstrated that particles that possess deformability that is comparable to RBCs exhibit longer circulation times.
- [176] Tsai, R. K. & Discher, D. E. Inhibition of “self” engulfment through deactivation of myosin-II at the phagocytic synapse between human cells. *J. Cell Biol.* 180, 989–1003 (2008). This was the first study to use CD47, a ‘marker of self’, on synthetic particles to obtain resistance to phagocytosis by macrophages.
- [177] Boyer, C. & Zasadzinski, J. A. Multiple lipid compartments slow vesicle contents release in lipases and serum. *ACS Nano* 1, 176–182 (2007).
- [178] Sengupta, S. et al. Temporal targeting of tumour cells and neovasculature with a nanoscale delivery system. *Nature* 436, 568–572 (2005).
- [179] Haghgooeie, R., Toner, M. & Doyle, P. Squishy non-spherical hydrogel microparticles. *Macromol. Rapid Commun.* 31, 128–134 (2010).

- [180] Oldenborg, P. A. et al. Role of CD47 as a marker of self on red blood cells. *Science* 288, 2051–2054 (2000).
- [181] Ruoslahti, E., Bhatia, S. N. & Sailor, M. J. Targeting of drugs and nanoparticles to tumors. *J. Cell Biol.* 188, 759–768 (2010).
- [182] Yoo, J., Chambers, E. & Mitragotri, S. Factors that control the circulation time of nanoparticles in blood: challenges, solutions and future prospects. *Curr. Pharm. Des.* 16, 2298–2307 (2010).
- [183] Bertram, J. P. et al. Intravenous hemostat: nanotechnology to halt bleeding. *Sci. Transl. Med.* 1, 11ra22 (2009).
- [184] Mitragotri, S. & Lahann, J. Physical approaches to biomaterial design. *Nature Mater.* 8, 15–23 (2009).
- [185] Kisak, E. T., Coldren, B. & Zasadzinski, J. A. Nanocompartments enclosing vesicles, colloids, and macromolecules via interdigitated lipid bilayers. *Langmuir* 18, 284–288 (2002).
- [186] Kubowicz, S., Baussard, J. & Lutz, J. Multicompartment micelles formed by self-assembly of linear ABC triblock copolymers in aqueous medium. *Angew. Chem. Int. Ed. Engl.* 44, 5262–5265 (2005).
- [187] Li, Z., Kesselman, E., Talmon, Y., Hillmyer, M. A. & Lodge, T. P. Multicompartment micelles from ABC miktoarm stars in water. *Science* 306, 98–101 (2004).
- [188] Utada, A. S. et al. Monodisperse double emulsions generated from a microcapillary device. *Science* 308, 537–541 (2005).
- [189] Nie, Z., Xu, S., Seo, M., Lewis, P. C. & Kumacheva, E. Polymer particles with various shapes and morphologies produced in continuous microfluidic reactors. *J. Am. Chem. Soc.* 127, 8058–8063 (2005).
- [190] Berkland, C., Pollauf, E., Pack, D. W. & Kim, K. Uniform double-walled polymer microspheres of controllable shell thickness. *J. Control Release* 96, 101–111 (2004).
- [191] Roh, K.H., Martin, D. C. & Lahann, J. Biphasic Janus particles with nanoscale anisotropy. *Nature Mater.* 4, 759–763 (2005). This was the demonstration of a novel technique for synthesizing nanoparticles with biphasic geometry.
- [192] Bhaskar, S., Hitt, J., Chang, S.W. L. & Lahann, J. Multicompartmental microcylinders. *Angew. Chem. Int. Ed. Engl.* 48, 4589–4593 (2009).
- [193] Dendukuri, D., Gu, S. S., Pregibon, D. C., Hatton, T. A. & Doyle, P. S. Stop-flow lithography in a microfluidic device. *Lab Chip* 7, 818–828 (2007).
- [194] Dendukuri, D., Pregibon, D. C., Collins, J., Hatton, T. A. & Doyle, P. S. Continuous-flow lithography for high-throughput microparticle synthesis. *Nature Mater.* 5, 365–369 (2006).
- [195] Gagliardi M. Biomimetic and bioinspired nanoparticles for targeted drug delivery. *Therapeutic Delivery* 8 (5), 289-299 (2017).
- [196] Luk BT, Zhang L. Cell membrane-camouflaged nanoparticles for drug delivery. *J. Control. Rel.* 220(B), 600–607 (2015).
- [197] Liu A, Verwegen M, de Ruiter MV, Maassen SJ, Traulsen CH-H, Cornelissen JJLM. Protein cages as containers for gold nanoparticles. *J. Phys. Chem. B.* 120(26), 6352–6357 (2016).
- [198] Bose RJC, Lee S-H, Park H. Biofunctionalized nanoparticles: an emerging drug delivery platform for various disease treatments. *Drug Discov. Today* 21(8), 1303–1312 (2016).
- [199] Copp JA, Fang RH, Luk BT et al. Clearance of pathological antibodies using biomimetic nanoparticles. *Proc. Natl Acad. Sci. USA* 111(37), 13481–13486 (2014).
- [200] Guo Y, Wang D, Song Q et al. Erythrocyte membrane-enveloped polymeric nanoparticles as nanovaccine for induction of antitumor immunity against melanoma. *ACS Nano* 9(7), 6918–6933 (2015).
- [201] Hui L, Qin S, Yang L. Upper critical solution temperature polymer, photothermal agent, and erythrocyte membrane coating: an unexplored recipe for making drug carriers with spatiotemporally controlled cargo release. *ACS Biomater. Sci. Eng.* 2(12), 2127–2132 (2016).
- [202] Luk BT, Fang RH, Hu C-MJ et al. Safe and immunocompatible nanocarriers cloaked in RBC membranes for drug delivery to treat solid tumors. *Theranostics* 6(7), 1004–1011 (2016).
- [203] Zhou H, Fan Z, Lemons PK, Cheng H. A facile approach to functionalize cell membrane-coated nanoparticles. *Theranostics* 6(7), 1012–1022 (2016).
- [204] Wang Q, Cheng H, Peng H, Zhou H, Li PY, Langer R. Non-genetic engineering of cells for drug delivery and cell-based therapy. *Adv. Drug Deliv. Rev.* 91, 125–140 (2015).

- [205] Suk JS, Xu Q, Kim N, Hanes J, Ensign LM. PEGylation as a strategy for improving nanoparticle-based drug and gene delivery. *Adv. Drug Deliv. Rev.* 99(A), 28–51 (2016).
- [206] Hu C-MJ, Fang RH, Luk BT, Zhang L. Polymeric nanotherapeutics: clinical development and advances in stealth functionalization strategies. *Nanoscale* 6(1), 65–75 (2014).
- [207] Yang Q, Lai SK. Anti-PEG immunity: emergence, characteristics, and unaddressed questions. *Wiley Interdiscip. Rev. Nanomed. Nanobiotechnol.* 7(5), 655–677 (2015).
- [208] Lin W, Ma G, Ji F et al. Biocompatible long-circulating star carboxybetaine polymers. *J. Mater. Chem. B* 3(3), 440–448 (2015).
- [209] Ye L, Zhang Y, Yang B et al. Zwitterionic-modified starch-based stealth micelles for prolonging circulation time and reducing macrophage response. *ACS Appl. Mater. Interfaces.* 8(7), 4385–4398 (2016).
- [210] Lin W, Ma G, Wu J, Chen S. Different in vitro and in vivo behaviors between poly(carboxybetaine methacrylate) and poly(sulfobetaine methacrylate). *Colloids Surf. B Biointerfaces* 146, 888–894 (2016).
- [211] Engler AC, Ke X, Gao S et al. Hydrophilic polycarbonates: promising degradable alternatives to poly(ethylene glycol)-based stealth materials. *Macromolecules* 48(6), 1673–1678 (2015).
- [212] Bludau H, Czapar AE, Pitek AS, Shukla S, Jordan R, Steinmetz NF. POxylation as an alternative stealth coating for biomedical applications. *Eur. Polym. J.* 88, 679–688 (2017).
- [213] Qi Y, Chilkoti A. Protein-polymer conjugation-moving beyond PEGylation. *Curr. Opin. Chem. Biol.* 28, 181–193 (2015).
- [214] Lowe S, O'Brien-Simpson NM, Connal LA. Antibiofouling polymer interfaces: poly(ethylene glycol) and other promising candidates. *Polym. Chem.* 6(2), 198–212 (2015).
- [215] Meyer RA, Meyer RS, Green JJ. An automated multidimensional thin film stretching device for the generation of anisotropic polymeric micro- and nanoparticles. *J. Biomed. Mater. Res. A.* 103(8), 2747–2757 (2015).
- [216] Ju X, Wang X, Liu Z, Xie R, Wang W, Chu L. Red-blood-cell-shaped chitosan microparticles prepared by electrospraying. *Particuology* 30, 151–157 (2016).
- [217] Merkel TJ, Jones SW, Herlihy KP et al. Using mechanobiological mimicry of red blood cells to extend circulation times of hydrogel microparticles. *Proc. Natl Acad. Sci. USA* 108(2), 586–591 (2011).
- [218] Chen K, Merkel TJ, Pandya A et al. Low modulus biomimetic microgel particles with high loading of hemoglobin. *Biomacromolecules* 13(9), 2748–2759 (2012).
- [219] Hu C-MJ, Fang RH, Luk BT et al. “Marker-of-self” functionalization of nanoscale particles through a top-down cellular membrane coating approach. *Nanoscale* 5(7), 2664 (2013).
- [220] Barclay AN, Van den Berg TK. The interaction between signal regulatory protein alpha (SIRP α) and CD47: structure, function, and therapeutic target. *Annu. Rev. Immunol.* 32, 25–50 (2014).
- [221] Rao L, Xu J-H, Cai B et al. Synthetic nanoparticles camouflaged with biomimetic erythrocyte membranes for reduced reticuloendothelial system uptake. *Nanotechnology* 27(8), 085106 (2016).
- [222] Ren X, Zheng R, Fang X et al. Red blood cell membrane camouflaged magnetic nanoclusters for imaging-guided photothermal therapy. *Biomaterials* 92, 13–24 (2016).
- [223] Luk BT, Hu C-MJ, Fang RH et al. Interfacial interactions between natural RBC membranes and synthetic polymeric nanoparticles. *Nanoscale* 6(5), 2730–2737 (2014).
- [224] Parodi A, Quattrocchi N, van de Ven AL et al. Synthetic nanoparticles functionalized with biomimetic leukocyte membranes possess cell-like functions. *Nat. Nanotechnol.* 8(1), 61–68 (2013). Interesting study on biomimetic white blood cell membranecoated particles with improved targeting properties.
- [225] Hu CMJ, Fang RH, Wang KC et al. Nanoparticle biointerfacing by platelet membrane cloaking. *Nature* 526(7571), 118–121 (2015).
- [226] Palomba R, Parodi A, Evangelopoulos M et al. Biomimetic carriers mimicking leukocyte plasma membrane to increase tumor vasculature permeability. *Sci. Rep.* 6, 34422 (2016).
- [227] He W, Frueh J, Wu Z, He Q. How leukocyte cell membrane modified janus microcapsules are phagocytosed by cancer cells. *ACS Appl. Mater. Interfaces* 8(7), 4407–4415 (2016).
- [228] He W, Frueh J, Wu Z, He Q. Leucocyte membrane-coated janus microcapsules for enhanced photothermal cancer treatment. *Langmuir* 32(15), 3637–3644 (2016).

- [229] Xuan M, Shao J, Dai L, Li J, He Q. Macrophage cell membrane camouflaged au nanoshells for *in vivo* prolonged circulation life and enhanced cancer photothermal therapy. *ACS Appl. Mater. Interfaces* 8(15), 9610–9618 (2016). Very interesting study involving macrophages cellmembrane-camouflaged particles for cancer treatment.
- [230] Xuan M, Shao J, Dai L, He Q, Li J. Macrophage cell membrane camouflaged mesoporous silica nanocapsules for *in vivo* cancer therapy. *Adv. Healthc. Mater.* 4(11), 1645–1652 (2015).
- [231] Chen Z, Zhao P, Luo Z et al. Cancer cell membrane-biomimetic nanoparticles for homologous-targeting dual-modal imaging and photothermal therapy. *ACS Nano* 10(11), 10049–10057 (2016).
- [232] Fang RH, Hu C-MJ, Luk BT et al. Cancer cell membrane-coated nanoparticles for anticancer vaccination and drug delivery. *Nano Lett.* 14(4), 2181–2188 (2014). Very interesting and innovative approach to target-specific cancer cells.
- [233] Li J, Ai Y, Wang L et al. Targeted drug delivery to circulating tumor cells via platelet membrane-functionalized particles. *Biomaterials* 76, 52–65 (2016).
- [234] Li J, Sharkey CC, Wun B, Liesveld JL, King MR. Genetic engineering of platelets to neutralize circulating tumor cells. *J. Control. Release* 228, 38–47 (2016). Reports an innovative approach to reduce circulating tumor cells with a biohybrid system.
- [235] Hu Q, Qian C, Sun W et al. Engineered nanoplatelets for enhanced treatment of multiple myeloma and thrombus. *Adv. Mater.* 28(43), 9573–9580 (2016).
- [236] Bobo D, Robinson KJ, Islam J, Thurecht KJ, Corrie SR. Nanoparticle-based medicines: a review of FDA-approved materials and clinical trials to date. *Pharm. Res.* 33(10), 2373–2387 (2016). Reports an updated list of US FDA-approved materials for medical uses.
- [237] Chertow GM, Dillon M, Burke SK et al. A randomized trial of sevelamer hydrochloride (RenaGel) with and without supplemental calcium. Strategies for the control of hyperphosphatemia and hyperparathyroidism in hemodialysis patients. *Clin. Nephrol.* 51(1), 18–26 (1999).
- [238] Reid G, Kao SC, Pavlakis N et al. Clinical development of TargomiRs, a miRNA mimic-based treatment for patients with recurrent thoracic cancer. *Epigenomics* 8(8), 1079–1085 (2016).
- [239] MacDiarmid JA, Mugridge NB, Weiss JC et al. Bacterially derived 400 nm particles for encapsulation and cancer cell targeting of chemotherapeutics. *Cancer Cell* 11(5), 431–445 (2007).
- [240] MacDiarmid JA, Amaro-Mugridge NB, Madrid-Weiss J et al. Sequential treatment of drug-resistant tumors with targeted minicells containing siRNA or a cytotoxic drug. *Nat. Biotechnol.* 27(7), 643–651 (2009).
- [241] Reid G, Pel ME, Kirschner MB et al. Restoring expression of miR-16: a novel approach to therapy for malignant pleural mesothelioma. *Ann. Oncol.* 24(12), 3128–3135 (2013).

‘Eutrophication’ is Malediction or Benediction in nature – An assessment

Debaleena Ghosh, Amlan De, Phanibhusan Ghosh* and Tarun Kumar De

Department of Marine Sciences, University of Calcutta,

35 B. C. Road, Kolkata- 700019

Abstract

Eutrophication in aquatic system is the proliferation of undesirable algae excessively by the influence of enriched level of nutritional elements. It may occur naturally and anthropogenic influences. Literature survey reveals that large numbers of undesirable consequences are there in course of eutrophication which has been termed as pollution menace because of reduction of ecosystem services with increase in biomass, decrease in biodiversity, appearance of anoxic state and unhygienic situation and also fish killing. But in the present study it has been highlighted that this could be thought of as very essential phenomenon that acts as benediction of nature to the biotic life of this earth. All these adverse effects in eutrophication are favorable for the process of carbon sequestration that reduces the green house gas content in the atmosphere, keep oxygen-carbon-dioxide balance and control climate change. In anoxic state, the rate of microbial degradation of organic matter decreases sequentially, produces harmful gases to reduce the food chain such that most fraction of organic matter is not further used or decomposed by respiration but could be sequestered in sediments and may buried to produce fossil fuel in the long run. Thus this phenomenon could be ascribed as the one of the most important methods for long-term storage of carbon-dioxide or other forms of carbon to either mitigate or differ global warming for avoiding the adverse effects of climate change.

Key-words: Eutrophication, Negative effects, Positive effects, Assessment.

Introduction

Eutrophication is originated from the Greek word ‘*eutrophos*’ meaning a well-nourished condition of an ecosystem[1]. It is defined as the process of enrichment of minerals and nutrients in the aquatic systems progressively. It can also be defined as the process in which excessive growth of plant or algal bloom is there due to presence of large amount of dissolved nutrients of the elements Phosphorous (P) and Nitrogen (N) in the system [2,3]. Eutrophication is of two types, natural and cultural or anthropogenic. Natural eutrophication occurs slowly on geological time scales [4] in which nutrients are introduced by organic matter degradation and from mineral rock scavenging by the action of lichens, mosses and fungi (5). Anthropogenic or cultural eutrophication is often a much more rapid process in which nutrients are added to a water body from any of a wide variety of polluting inputs including untreated or partially treated sewage, industrial wastewater and fertilizer from farming practices containing excess nitrogen or phosphorus nutrients which, stimulate algal and aquatic plant growth.

The phenomenon, eutrophication has been considered as serious threats for its disruption in ecosystem services, could cause a great source of pollution in the aquatic systems including

freshwater, terrestrial and coastal areas [6]. The World Resources Institute has mentioned that there are 375 hypoxic coastal zones in the world, situated in coastal areas in Western Europe, the Eastern and Southern coasts of the US, and East Asia, particularly in Japan [7]. Moreover studies have also highlighted that about two thirds of USA's coastal areas and Bays are affected by this phenomenon. The United Nations Environmental Programme [8] has marked that about 146 numbers of areas in the vicinity of coast have been affected as oxygen starved zones in the world. Besides, it has also been assessed that the fish production in inland and brackish areas has reduced significantly after the cultivation only a few years due to this event. For this, concerted efforts are there to adopt the strategy to cope with this problem by means of eco-restoration for the stability of these ecosystems. The state of eutrophication experiencing a ecosystem is distinctly manifested through changes of some water quality components of biological and chemical origin [9,12]. During the literature survey on the effects of eutrophication, it has been identified that it is always and everywhere treated as pollution with harmful effects [10,11] to the society as well as to the mankind with no positive role. But, this event occurs in nature and it is true that any phenomenon occurring in nature must have some positive roles to play.

Present study is an attempt to highlight the important aspects of other phenomenon that play vital role for the protection of our immediate environment through the process of carbon sequestration by which excess green house gas in the form of CO₂ is removed and keep O₂-CO₂ balance in the atmosphere.

Maledictions:

The maledictions could be termed as pollution effects or negative effects that appear to the human society because human beings always deserve for the inherited benefits from the aquatic ecosystems. If there are any negative or harmful consequences imparted by the natural system that affect their gains then, these are subscribed as curse or maledictions. Nutritional elements may be introduced in the water bodies from various point and non-point sources (Fig1). Opportunistic algae can able to utilize the abundant nutrient by some special mechanisms [12] and proliferate extensively and sometime changes the color (Fig-2) depending on the population density of the algal components. As more plant material becomes available as a food resource, there are associated increases in invertebrates and fish species.

As the process continues, the biomass of the water body increases but biological diversity decreases [10,11]. The visible effect of eutrophication is often nuisance algal blooms that can cause substantial ecological degradation in water bodies and associated streams [7]. With more severe eutrophication, bacterial degradation of the excess biomass results in oxygen consumption, which can create a state of hypoxia at least in the bottom sediment and deeper layers of water. This anoxic environment kills off aerobic organisms (e.g. fish and invertebrates) in the water body (Fig-3). This also affects terrestrial animals, restricting their access to affected water (e.g. as drinking sources). Selection for algal and aquatic plant species that can thrive in nutrient-rich conditions can cause structural and functional disruption to entire aquatic ecosystems and their food webs, resulting in loss of habitat and species biodiversity.[10,11].



Fig-1. Point and non-point sources of nutrients pollution mixing in the aquatic system.



Fig-2. The changing of color of the aquatic systems due to various algal developments during eutrophication.

Adverse effects of eutrophication on lakes, reservoirs, rivers and coastal marine waters are as follows.

- Increased biomass of undesirable phytoplankton with severe reduction in water quality like decrease in sunlight penetration, increase in turbidity, release of cyto-toxine to kill the other algal community.
- This result in decrease in diversity of aquatic organisms and ultimately reduce the food chain.
- Biomass of macrophytic, benthic and epiphytic algae also increased abruptly.
- Disrupt normal functioning of the ecosystem.



Fig-3. Effect of eutrophication (Fish killing).

- Water becomes cloudy and decreases in water transparency, taste and odor.
- Create problems in water treatment for various colors like shade green, yellow, brown, or red due to presence of various types of algal community.
- Lack of aerial oxygen in water due to microbial degradation of dead algae.
- The incidences of fish killing increased.
- Decreases the resource values of the water bodies like aesthetic values, recreation, fishing, hunting etc.
- Produces bad odor due to anaerobic microbial degradation of organic matter producing phosphin (PH_3), ammonia (NH_3), hydrogen sulfide (H_2S) and the green house gas, methane (CH_4).

- Occurrence of health related problems.
- The aquatic systems become unhygienic.

Benedictions:

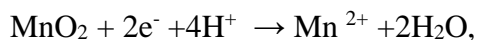
The benedictions of eutrophication could be the positive effects that are beneficial to the mankind and this chiefly happens through another natural process of carbon sequestration (CS) by which long term storage of CO₂ or other forms of carbon takes place. It has been advocated [13] that CS could be the most effective natural method to remove the excess green house gases (CO₂) either to mitigate global warming as well as climate change [14]. Major sink of carbon takes place by gradual deposition of organic matter in soil or sediments in the form of surface litter or bottom deposition in aquatic bodies and soil organic carbon pool is about 4.2 times the entire atmospheric pool and about 5.7 times the biotic pool [15].

It has been known that Eutrophication causes anoxic condition due to utilization of dissolved oxygen present in aquatic medium by microbial community for degradation of enriched organic matter and ultimately results in anaerobic condition of the system. The appearance of this state may be natural or manmade and if natural, then it must have some sorts of necessity in this natural ecosystem with some positive implication for the sustenance of biotic community on this earth. Although, during its appearance, there may have some undesirable consequences at the initial stage but it must have to overcome some stresses imparted on the ecosystem that would be relieved at the end through the attainment of dynamic equilibrium state. Because, the nature can meet all the demands necessary of survival of life but cannot quench the greed of all life forms, specially the human beings and as a result, eutrophication is known to be enhanced at a high rate by anthropogenic activities.

At this anoxic condition that appeared by natural or manmade sources, the anaerobic bacteria can sustain by taking oxygen from the oxygenated compounds present in combined form like nitrate (NO₃), manganese oxide (MnO₂), sulphate (SO₄) and carbon-dioxide (CO₂) and for this, these oxygenated compounds are termed as alternative electron acceptors[16,17]. These compounds are reduced to produce the end products like ammonia (NH₃), mangnic (Mn⁺⁴) of MnO₂ to manganus (Mn⁺²), hydrogen sulfide (H₂S) and the green house gas methane (CH₄) respectively.



This reaction occurs at a redox potential of 250 mV.



At redox potential of 225 mV,



At extreme reduced condition below the redox potential -200 mV



At this, some extra energy is used up by the microbes to avail this bound form of oxygen and these results in slow rate of organic matter degradation in comparison to the aerobic degradation process performed by aerobic or facultative bacterial community [18]. Besides, all these electron acceptors are used in a definite sequence depending on the gradual decrease in Gibbs free energy and redox potential values (16) and as a consequence, the organic matter decomposition rates also decreases as follow order..

NO_3 reduction rate > Manganese reduction rate > Ferric reduction rate > Sulphate reduction rate > CO_2 reduction rate.

The intensity of anaerobic state is usually expressed in terms of redox potential values. At the extreme redox zone, CO_2 is reduced by methane forming bacteria [20] and this rate is the slowest. These biochemical reactions are very sensitive, substrate specific and depend on any change in environmental condition [21].

From the above discussion it is clear that anaerobic state provides large amount of organic matter may be degraded or partially degraded form. There are several mineralization steps at anaerobic condition occurring sequentially with higher to lower rates of biochemical transformation. It then appears that the significance of this sequential decrease in rates is to permit sufficient time for the system. Within this period, dissolved organic matter in aquatic phase may undergo polymerization to form macro molecules and get deposited at the bottom sediment under the influence of flocculation and sedimentation [19, 22]. On the other hand, in anaerobic condition, the end products of these biochemical reactions are toxic in nature (NH_3 , H_2S etc). These toxic substances might play harmful effects to the higher trophic level organisms for their survival and ultimately may kill them. As a result, the length of food chain is reduced. At this, the respiratory loss of carbon in the form of CO_2 is minimized. All these incidents take place in order to reduce the loss of organic matter through microbial decomposition. This obviously provides opportunity to the present organic matter to accumulate and ultimately buried in the soil and may undergo digenesis by the influence of high pressure and temperature to form fossil fuel in the long run. Hence the anaerobic state might be regarded as very important natural condition which appears as a result of enrichment of organic matter or nutritional elements that eventually produce organic matter through eutrophication. This leads to natural carbon sequestration in any aquatic system. Hence, the larger the tenure of anaerobic state the more will be the removal of organic matter from the sedimentary environment. Hence, the phenomenon of eutrophication may appear to sequester the prevailing enriched source of organic production to reduce the green house gas level and control the climate change making the balance between O_2 - CO_2 cycle in nature and serve as benedictions.

Conclusion:

Eutrophication is a phenomenon of the aquatic body in which undesirable algal blooms takes place by the influence of excess amount of nutritional substances. It causes so many harmful consequences which are not at all desirable to our human society because of loss of various ecosystem services, appearance of anaerobic conditions; reduce in biodiversity, killing of

animals, unhygienic state etc. Along with this, present study emphasizes the positive roles of this phenomenon that may play as benediction of the nature on the biotic life in this earth. All those harmful effects as observed during eutrophication may create great favorable condition in the aquatic system for carbon sequestration through deposition of organic matter in bottom sediments and ultimately buried in soil to produce fossil fuel in the geologic time scale. Thus this phenomenon could be ascribed as the one of the most important methods by which long-term storage of carbon-dioxide or other forms of carbon can take place in order to either mitigate or differ the great menace of global warming and avoiding the adverse effects of climate change.

Acknowledgement:

Authors are grateful to the authority of the library of this department for providing adequate support and services during literature survey.

References:

- [1]. *"eutrophia"*, *American Heritage Dictionary of the English Language (Fifth ed.)*, Houghton Mifflin Harcourt Publishing Company, 2016, retrieved 10 March 2018.
- [2]. Hutchison, G. E. 1973. Eutrophication. *American Scienc*, 61:269-279.
- [3]. Callisto, Marcos; Molozzi, Joseline and Barbosa, José Lucena Etham .2014. "Eutrophication of Lakes" in A. A. Ansari, S. S. Gill (eds.), *Eutrophication: Causes, Consequences and Control*, Springer Science+Business Media Dordrecht. doi:10.1007/978-94-007-7814-6_5. ISBN 978-94-007-7814-6.
- [4]. Selman, Mindy (2007) *Eutrophication: An Overview of Status, Trends, Policies, and Strategies*. World Resources Institute.
- [5]. S. Mith, V. H.; Tilman, G. D and Nekola, J. C. 1999. "Eutrophication: Impacts of excess nutrient inputs on freshwater, marine, and terrestrial ecosystems". *Environmental Pollution (Barking, Essex : 1987)*. **100** (1–3): 179–196. doi:10.1016/S0269-7491(99)00091-3. PMID 15093117.
- [6]. Chislock, M.F.; Doster, E.; Zitomer, R.A.; Wilson, A.E. 2013. Eutrophication: Causes, Consequences, and Controls in Aquatic Ecosystems. *Nature Education Knowledge*. **4** (4): 10. Retrieved 10 March 2018.
- [7]. Rabalais, N. N. 2002. Nitrogen in aquatic ecosystems. *AMBIO: A Journal of the Human Environment*. **31** (2):102–112. doi:10.1579/0044-7447-31.2.102. PMID 12077998. S2CID 19172194.
- [8]. UNEP, 2006. The state of the marine environment: trends and processes, United Nations Environment Programme, The Hague, pp 28.
- [9]. Bhattacharya, S, Ghosh, P.B and Das, P.K. 2003. Understanding some physic-chemical components for estimation of eutrophication of an aquatic ecosystem, *International journal of Management & Technology*, 2(1):64-66.
- [10]. Smith, V. H. 2006. Responses of estuarine and coastal marine phytoplankton to nitrogen and phosphorus enrichment. *Limnology and Oceanography*, 51: 377-384.
- [11]. Bishop, M. J., Powers, S. P., Porter, H. J and Peterson, C. H. 2006. Benthic Biological effects of seasonal hypoxia in a eutrophic estuary. Predate rapid coastal development, *Estuarine Coastal Shelf Sciences*, 70:415-422.
- [12]. Das, P. K, Bhattacharya, S and Ghosh P.B. 2012. Method of interpretation of dissolved oxygen analysis for assessing aquatic ecosystem, 13(2):32-35.
- [13]. Adhikari, S, Bajracharya, R and Sitaula, K, 2009, " A Review of Carbon dynamics and sequestration in wetlands," *Journal of wetland ecology*, 2: 42-46.
- [14]. Hessen, D O, Agren, G I, Anderson, T R, Elser, J J and De Ruiter, P C, 2004, "Carbon sequestration in ecosystem, The role of stoichiometry", *Ecology*, 85(51) : 1179-1192.
- [15]. R. Lal, 2004, "Soil Carbon Sequestration Impacts on Global Climate Change and Food Security", *Science*, 304:11.
- [16]. Laanboek, H. J. 1990. Bacteria cycling of minerals that affect plant growth in waterlogged soil, a review, *Aquatic Botany*, 38:109-125.

- [17]. Mukherjee, S and Ghosh, P.B. 2012. Implication of anaerobic condition on carbon sequestration in wetland sediment, Proceedings of the Regional Conference of the International Network of Women Engineers & Scientists (INWES), New Delhi, India.
- [18]. Reddy, K. R and Graetz, D. A. 1988. Carbon and nitrogen dynamics in wetland soils, the Ecology and Management of Wetland, 7:307-318.
- [19] Kranck, K 1973, Flocculation of Suspended sediments in the sea, Nature, 246 :348-350.
- [20]. Ward D.M. and M. R. Winfrey. 1985, Interactions between methanogenic and sulphur reduction bacteria in sediment. Advance Aquatic Microbiology, 3: 141-179.
- [21]. Lovely D.R. and M J Clung. 1982, Intermediary metabolism of organic matter in the sediments of a eutrophic lake. Appl, Environmental Microbiology. 43:552-60.
- [22]. Reddy, K.R and Graetz, D.A. 1988, Carbon and nitrogen dynamics in wetland soils, The ecology and management of wetland, 7: 307-318.

Posterior Parietal Cortex Dysfunction is Central to Working Memory Storage and Broad Cognitive Deficits in Schizophrenia

Aniket Hazra*, Atri Panda , Priyanshu Sarkar

Department of Computer Science and Engineering (AI), Institute of Engineering and Management, Kolkata-700091

Abstract

Working memory (WM) deficiencies in patients with schizophrenia (PSZ) are thought to be caused by PFC dysfunction, but few research have looked at non-manipulated measures of WM storage. Storage capacity is more closely tied to the posterior parietal cortex (PPC) than the frontal cortex (PFC) in neurotypical people, suggesting that impairments in WM storage capacity in schizophrenia that are associated with widespread cognitive deficits may be related to neuronal activity in the PPC. While receiving fMRI, 37 PSZ and 37 matched healthy control volunteers of both sexes conducted a change detection test with varied set sizes. The assignment was created to emphasis WM storage while requiring minimal top-down management. BOLD activity correlated with the number of items kept in WM (K), as determined by task performance at a particular set size, according to whole-brain analyses. Independent of set size, K values predicted BOLD activity in the PPC, including the superior and inferior parietal lobules, intraparietal sulcus, and middle occipital gyrus, across groups. In the left PPC, whole-brain interaction analysis revealed that PSZ had much less K-dependent signal modulation than healthy control participants, a finding that could not be explained by a smaller K value range. The slope between K and PPC activation accounted for 43.4 percent of the variations in broad cognitive performance across groups. These findings suggest that PPC dysfunction is linked to WM storage abnormalities in PSZ and may play a role in schizophrenia's widespread cognitive deficiencies.

Keywords: working memory; schizophrenia; fMRI; posterior parietal cortex

Introduction

Working memory (WM) impairments are thought to be a key component of the cognitive deficiencies linked to schizophrenia. WM, on the other hand, is a complex construct that entails both short-term information storage and active modification, prioritizing, and rehearsal of that information. The majority of functional neuroimaging protocols used to investigate the basis of WM abnormalities in schizophrenia included manipulating stored content or allowing active rehearsal, integrating the storage and executive control parts of WM. The bulk of these investigations found anomalies in PFC recruitment in persons with schizophrenia (PSZ).

These PFC anomalies may indicate defective WM executive control mechanisms rather than WM storage, according to basic cognitive neuroscience research. The importance of PFC in executive control activities in healthy people is well known; fact, these functions have been proposed to explain most observations of persistent PFC activity during delayed-response task retention.

Individual variations in PFC recruitment can predict WM storage capacity, although this appears to be due to the action of top-down storage resource management systems. Intraparietal sulcus (IPS) and occipital activity patterns, on the other hand, better indicate storage capacity restrictions in general. There is significant evidence that PPC-based processes are fundamental to WM storage, regardless of whether they influence item representations or the preservation of attention over things whose attributes are represented in sensory cortex.

Pure indicators of storage capacity (the number of representations that can be retained simultaneously in WM) have been found to be significantly lower in PSZ compared to healthy control individuals (HCS) in recent years. In both PSZ and HCS, WM storage capacity predicted global cognitive skills, accounting for 40% of the between-group variation in intelligence and cognitive areas relevant to schizophrenia. These findings are based on visual change detection tasks, which stress WM storage processes (i.e., material encoding and maintenance but not manipulation) and are not favourable to verbal rehearsal tactics. A test array is offered after a brief presentation (100–200 ms) of a varied number of items, followed by a short retention interval and then a test array. Participants must indicate if the test array matches the sample array exactly or if one item has altered.

Basic cognitive neuroscience validated the PPC as a crucial factor of WM storage capacity using this paradigm. Activation of the IPS and intraoccipital sulci, but not the PFC, was linked to the amount of items kept in WM and individual variations in WM capability in fMRI investigations. These findings are supported by persistent event-related potentials (ERPs), which appear to emerge from PPC and whose size is proportional to the number of things kept in WM and asymptotes at an individual's storage capacity. In PSZ, the ERP impact is diminished. PPC dysfunction was commonly reported as part of wider network abnormalities in schizophrenia in fMRI studies utilising multiple cognitive tasks; nonetheless, PPC dysfunction has never been considered a critical component.

The goal of this work was to identify the neuroanatomical correlates of WM storage capacity deficits in schizophrenia, with PPC being a key player.

Materials and Methods

1.1 Subjects

Forty outpatients are scheduled to gather. The fourth edition of the Diagnostic and Statistical Manual of Mental Disorders (DSM-IV) This research included 41 people who met the criteria for schizophrenia or schizoaffective disorder (N 7) and 38 HCS. A best-estimate technique was used to make the diagnosis, which included information from a Structured Clinical Interview for DSM-IV (SCID) and a review of medical data. Due to significant head motion (criterion described below), data from 1 HCS and 3 PSZ were omitted from analysis, leaving N=37 per group. The demographic features of these participants are summarised in Table 1. PSZ had less years of schooling and scored worse than HCS on neuropsychological tests of cognitive functioning, including the MATRICS Consensus Cognitive Battery (MCCB), which is meant to offer an evaluation of major cognitive domains compromised in schizophrenia. Although there was a trend toward lower parental education in PSZ compared to HCS, we discovered no significant or trend associations between parental education and any of the key dependent variables, therefore this minor and insignificant variation cannot explain the results provided below.

Table 1. Demographics of Participants

	PSZ (N = 37)	HCS (N= 37)	Statistics
Age (yr)	36.3 ± 11.2	37.0 ± 11.7	$t_{(72)} = 0.25$
	(range 19 –55)	(range 21–55)	$p = 0.8$
Male/female	23:14	23:14	$\chi^2 = 0$
			$p = 1$
Black/white/other	12:21:4	14:23:0	$\chi^2 = 4.25$
			$p = 0.12$
Education (yr)	12.8 ± 2.1	15.5 ± 1.9	$t_{(72)} = 5.71$
			$p < 0.001$
Parental education (yr) ^a	13.5 ± 2.7	14.7 ± 2.6	$t_{(72)} = 1.89$
			$p = 0.062$
Estimated IQ ^{b,f}	99.5 ± 14.8	115.9 ± 8.8	$t_{(68)} = 5.54$
			$p < 0.001$
MCCB ^{c,f}	37.1 ± 12.9	53.6 ± 7.8	$t_{(68)} = 6.39$
			$p < 0.001$
WRAT 4 ^{d,f}	98.6 ± 17.0	115.1 ± 13.0	$t_{(68)} = 4.53$
			$p < 0.001$
WTAR ^{e,f}	100.2 ± 18.2	115.8 ± 7.1	$t_{(68)} = 4.61$
			$p < 0.001$

a - Average over maternal and paternal education. b- Data missing for 4 HCS. c - MATRICS Consensus Cognitive Battery Composite Score. d - Test of Broad Achievement. e - Adult Reading(Wechsler Test). f - Data missing for 4 HCS

PSZ were stably treated rehabilitants with a total score of 30.1 ± 7.1 (mean \pm SD) on the Detail Psychiatric Rating Scale (range 21 – 47), 22.7 ± 13.0 on the Scale for the Assessment of Negative Symptoms (range 2 – 58), 17.5 ± 12.4 on the Detail Negative Symptom Scale (range 0 – 65), 22.4 ± 6.5 on the Position Of Performing Scale (range 6 – 36), and an average overall global standing of 3.0 ± 0.8 on the Multidimensional Scale of Independent Functioning (range 2–5). All PSZ were on antipsychotic drug, which included 28 alternate- generation antipsychotics, 4 first- generation antipsychotics, and 5 both. Sixteen PSZ were also given antidepressants, mood stabilisers, anxiolytics, and antiparkinsonian medicines. One case was on methylphenidate, while the other was taking varenicline. Medication and doses have remained unchanged for the previous four weeks. Drug or alcohol misuse in the previous 6 months was an exclusionary factor for both PSZ and HCS, as confirmed by targeted screening questions, chart review (if available), the SCID, and urine and breathalyser tests. Color blindness was similarly exclusionary when tested with the Ishihara plates. HCS was found through internet advertising, leaflets, and word of mouth. With the exception of one participant who was on carbamazepine as a muscle relaxant, HCS had no Axis 1 or 2 diagnoses, no self-reported family history of psychosis, and were not using any psychiatric medication, according to a SCID. Participants supplied informed permission for a procedure authorised by the University of Maryland Baltimore's Institutional Review Board. Before PSZ signed the permission form, the investigator officially evaluated fundamental grasp of research expectations, hazards, and what to do if suffering discomfort or terminating participation in the presence of a witness. Everyone who took part was compensated for their time.

Procedure

On a different day prior to the MR scan, participants were agreed to and screened. They were told not to drink any caffeine on the day of the scan. Participants received task instructions and completed a short practise version of the change detection task on a desktop computer on the day of the scan. The scanner was then used to conduct the change detection job. Following the first four work blocks, an anatomy scan was collected. On a different day, neuropsychological tests and psychiatric ratings were done. Neuropsychological tests of cognitive functioning were completed within 6 months of the scan session for all participants (mean \pm SD, 55.8 ± 51.6 d), with the exception of 6 of the 74 participants (all PSZ), for whom we used test scores obtained as part of a previous study (276 to 608 d prescan) due to scheduling issues. This was judged suitable due to the observed temporal stability of neuropsychological cognitive assessments in PSZ. Within 3 months of the scan (34.7 ± 30.0 d), psychiatric scores were collected.

Task paradigm

The paradigm was initially described by Luck and Vogel (1997). Participants watched a 200 ms encoding array of 1, 2, 4, 6, or 7 squares on a black background ($\sim 1 \times 1^\circ$ viewing angle) (Fig. 1). From a palette of red, magenta, purple, blue, teal, cyan, green, olive, yellow, and white, each square was painted in a different colour at random. Verbal rehearsal attempts were complicated by the short encoding period and the fact that most of the colours could not be easily divided into easily nameable groupings. One of the squares from the encoding array returned for 2000 ms at its original place after a blank-screen delay of varied time (1100, 1650, 2200, 2750, 3300, 3850, or 4400 ms). If the colour of this test item has changed after the first presentation, make an index finger response, and if the colour remained the same, make a middle finger answer (50 percent probability). The new colour was chosen at random from the colours that were not included in the previous encoding array when the colour was altered.

A variable intertrial interval was used to separate the trials (2000, 2500, 3000, 3500, 4000, 4500, or 5000). Throughout the activity, a white fixation cross ($\sim 0.66 \times 0.66^\circ$ viewing angle) remained in the middle of the display. The cross functioned as a spatial reference point; participants were not required to maintain their gaze fixed on it. The task was presented in eight 4:56 minute runs of 35 trials each, with seven trials of each set size presented in random order. After each run, the scanner was turned off, and the researcher communicated with the subject through intercom (the participant responded by button press). The assignment took about 45 minutes to complete.

It's critical to distinguish between activity due to information storage and activity related to task difficulty, display complexity, and other factors when studying brain activity related to WM storage. We centred our studies on the amount of items actually held in WM for a given set size, abbreviated *K*, which was calculated from performance as explained below, to stress real WM storage over task demands. As set size grows, *K* rises, plateaus around an individual's WM capacity (*K*_{max}), and then falls as a subset of the array must be picked for encoding with ever higher set sizes. This results in an inverted U-shaped *K* dose–response curve in respect to set size, with many factors impacting the ascending arm (limited number of items accessible for storage), the descending arm (selection demands), and the peak region of the curve (*K*_{max}). As a result, none of these factors can account for any BOLD activity that is linearly connected to *K*. Task difficulty or selection demands, which develop with increasing set size even beyond the individual's WM capacity, have a distinct connection to set size than *K*-related signal. *K*-related variance provides a relatively pure reflection of the number of simultaneously active representations under the current task conditions, with relatively little influence of executive processes that contribute to performance indices on most other WM tasks.

Because the *K*-related signal represents real WM storage rather than task demands, utilising *K* as the regressor of interest efficiently removes confounds linked to task performance differences across groups. In other words, like in prior fMRI investigations, our regression technique revealed clusters of voxels whose BOLD activity changed linearly with participants' behaviorally evaluated *K*. Because set size was included as a regressor of no interest, all discovered signals mirrored *K* regardless of set size.

MRI

T2*-weighted BOLD effects were measured using a 3-tesla Tim Trio scanner (Siemens) that collected whole- brain EPI images (4 mm oblique [13.5°] axial slices, 128 x 128 matrix, FOV = 22 x 22 cm, TR = 2 s, TE = 27 ms, FA = 90°). Anatomical reference was given via an axial T1-weighted image (MPRAGE) (0.8 mm³ voxels, TR = 2.2 s, TE = 2.83 ms, FA = 13°).

AFNI was used to process the data. Each book was compared to a reference volume. The six motion correction factors were combined to create a composite motion index for each participant. There was no difference in these scores between HCS and PSZ ($t_{(72)} = 1.10$, $p > 0.27$). TRs with a displacement of more than 0.5 mm or a rotation of more than 0.5° relative to the preceding TR were censored from the time series. Participants having more than 304 (25%) censored TRs were eliminated from the study. This was the case for 1 HCS and 3 PSZ. There was no difference in the number of censored TRs across groups ($t_{(72)} = 0.02$, $p > 0.9$).

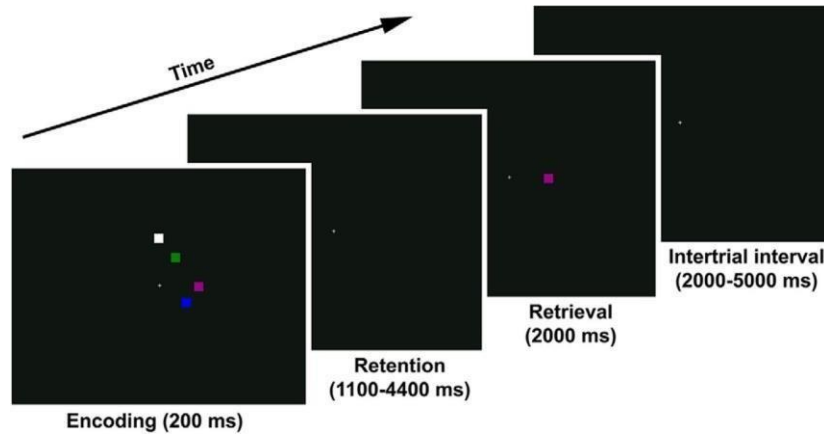


Fig 1. The task of detecting changes. Each encoding array had one, two, four, six, or seven pieces. The goal was to determine if the test item was the same colour as the encoding array's related item or had changed to a different colour. A no-change experiment at set size 4 is shown below.

First-Level Analysis

Voxelwise multiple regression was used to examine the time series as an event-related design. Convolved with a model hemodynamic response function and its temporal derivative, regressors were defined as a delta function, time-locked to the commencement of each encoding array. The five set sizes were represented by regressors (1, 2, 4, 6, and 7). The time series was analysed as a duration-modulated block design using the dmBLOCK option in AFNI, with duration indicating the length of the retention period on each trial, and very comparable findings were produced. On trials in which the participant did not reply or replied prematurely, regressors of no interest corresponded to the commencement of the retrieval array, as well as the onset of the encoding and retrieval array. The six motion parameter curves were also included as non-interesting regressors. Pearson correlations between the time history of the signal and each of the five regressors of interest and each of the six motion regressors were determined for each participant. Only 12 of the 2220 associations were significant when uncorrected, and none survived multiple comparison correction. The average correlation between stimulus-related signal and motion did not change between the two diagnostic groups ($t_{(72)} = 0.075$, $p > 0.9$). The average voxelwise amplitude of signal change caused by each of the five set sizes was calculated for each patient. These maps were resampled to a $1 \mu\text{l}$ resolution, transformed to a standard coordinate system, then blurred spatially using a Gaussian 5 mm root mean square isotropic kernel.

Second-Level Analysis

On the 370 maps, whole-brain voxelwise multiple linear regression was done (one map for each set size for each of the 74 subjects). The first study was intended to determine areas whose signal was connected to current WM storage regardless of diagnostic group membership. K , as determined from performance (see below), was the regressor of interest in this research. Group (HCS, PSZ), the group K interaction, set size (1, 2, 4, 6, 7) and subject were included in the model as uninteresting regressors. Based on Monte Carlo simulations, a voxelwise $p < 0.001$ paired with a $946\mu\text{l}$ clustersize cutoff resulted in an overall $p < 0.05$. A second whole-brain

analysis was conducted to identify locations where K-related activity varied between groups (i.e., areas in which the function relating K to BOLD activity differed between PSZ and HCS). The group K interaction was the regressor of interest in this research, with K, group, set size, and subject included in the statistical model as regressors of no interest. Based on Monte Carlo simulations, a voxelwise $p < 0.001$ coupled with a 466 μ l clustersize cutoff resulted in an overall $p < 0.05$. BOLD activity was averaged within each of the resultant clusters for each individual at each set size.

Experimental Design and Statistical Analysis

Cowan (2001) developed the formula used to transform performance into an estimate of K, and it has been verified as the model of choice for single-probe change detection tasks like the one used in this study:

$$K = \text{set size} * (\text{hit rate} - \text{false alarm rate})$$

In the absence of any WM representation, full guessing yields a K estimate of 0 according to this formula. K is largely restricted by the number of objects given in the lower set sizes (1 and 2), whereas K is mostly limited by an individual's working memory capacity in the bigger set sizes. K is also influenced by the individual's ability to pick a subset of objects for storage at specified sizes that considerably exceed capacity (6 and 7). We extract brain signal indicative of the number of items currently stored by employing K as the regressor of interest over a wide range of set sizes, regardless of the various factors that may contribute to the variance within.

Diagnostic group was a between-subject factor, and set size was a within-subject factor, in a 2-factor ANOVA for repeated measurements. The proportion of trials in which no answer was given was a supplemental performance metric. There were no reaction times reported.

Each participant's regional average BOLD activity at each set size was paired with K at this set size, and the five BOLD-K pairs were entered into a linear regression model ($\text{BOLD} = a + b \times K$) to get the slope, b, of the relationship between K and BOLD signal for each individual. This is a measure of how much the BOLD activity in that location changes in relation to the quantity of data stored in WM. All statistical analyses involving slope used nonparametric tests, such as one-sample Wilcoxon signed rank tests for comparisons against zero, Mann–Whitney U tests for group comparisons, and Spearman rho correlations to test associations with cognitive measures, due to the non-normality of the slope coefficient distribution. When utilising parametric testing, the similar pattern of findings was found.

Results

Behavioral Task Performance

In HCS and PSZ, Figure 2 shows the number of objects saved in WM (K) as a function of set size. The predicted inverted U-shaped dose–response curve was seen in both groups, with HCS and PSZ storing the most items at set size 4 (main impact of set size: $F_{(4,288)} = 27.9$, $p < 0.001$). Overall, PSZ had lower K than HCS, as evidenced by a main effect of group ($F_{(1,72)} = 535.5$, $p < 0.001$). This change was most noticeable for the three larger set sizes, resulting in a flattening of the PSZ curve (group x set size interaction: $F_{(4,288)} = 3.47$, $p = 0.009$).

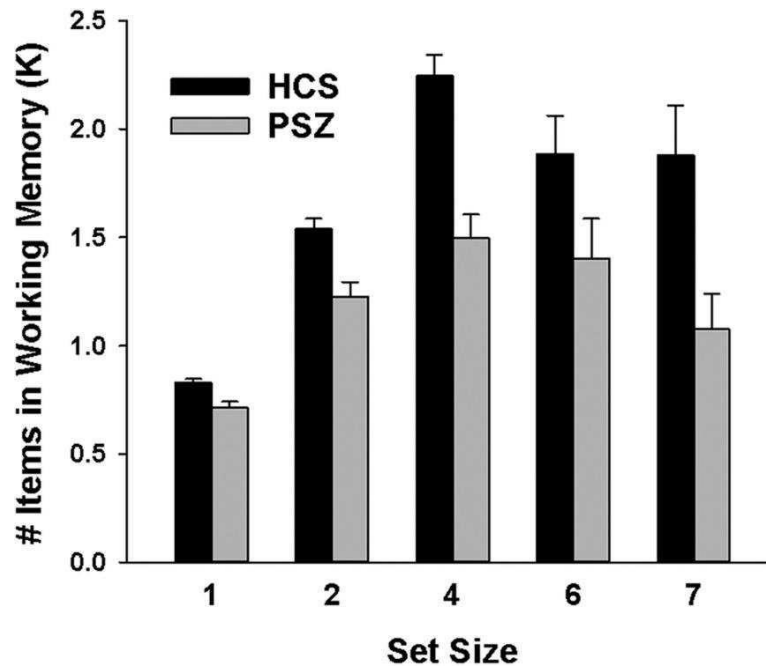


Fig 2. Task accomplishment. In patients with schizophrenia (PSZ) and healthy control participants, the mean (\pm SEM) number of items kept in working memory (K) was compared (HCS).

Overall, no-response trials were uncommon. They were unaffected by set size ($F_{(4,288)} = 1.15$, $p = 0.335$), and there was no set size-group interaction ($F_{(4,288)} = 0.72$, $p = 0.580$). However, a main effect of group ($F_{(1,72)} = 4.62$; $p = 0.035$) revealed that no-response trials were more common in PSZ ($3.3 \pm 4.2\%$) than in HCS ($1.6 \pm 2.7\%$).

1.1 MRI

1.1.1 K main effect

As a preliminary step, we wanted to see if PPC was actually crucial to WM storage mechanisms, as prior research had shown. There were three clusters that showed a linear activation shift with K across groups (Table 2; Fig. 3). On the right, the biggest cluster included many PPC areas, including the superior and inferior parietal lobules (SPL, IPL), IPS, and the middle occipital gyrus. Two distinct clusters of symmetrical left PPC and middle occipital gyrus areas were discovered. More items were kept in WM in all three clusters, indicating that they were more active (Fig. 4). These areas resemble K-related clusters discovered in prior change detection studies involving healthy young people.

Table 2. Clusters shown to have a linear activation change with items kept in working memory (K)^a

Region	Side	Volume (μ)	Center of mass (mm)		
			LR	PA	IS
Superior and inferior parietal lobule, precuneus, middle occipital gyrus	R	11718	27.5	-60.2	42.6
Superior and inferior parietal lobule, precuneus	L	7991	-24.8	-61.7	46.6
Middle occipital gyrus	L	2430	-27.8	-76.8	19.2

- LR = left-right; IS = inferior-superior.
- PA = posterior-anterior
- IS = inferior-superior.

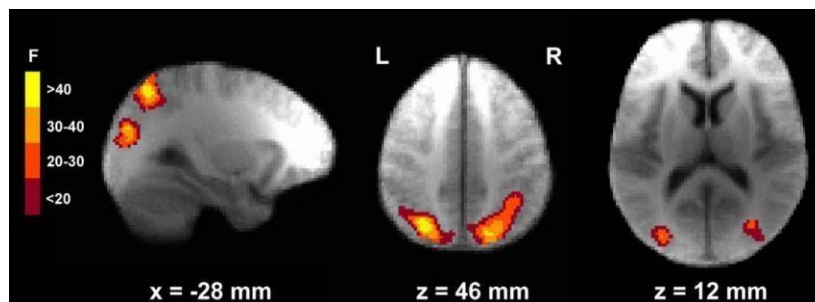


Fig 3. The K regressor found regions linked with WM storage. Clusters of voxels showing a substantial linear signal shift with the number of items kept in working memory (K), regardless of set size, are shown below. In Talairach space, group activation maps are superimposed on anatomical scans and averaged across all 74 individuals.

1.1.2 K x group interaction

A single cluster, containing SPL, IPL, and IPS, was identified as demonstrating a K group interaction in the left PPC (Table 3; Fig. 5). 94% of this region overlapped with the left PPC region, which was identified as having a K major impact in the previous section. Activation of this area rose in HCS, but not in PSZ, since more objects were kept in WM (Fig. 6). In HCS, the average slope of this relationship was substantially greater than zero ($Z = 4.34$, $p < 0.001$). PSZ slope was considerably less than HCS ($U = 364.5$, $p < 0.001$) and did not deviate from zero ($Z = 1.49$, $p = 0.14$).

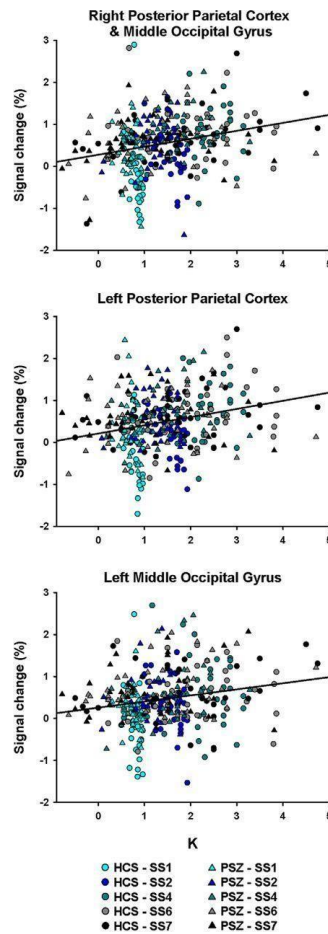


Fig 4. Change in K-dependent activation. In the three clusters shown in Figure 3 and reported in Table 2, scatter plots depict the association between K and activation. Each participant with schizophrenia (PSZ; triangles) and each healthy control subject (HCS; circle) provide five data points to each graph, one for each set size

Table 3. In HCS and PSZ, a cluster exhibiting a distinct linear activation change with K (designated as a K group interaction)

Region	Side	Volume (μ l)	Center of mass (mm)		
			LR	PA	IS
Superior and inferior parietal lobule	L	1941	23.7	61.8	45.9

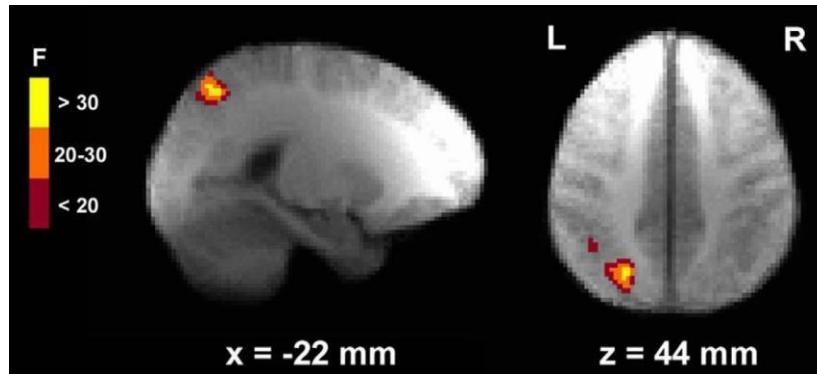


Fig 5. The $K \times$ group interaction regressor identifies the region. The left posterior parietal cortex (PPC) area illustrated here shows a difference in K -dependent signal change between healthy control subjects and schizophrenia participants. In Talairach space, group activation maps are superimposed on anatomical scans and averaged across all participants.

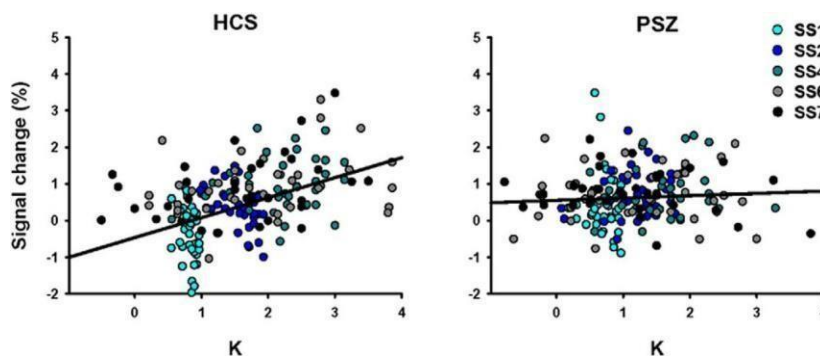


Fig 6. Differential K -BOLD correlations in schizophrenia patients and healthy control individuals (HCS) (PSZ). Scatter plots depict the association between K and activation in the left PPC area, as shown in Figure 5 and described in Table 3, for HCS and PSZ, individually. Each participant gives five data points to the graph, one for each of the five set sizes (SS).

To see if the lack of K -dependent modulation of this area in PSZ might be explained by the narrower range of K values in PSZ vs HCS, we recalculated slope values for all individuals using only K -BOLD data pairings with $K \leq 2$. Because K was always 2 for set sizes 1 and 2, all participants had at least two data pairings that met this requirement, while the majority (64 of 74) had at least three. While the variance of K values differed considerably across groups in the whole dataset ($F = 5.41$, $p < 0.021$, Levene's test), it no longer did in this sample of data pairings ($F = 0.67$, $p = 0.415$). Slopes based on the K -capped subset remained considerably greater than zero in HCS ($Z = 4.40$, $p < 0.001$) and now crossed the significance threshold in PSZ ($Z = 2.03$, $p = 0.042$), although they were still significantly smaller in PSZ than in HCS ($U = 421.0$, $p = 0.004$). This indicates that the group variation in K -BOLD slope was not caused by differences in K value ranges.

Figure 7 depicts the average BOLD signal within this area at each set size. The activation pattern across set sizes paralleled the one found with K , as predicted (Fig. 2). The greatest group difference in BOLD signal was observed at set size 1, where average PPC activity was dropped

below baseline in HCS but elevated above baseline in PSZ. This shows that failing to suppress BOLD activity at set size 1 may contribute to PSZ's flatter K-BOLD slope. To investigate this, we calculated Spearman correlations between the BOLD signal at set size 1 and the slope of the K-BOLD function and discovered a substantial negative association in both groups (HCS: $r = 0.50$, $p = 0.002$; PSZ: $r = 0.42$, $p = 0.009$). We identified only positive trends when we computed the same correlation for set size 4 (the set size with the highest average BOLD signal and K values in both groups). Thus, the steepness of the K-BOLD slope reflected the proclivity to restrict PPC activation when WM storage needs were low, at least as much as the proclivity to activate PPC when WM storage demands were high.

1.1.1 Relationship with cognition

We linked the K-BOLD slope coefficient with K at set size 4 to see if left PPC signal modulation with the amount of items presently kept in WM (K) was related to WM capacity (Kmax). Because it is least constrained by the number of items shown at small set sizes or by selection demands at big set sizes, K at set size 4 is the closest task-derived estimate of Kmax. Given that the K-related BOLD signal at set size 4 contributed to the definition of the left PPC cluster and slope coefficient, we calculated partial correlations controlling for the average regional BOLD signal at set size 4, likely underestimating the correlation but alleviating concerns about bias due to "double-dipping". HCS ($R_{(34)} = 0.41$, $p = 0.014$) and PSZ ($R_{(34)} = 0.47$, $p = 0.004$) both revealed significant partial correlations. We linked the single-participant K-BOLD slope coefficients with the MCCB composite score to see if the degree of K-dependent signal modulation in this left PPC area was predictive of broad cognitive ability (Fig. 8). Both HCS ($R_{(33)} = 0.47$, $p = 0.006$) and PSZ ($R_{(37)} = 0.38$, $p = 0.021$) had significant Spearman correlations. We also looked at exploratory correlations between the K-BOLD slope and the seven MCCB subdomains, and found that only the WM domain had significant correlations with the slope coefficient in both groups (HCS: $R_{(33)}$

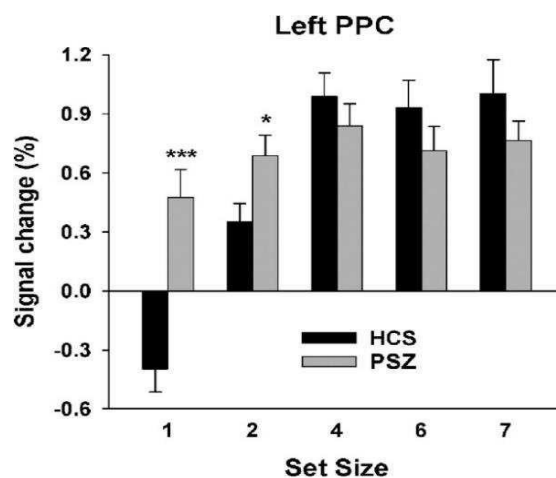


Fig 7. Set size activates the left posterior parietal cortex (PPC). BOLD activity average (SEM) for each set size in the region with a K group interaction (Fig. 5; Table 3) for healthy control subjects (HCS) and people with schizophrenia (PSZ). HCS versus PSZ independent-samples t test: *** $p < 0.001$; * $p < 0.05$

=0.43, $p = 0.01$; PSZ: $R_{(37)} = 0.41$, $p = 0.012$), though other correlations were significant in one or the other (HCS: $R_{(33)} = 0.43$, $p = 0.01$; PSZ: R (Table 4). However, because these exploratory analyses did not account for multiple comparisons, the pattern of statistical significance should be interpreted with care

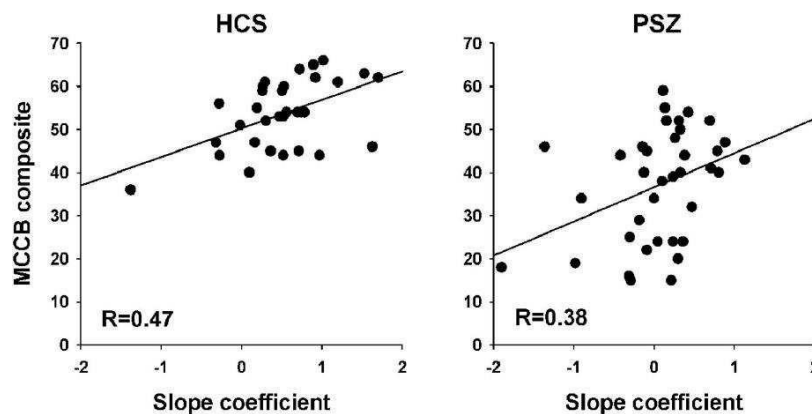


Fig 8. Correlations of slope and MCCB. The slope coefficient and the MCCB composite score in HCS and PSZ are related to the degree of K-dependent signal change in the left PPC (Fig.5; Table 3).

We used an ANCOVA model with diagnostic group as the independent variable and MCCB composite score as the dependent variable to see how much K-dependent signal change in the left PPC could explain the huge group difference in the MCCB composite (Table 1). Then, as a covariate, we included the K-BOLD slope coefficient to see how much between-group variation the coefficient might account for. The slope coefficient ($F_{(1,67)} = 13.6$, $p < 0.001$) was a significant covariate. In all models, diagnostic group was significant at $p < 0.001$; however, incorporating the slope coefficient as a covariate reduced the variation explained by the group component by 43.4%. Although causality cannot be proved based on these findings, a lack of PPC signal modulation with current WM content can statistically explain for more than 40% of the schizophrenia-related broad cognitive loss indicated by the MCCB.

1.1.2 Relationship with Medication

Antipsychotic medicines were translated to daily chlorpromazine-equivalent doses according to Andreasen et al. (2010) and associated with slope values to see if the K-BOLD slope coefficient, as the major quantitative outcome measure, may be connected to PSZ's usage of psychotropic medications. The Spearman correlation ($R_{(37)} = 0.17$, $p > 0.3$) was not significant. Furthermore, there was no difference in the slope coefficient between PSZ who used antidepressant medication ($U = 139.0$, $p > 0.3$) or PSZ who did not use anxiolytic medication ($U = 146$, $p > 0.7$).

Table 4. Correlations between the K-BOLD slope coefficient and the MCCB composite score and subscales: Spearman rho and significance levels

	HCS (N = 33) ^a	PSZ (N = 37)
MCCB composite	R = 0.47, = 0.006	R = 0.38, = 0.021
Processing speed	R = 0.33, = 0.059	R = 0.44, = 0.006
Attention/vigilance	R = 0.39, = 0.027	R = 0.26, = 0.115
Working memory	R = 0.44, = 0.010	R = 0.41, = 0.012
Verbal learning	R = 0.44, = 0.018	R = 0.11, = 0.501
Visual learning	R = 0.17, = 0.347	R = 0.34, = 0.043
Reasoning/problem solving	R = 0.09, = 0.631	R = 0.36, = 0.029
Social cognition	R = -0.03, = 0.850	R = 0.17, = 0.318

a - Four HCS do not have MCCB data.

2. Conclusion

The goal of this study was to find neuroanatomical correlates of WM storage abnormalities in PSZ using a performance-based estimation of the number of items kept in WM (K). In PSZ, WM storage capacity is significantly diminished and is closely linked with overall cognitive function. The goal was to address the neurological basis of this deficit using approaches that prioritise storage while reducing manipulation and rehearsal demands. Activity in the posterior parietal and occipital areas differed among groups in a K- dependent way, regions that were very similar to those discovered by Todd and Marois (2004, 2005) using similar techniques. There was no evidence of PFC involvement in WM storage, as in earlier investigations. This is in stark contrast to studies that used WM paradigms that required active prioritising or modification of the stored content, as well as active rehearsal.

The key conclusion of this study was that PSZ had reduced K-dependent activity modulation in the left PPC area, which included SPL, IPL, and IPS. Despite the fact that this data is correlated, there are grounds to suspect that a lack of flexible adaptation of PPC neuronal activity with the quantity of items stored in WM is a crucial mechanism explaining WM storage deficiencies in schizophrenia:

First, the combination of experimental design and analytic technique rules out the possibility that the absence of differential PPC modulation in PSZ is just a reflection of lower WM storage involvement. A shallow slope of the K-PPC signal relationship does not indicate low K, but rather less change in PPC signal as K changes. A lower average K does not always imply a lower degree of PPC signal change per unit of K change. Furthermore, the shallower K-BOLD slope in PSZ than in HCS was not due to a smaller range of K values in PSZ: slopes in PSZ were shallower than in HCS even when the study was restricted to situations with K values no greater than 2, a range in which K-related variance was matched between groups.

Second, individual variances in slope were not only due to PSZ's failure to recruit the PPC with more WM goods. Indeed, although both ends certainly contributed, there were more robust relationships between slope coefficients and activity at set size 1 than activity at set size 4. As a result, the PPC impairment in PSZ may best be defined as a lack of flexibility in activity modification in response to present WM material.

Another significant finding was that the lack of K-dependent PPC modulation predicted broad cognitive performance in both diagnostic groups and accounted for 43 % of the MCCB composite's schizophrenia-related deficiency. Previous research has found that WM storage capacity is a reliable predictor of conventional measures of fluid intelligence and general aptitude, with WM storage capacity deficits accounting for 40% of broad cognitive impairment in PSZ. The current data suggests a brain link for this possible fundamental cognitive loss, explaining a roughly equal percentage of schizophrenia-related impairment in a wide cognitive functioning test that was unrelated to our behavioral assessment of WM storage. PPC impairment, albeit understudied in this setting compared to PFC, is believed to be fundamental to cognitive difficulties linked with schizophrenia. Our findings, when taken with previous research, show that PFC and PPC are the substrates of fundamentally separate core functional deficits in schizophrenia, with a PFC site for decreased executive control of WM and a PPC location for lower storage capacity. Despite distinct underlying neuropathology, this might be true in various clinical groups with WM dysfunction.

The current study makes no judgement on whether WM representations are truly stored in PPC or if this area implements attentional processes that influence information storage in sensory cortex. The two perspectives would give distinct interpretations to the current finding. A lack of flexibility in PPC activity in relation to present WM information might indicate a faulty storing mechanism. On the other hand, the data might indicate a lack of flexibility in allocating attentional resources to representations stored in the visual cortex. Given that a K group interaction was not observed in visual cortex despite its sensitivity to the K regressor, item representations may not be degraded per se, according to this viewpoint. Instead, insufficient attentional resources may be assigned to greater numbers of representations, while an overabundance of attentional resources is allocated to smaller numbers (see overactivation in PSZ at set sizes 1 and 2). Additional study would be required to provide conclusive evidence in favour of either viewpoint.

While the task paradigm and analytical technique (with K as the regressor of interest) clearly separated activity related to WM storage (as opposed to manipulation), the current study did not aim to separate encoding-related activity from maintenance- and retrieval-related activity. The extensive retention periods required would most likely activate long-term memory and memory systems mediated by the medial temporal lobe. Reduces in a K-related posterior ERP in PSZ began during encoding and remained throughout the 800 ms maintenance interval, according to an ERP research whose paradigm and temporal parameters were very similar to those utilised here. Todd and Marois (2004) found that the PPC is involved in both encoding and maintenance, but not retrieval, employing a method identical to ours but included a substudy with longer retention intervals. Linden et al. (2003) demonstrated inverted U-shaped IPS activity with set size during encoding and the early sections of the maintenance phase, but not retrieval, using a delayed recognition test with consecutively presented abstract form stimuli and a 12 s retention gap. Bittner et al. (2015) reported set size-dependent hypoactivation of frontal, parietal, and temporal areas largely during encoding and early in the retention phase, but not

during retrieval, using the same paradigm in adolescents with schizophrenia. Retrieval-related activity was accounted for in our investigation by a different regressor of negligible interest, and so had little or no contribution to the observed signal, which is consistent with our findings.

Performance confounds are further avoided by regressing for activity related to the number of things actually represented in WM rather than the number of items on display. The issue in fMRI research comparing cognitive processes between diagnostic groups is that tasks must test the deficiencies under study, yet the ensuing performance discrepancy between groups causes unequal involvement of these systems. As a result, disparities in activation may indicate a lack of involvement by PSZ rather than a mechanism underlying the performance deficiency. Anticevic et al. (2013) used a delayed match-to-sample task to approximate performance between groups by making the two to-be-encoded stimuli for PSZ and HCS more different. PSZ revealed hypoactivation in several PFC areas, while no impact was detected in PPC. Given the extended encoding (4.4 s) and latency periods (15.4 s), variations in PFC recruitment might have been related to task set maintenance and proactive interference prevention, which affects WM paradigm performance but not the conventional change detection task performed here. Furthermore, in the Anticevic et al. (2013) investigation, the lower perceptual demands for PSZ compared to HCS may have decreased the requirement for complicated PFC-mediated encoding and maintenance techniques. A small-N research utilising a colour change detection task identical to that utilised here, with set sizes 1, 2, and 4, produced results that were more congruent with the current experiment. Prior to fMRI scanning, intensive task training was used to obtain almost identical performance between HCS and PSZ. Due to over-recruitment at set sizes 1 and 2, task-positive and, most notably, PPC areas changed less as a function of set size in PSZ under these conditions.

Although we did not examine the pathophysiological foundations of the attenuated PPC adjustment with current WM content, based on the literature on neuronal oscillation anomalies in PSZ, some hypothesis may be warranted. Raffone and Wolters (2001) used a neural network model to show that WM storage limits could be explained by a balance between synchronisation mechanisms that keep neural assemblies in a coherent oscillatory state and desynchronisation between assemblies that code for different to-be-distinguished objects or features. The neuropathology of schizophrenia is significantly overlapping with the neurobiology, allowing both fast and slow oscillatory activity, with deleterious consequences for the orchestration of both local and distant brain activity. Thus, in PPC, the decreased flexibility of WM storage-related activities might be a local manifestation of generally defective neural synchronisation mechanisms.

Finally, areas of the PPC and occipital cortex were identified as being engaged in WM storage activities utilising the task-derived number of items presently held in WM (K) as a regressor, as previously demonstrated in young healthy volunteers using comparable technique. PSZ had less K -dependent activity modulation in the left PPC, which could not be explained by a limited range of K values. K -dependent PPC modulation was found to have a strong relationship with broad cognitive ability, accounting for 43% of the schizophrenia-related loss. PPC failure, we believe, lies at the heart of WM storage abnormalities in PSZ, as well as cognitive problems associated with schizophrenia in general.

References

- [1] Andreasen NC, The Scale for the Assessment of Negative Symptoms (SANS) (1984)

- [2] Andreasen NC, Pressler M, Nopoulos P, Miller D and Ho BC, Antipsychotic dose equivalents and dose-years: a standardized method for comparing exposure to different drugs (2010)
- [3] Barch DM and Ceaser A, Cognition in schizophrenia: core psychological and neural mechanisms (2012)
- [4] Andreasen NC, The Scale for the Assessment of Negative Symptoms (SANS) (1984)
- [5] Andreasen NC, Pressler M, Nopoulos P, Miller D and Ho BC, Antipsychotic dose equivalents and dose-years: a standardized method for comparing exposure to different drugs (2010)
- [6] Barch DM and Ceaser A, Cognition in schizophrenia: core psychological and neural mechanisms (2012)
- [7] Barch DM, Moore H, Nee DE, Manoach DS and Luck SJ, CNTRICS imaging biomarkers selection: working memory (2012)
- [8] Callicott JH, Mattay VS, Verchinski BA, Marenco S, Egan MF and Weinberger DR, Complexity of prefrontal cortical dysfunction in schizophrenia: more than up or down (2003)
- [9] Cowan N, The many faces of working memory and short-term storage (2017)
- [10] Cox RW, AFNI: software for analysis and visualization of functional magnetic resonance neuroimages (1996)
- [11] Curtis CE and D'Esposito M, Persistent activity in the prefrontal cortex during working memory (2003)
- [12] Edin F, Klingberg T, Johansson P, McNab F, Tegnér J and Compte A, Mechanism for top-down control of working memory capacity (2009)
- [13] Emrich SM, Riggall AC, Larocque JJ and Postle BR, Distributed patterns of activity in sensory cortex reflect the precision of multiple items maintained in visual short-term memory (2013)
- [14] Erickson MA, Hahn B, Leonard CJ, Robinson B, Gray B, Luck SJ and Gold J, Impaired working memory capacity is not caused by failures of selective attention in schizophrenia (2015)
- [15] Glahn DC, Ragland JD, Abramoff A, Barrett J, Laird AR, Bearden CE and Velligan DI, Beyond hypofrontality: a quantitative meta-analysis of functional neuroimaging studies of working memory in schizophrenia (2005)
- [16] Hartshorne JK, Visual working memory capacity and proactive interference (2008)
- [17] Jenson A, Wixted JT, Hopkins RO and Squire LR, Visual working memory capacity and the medial temporal lobe (2012)
- [18] Kane MJ and Engle RW, Working-memory capacity, proactive interference, and divided attention: limits on long-term memory retrieval (2000)
- [19] Lee J and Park S, Working memory impairments in schizophrenia: a meta-analysis (2005)
- [20] Linden DE, The working memory networks of the human brain (2007)
- [21] Luck SJ and Vogel EK, The capacity of visual working memory for features and conjunctions (1997)
- [22] Makovski T and Jiang YV, Proactive interference from items previously stored in visual working memory (2008)
- [23] Minamoto T, Yaoi K, Osaka M and Osaka N, The rostral prefrontal cortex underlies individual differences in working memory capacity: an approach from the hierarchical model of the cognitive control (2015)
- [24] Overall J and Gorman D, The brief psychiatric rating scale (1962)
- [25] Robitaille N, Grimault S and Jolicoeur P, Bilateral parietal and contralateral responses during maintenance of unilaterally encoded objects in visual short-term memory: evidence from magnetoencephalography (2009)
- [26] Talairaque J and Tournoux P, Co-planar stereotaxic atlas of the human brain (1988)
- [27] Uhlhaas PJ and Singer W, High-frequency oscillations and the neurobiology of schizophrenia (2013)
- [28] Wechsler D, Wechsler Test of Adult Reading (WTAR) (2001)

Synthesis, antibacterial activity study, molecular docking and molecular properties prediction of new organo phosphonate derivatives

Jhonsee Rani Telu¹, Naveen Kuntala¹, Venkanna Banothu², Bala Divya Mallavarapu¹, Sarbani Pal^{3*} and Jaya Shree Anireddy^{1*}

¹Centre for Chemical Sciences and Technology, Institute of Science and Technology, Jawaharlal Nehru Technological University Hyderabad, Kukatpally, Hyderabad-500085, India

²Centre for BioTechnology, Institute of Science and Technology, Jawaharlal Nehru Technological University Hyderabad, Kukatpally, Hyderabad-500085, India

³Department of Chemistry, MNR Degree & PG College, Kukatpally, Hyderabad-500072, India

Abstract

A series of organophosphorous compounds (**3a-3m**) containing phosphonate functional group have been synthesized efficiently with high speed and good yield. All the compounds were correctly characterized using different spectroscopic techniques IR, Mass, ¹H, ¹³C and ³¹P-NMR). These compounds were screened for their antibacterial activity. All the synthesized derivatives showed good antibacterial activities. **3g** compound showed the best activity against one Gram-positive (*Staphylococcus aureus*) and two Gram-negative (*Escherichia coli* and *Klebsiella pneumoniae*) species. In order to predict binding interaction between active site of bacterial enzyme and **3g**, molecular docking was performed, into the crystal structures of DNA-gyrase cleavage complex of *S. aureus* (Gram+ve) with PDB_ID:5CDQ and the cleavage complex of topoisomerase Top. IV of *K. pneumoniae* (Gram-ve) with PDB_ID:5EIX using autodock/vina, an open source software. The molecule showed strong interaction due to H bonding, pi- pi interaction and hydrophobic interaction with active site amino acids. The synthesized compounds were also submitted to drug likeness model programs e.g molinspiration and osiris to predict bioavailability and toxicity profiles which are important for selection of the best drug candidate among all synthesized compounds. With these results we conclusively demonstrated the selected structural analogues can act as potential antibacterial agents.

Key words: Phosphonate derivatives, Antibacterial activity, Molecular docking, Molinspiration and Osiris.

1.Introduction

Phosphonates, surrogates of natural phosphates, bioisosteres of carboxylates, are one of the important classes of organic compounds presently as it has immense applications due to their fascinating biological activities such as antibacterial, antifungal, antiviral, anticancer agents, bone targeting agents and also acts as enzyme inhibitors [1][2][3][4]. Beyond medicinal chemistry organophosphonates have also other applications[5].

A number of methods have been reported for the preparation of phosphonates. The general method for the preparation of hydroxyl phosphonates and their related species is Abramov and Pudovik reaction [6][7]. The reaction of aldehydes with dialkyl phosphite in the presence of a base to give hydroxyl phosphonates as a product. The Michaelis-Arbuzov reaction is one of the essential method for the preparation of phosphonates via P-C bond formation[8][9]. It involves the reaction of an alkyl/aryl halide with dialkyl phosphite to give alkyl phosphonates. As it has been reported antibacterial activity of phosphonates we designed a series of new phosphonate derivatives and synthesized these compounds by grinding, green chemistry approach. It was time saving, extremely efficient, convenient, and eco-friendly method. Due to growing rate of bacterial resistance and increasing number of infections our health is facing biggest threat. The process of discovery of new antimicrobial agent is expensive and time consuming, directing to diminishing interest of pharmaceutical industries in it. On an average, research and development of anti-infective drugs takes around 15-20 years, and can cost more than \$1000 million. The cost of bringing a new product to the market is increasing at a rate of 10% per annum. Therefore based on urgent requirement we wanted to study anti-bacterial activity of these compounds, how effectively they bind with target by the docking analysis which in its turn depends on various parameters like H-bond donors, H-bond acceptors, molecular weight and calculated Log P (CLogP) value and Lipinski rule of five which predicts the absorption or permeation for orally active compounds. During drug development, safety is very crucial issue, including a variety of toxicities, adverse drug effects and drug -drug interaction. The computational method was used in prediction of chemical toxicity of designed molecules.

2. Materials and Methods

2.1. Chemistry

Melting points were determined by using Bio-technics melting point apparatus and open glass capillary method was followed. IR spectra were recorded on Bruker-Tensor 27 spectrometer using KBr pellets. $^1\text{H-NMR}$ and $^{13}\text{C-NMR}$ spectra were obtained using a Bruker ACF-300 machine or a Varian 300 or 400 MHz spectrometer, and the solvent CDCl_3 or DMSO-d_6 was used with tetramethylsilane as an internal reference. The ^{31}P NMR spectra were obtained using a Bruker-AVANCEIII 400 MHz spectrometer, and DMSO-d_6 was used as a solvent. The mass spectra were obtained using a Jeol JMC D-300 instrument (electron ionization at 70 eV). TLC (thin layer chromatography) on precoated silica gel plates were used to monitor the progress of reactions. Column chromatography was carried out by using silica gel (100–200 mesh, SRL, India) [10–20 times (by weight) of the crude compound.

2.1.1. General Procedure for Compounds 3a to 3d

A suspension of 1 (1.0 mmol), anhydrous magnesium chloride (0.1 g, 1.0 mmol), triethylamine (0.3 g, 3.0 mmol), and dimethyl phosphite (2, 0.136 g, 1.1 mmol) were taken in a dry mortar [10]. The mixture was ground for 10 min until a paste is obtained (TLC was used to monitor the reaction progress). Once the reaction was completed, extracted with EtOAc(3×5 ml). The organic layers were collected, combined, and evaporated under vacuum. The purification of crude compound was carried out using column chromatography on silica gel using petroleum ether/EtOAc as eluent to furnish the expected compounds (3a-3d).

2.1.2. General Procedure for Compound 3e to 3m

A mixture of azide (0.53 mmol), an appropriate terminal alkyne (0.53 mmol), CuSO₄•5H₂O (65 mg, 0.26 mmol), sodium ascorbate (52 mg, 0.26 mmol) and DMF (5 ml) were taken in a mortar. The mixture was ground for 10-15 min until a paste is obtained. The progress of the reaction was monitored by TLC. Once the reaction was completed, crushed ice was added and extracted with EtOAc (3×5 ml) using separating funnel. The organic layers were collected, combined, dried using anhydrous Na₂SO₄, filtered, and evaporated under vacuum. The purification of crude compound was carried out using column chromatography on silica gel using petroleum ether/EtOAc as eluent to furnish the expected (3e-3m).

2.2. Biology: Antibacterial activity

After preparing a small library of organo phosphonates (3a-3m) all these compounds were subjected to evaluation of their antibacterial properties against a gram-positive (*Staphylococcus aureus*) and two gram-negative (*Escherichia coli* and *Klebsiella pneumoniae*), at a concentration of 0.2 mg per 100 µl. An agar-well diffusion method was used for the assay of the test compounds [11][12]. The agar-well diffusion is a simple and widely method used test to study the susceptibility of bacteria with various compounds. If a compound inhibits the growth of bacteria, the area around the paper disc will not have bacterial growth which means that showed a halo appearance referred to as zone of inhibition. The size of zone of inhibition is dependent on the compound effectiveness to prevent the growth of the bacterium. This method was employed for the evaluation of the antibacterial activity of the given compounds. Amoxycillin and Ciproflaxacin were used as positive references at a concentration of 0.02 mg per 100 µl. DMSO was used as a negative control. The diameter of inhibition zone (DIZ) around each well was measured in mm to determine the activity of those compounds when compared with that of the reference compounds (Amoxycillin & Ciproflaxacin).

2.3. Molecular Docking Study

Molecular docking studies of molecules 3g into the crystal structures of DNA-gyrase cleavage complex of *S. aureus* (Gram-positive bacteria) with PDB_ID:5CDQ and the cleavage complex of topoisomerase Top. IV of *K. pneumonia* (Gram-negative bacteria) with PDB_ID:5EIX were carried out using Autodock Vina open source molecular docking software[13][14]. We have

generated a grid box with desired parameters around the active site of DNA-gyrase cleavage complex of *S. aureus* (PDB_ID:5CDQ) as centre: $x=40.123$, $y=-46.732$, $z=64.933$ and grid box size: $x=22$, $y=36$, $z=26$. We have generated a grid box with desired parameters around the active site of topoisomerase Top. IV of *K. pneumonia* (PDB_ID:5EIX) as centre: $x=183.18$, $y=28.952$, $z=-7.879$ and grid box size: $x=22$, $y=32$, $z=32$. We generated 20 conformations in each docking output by using advanced Genetic algorithm method in Vina. Protein/DNA complex and molecule input preparations and docking output analysis were carried out using MGLTools-1.5.6 software.

2.4. Molinspiration calculations and Drug-Likeness

Molecular properties such as partition coefficient (Log P), topological polar surface area (TPSA), hydrogen bond donors (HBD) and hydrogen bond acceptors (HBA), rotatable bonds (nrotb), number of atoms (natoms), molecular weight, and violations of Lipinski's rule of five were calculated to evaluate the drug likeness of the synthesized compounds.[15] Lipinski's rule of five filter the drug like molecules and states that a potential molecule is orally active if it's (a) molecular weight is ≤ 500 da, (b) $\log P \leq 5$, (c) number of hydrogen bond acceptors ≤ 10 , (d) number of hydrogen bond donors ≤ 5 . The logP value of a compound indicates the logarithm of its partition coefficient between n-octanol and water $\log (c \text{ octanol} / \text{water})$ used to measure the compound's hydrophilicity [16][17]. Lipophilicity is an important parameter which plays a vital role in physicochemical property in the medicinal field. Lipophilicity contributes to the ADME properties of drugs by contributing to their solubility, permeability through membranes, potency, selectivity, promiscuity, pharmacokinetics, impacting their metabolism [18]. It also affecting their pharmacodynamic and toxicological profile. Low hydrophilicities associated with high logP values which cause poor absorption or permeation. The reasonable probability of being well absorbed; if the compounds logP value must not be greater than 5.0.

2.5. Insilico bioactivity study and Osiris Toxicity Study

Molinspiration software version 2020 (<http://www.molinspiration.com>) was used to predict the bioactivity score for drug targets including enzymes, nuclear receptors, kinase inhibitors, GPCR ligands, and ion channel modulators. The bioactivity score of selected compounds were evaluated using the tool Molinspiration Cheminformatics server. In this computational method, large chemical databases are analyzed in order to identify potential new structural candidates. In the Molinspiration tool, the miscreen engine first analyze a training set of active structures (in extreme case even single active molecule is sufficient to build a usable model) and compares it with inactive molecules by using sophisticated Bayesian statistics. Only SMILES or SDfile structures of selected active molecules are sufficient for the training, no information about the active site or binding mode is necessary. The toxicity study of synthesized compounds was evaluated by using Osiris software[19]. Toxicity related risks such as (tumorigenicity, mutagenicity, irritation and reproduction effectivity) was calculated by using Osiris.

3. Results and Discussion

3.1. Synthesis of phosphonate derivatives

The designed organo phosphonates were prepared by grinding carbonyl compounds dimethylphosphite anhydrous magnesium chloride and triethylamine taken in a mortar. The mixture was subjected to grinding for 10-15 min (Fig-1) to complete as represented in scheme-1. After completion of step 1, in next step, azides having benzoxepine motif were allowed to add along with sodium ascorbate, copper sulphate penta hydrate and few drops of DMF and again allowed to grind for few min (Fig-2) to synthesize triazoles (3e-3m). Yield is reported in Table-1.

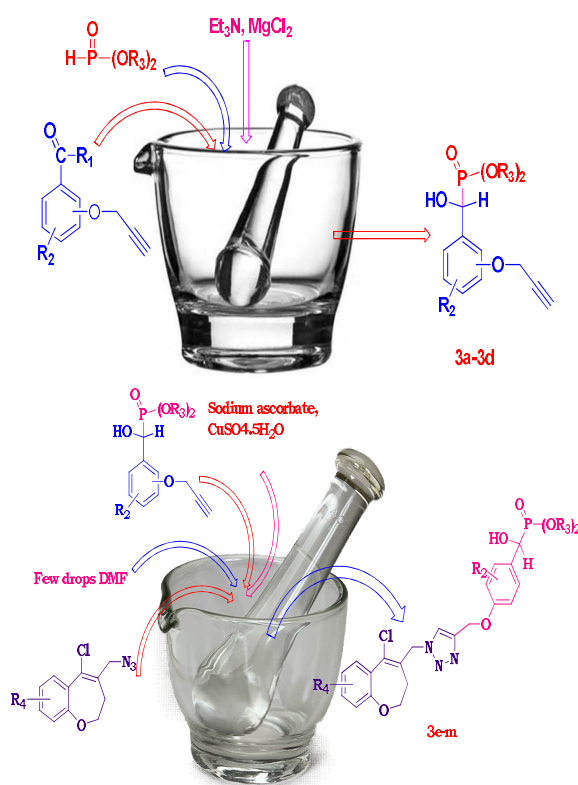


Fig 1. Synthesis of organophosphonates by grinding

Fig 2. Synthesis of benzoxepine phosphonate triazoles by grinding

Scheme -1: Synthesis of organophosphonates

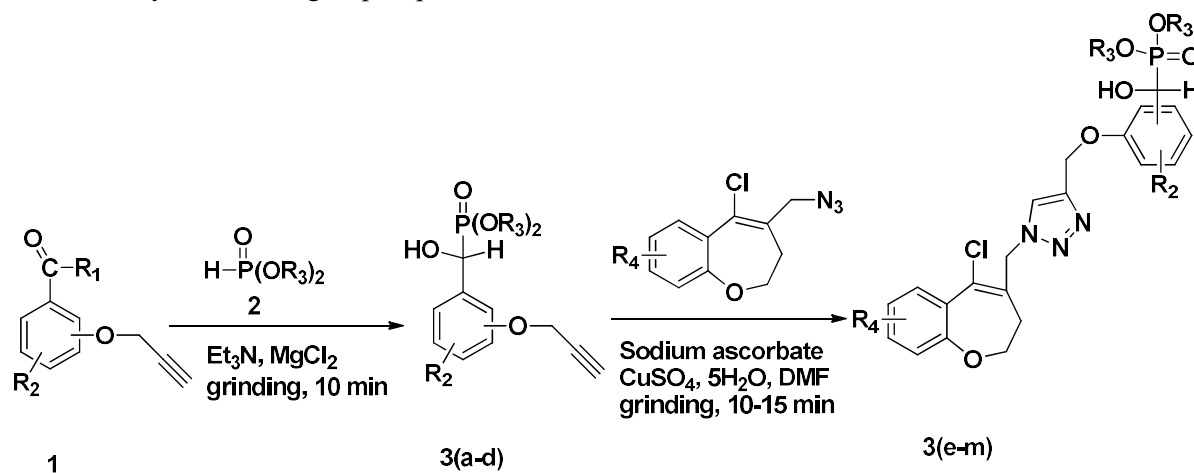


Table-1: The yield of hydroxy phosphonates 3a-3m

Code of molecules	R ₁	R ₂	R ₃	R ₄	% Yield
3a; <i>p</i> -OH	H	H	CH ₃	-	75%
3b; <i>m</i> -OH	H	H	CH ₃	-	70%
3c; <i>p</i> -OH	CH ₃	H	CH ₃	-	90%
3d; <i>p</i> -OH	H	<i>m</i> -OCH ₃	CH ₃	-	85%
3e; <i>o</i> -OH	H	H	CH ₃	<i>o</i> -CH ₃	90%
3f; <i>m</i> -OH	H	<i>p</i> -OCH ₃	CH ₃	<i>p</i> -Cl	85%
3g; <i>p</i> -OH	H	<i>m</i> -OC ₂ H ₅	C ₂ H ₅	<i>p</i> -CH ₃	90%
3h; <i>p</i> -OH	H	<i>m</i> -OC ₂ H ₅	CH ₃	<i>p</i> -Cl	75%
3i; <i>p</i> -OH	H	H	CH ₃	<i>o</i> -CH ₃	70%
3j; <i>o</i> -OH	H	H	CH ₃	<i>o</i> -Cl	90%
3k; <i>p</i> -OH	H	<i>m</i> -OCH ₃	CH ₃	-	90%
3l; <i>m</i> -OH	H	<i>o</i> -OCH ₃	C ₂ H ₅	<i>p</i> -CH ₃	85%
3m; <i>p</i> -OH	H	<i>m</i> -OC ₂ H ₅	C ₂ H ₅	<i>p</i> -Cl	90%

A total of 13 compounds were synthesized and characterized by using IR, NMR (¹H, ¹³C, ³¹P) and Mass spectrometry. The selected ¹H and ¹³C spectral data of molecule **3g** are shown in the **Fig-3** and **Fig-4**. In IR spectra, the absorption of the -OH moiety appeared in the range of 3265-3260 cm⁻¹ present in the compound. In ¹H NMR the three singlets near δ 8.30, 5.51 and 5.16 were due to the 1,2,3-triazole ring proton, NCH₂ and OCH₂ respectively. In ¹³C NMR spectrum

the signals for five methylene carbon atoms attached to oxygen appeared at δ 69.6, 68.3, 62.1, 61.5 and 55.3 ppm respectively. The signal appeared at 78.3 ppm was due to the -CH(OH)- moiety. The signal appeared at δ 51.8 ppm was due to the NCH₂ moiety. The signal appeared at δ 30.5 ppm was due to the CH₂ moiety attached to carbon of seven membered ring of benzoxepine. The presence of -PO(OC₂H₅)₂- group was further confirmed by the signal at δ 24.5 in the ³¹P NMR spectrum.

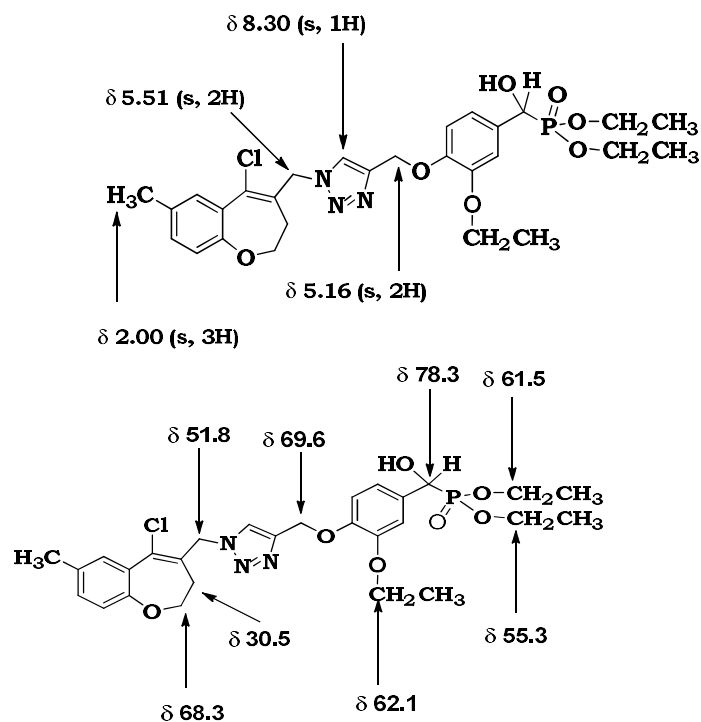


Fig 3. ¹H NMR of Compound 3g

Fig 4. ¹³C NMR of Compound 3g

3.2. Biology

Having prepared organo phosphonates (**3a-3m**), they were then evaluated for antibacterial activity against three different bacterial strains that includes one Gram-positive (*S.aureus*) and two Gram-negative (*K.pneumoniae*, *E.coli*) species. While most of the compounds showed moderate to reasonable activities against all the bacterial strains **Table-2**. Compound **3g** showed best antibacterial activity whereas **3f** and **3i** showed next level activity against all three strains. **3e**, **3f**, **3i**, **3j**, **3k** and **3m** showed good activity against *S.aureus*(+ve), **3f**, **3i** and **3l** showed good activity against *E.coli*(-ve). **3f**, **3i**, **3j**, **3k** and **3m** showed good activity against *K. pneumoniae* (-ve). In general compounds having terminal alkyne groups (**3a**, **3b**, **3c** and **3d**) showed inferior activity. The activity of all the compounds (**3a-3m**) was also influenced by position and nature of substituents as for example ethyl, methyl and chloro etc on aromatic rings.

Table 2. Antibacterial assessment of synthesized compounds using three bacterial strains.

S.No	Code of molecules	Zone of inhibition (Diameter in mm) at conc. 200 µg per 100 µl well (4 mg/500 µl DMSO)		
		<i>S. aureus</i> (G+ve)	<i>E. coli</i> (G-ve)	<i>K. pneumoniae</i> (G-ve)
1	3a	11 ± 0.31	11 ± 0.51	09 ± 0.08
2	3b	09 ± 0.13	11 ± 0.10	09 ± 0.09
3	3c	09 ± 0.12	12 ± 0.14	09 ± 0.08
4	3d	12 ± 0.13	13 ± 0.53	09 ± 0.13
5	3e	14 ± 0.19	13 ± 0.16	12 ± 0.15
6	3f	14 ± 0.23	15 ± 0.55	15 ± 0.45
7	3g	17 ± 0.31	16 ± 0.52	17 ± 0.34
8	3h	13 ± 0.19	12 ± 0.16	13 ± 0.15
9	3i	14 ± 0.25	15 ± 0.53	14 ± 0.46
10	3j	14 ± 0.32	13 ± 0.51	14 ± 0.33
11	3k	14 ± 0.32	13 ± 0.16	15 ± 0.13
12	3l	13 ± 0.14	14 ± 0.20	13 ± 0.14
13	3m	14 ± 0.32	13 ± 0.16	15 ± 0.43
14	Amoxicillin	28 ± 0.35	29 ± 0.25	31 ± 0.23
15	Ciprofloxacin	34 ± 0.51	32 ± 0.29	36 ± 0.38

3.3 Molecular Docking study

Next in order to understand host guest interaction **3g** was subjected to molecular docking. **Table-3** shows the binding affinity of **3g** molecule towards DNA-gyrase cleavage complex of *S. aureus* and topoisomerase Top. IV of *K. pneumoniae* organism's DNA binding site analysed using molecular docking studies. The binding affinities of the molecules are showing strong interaction energies with the DNA active site.

Table 3. Binding affinity of compound **3g**

Code of molecule	Binding energy (in kcal/mol)	
	3g	5CDQ
-8.40		-8.70

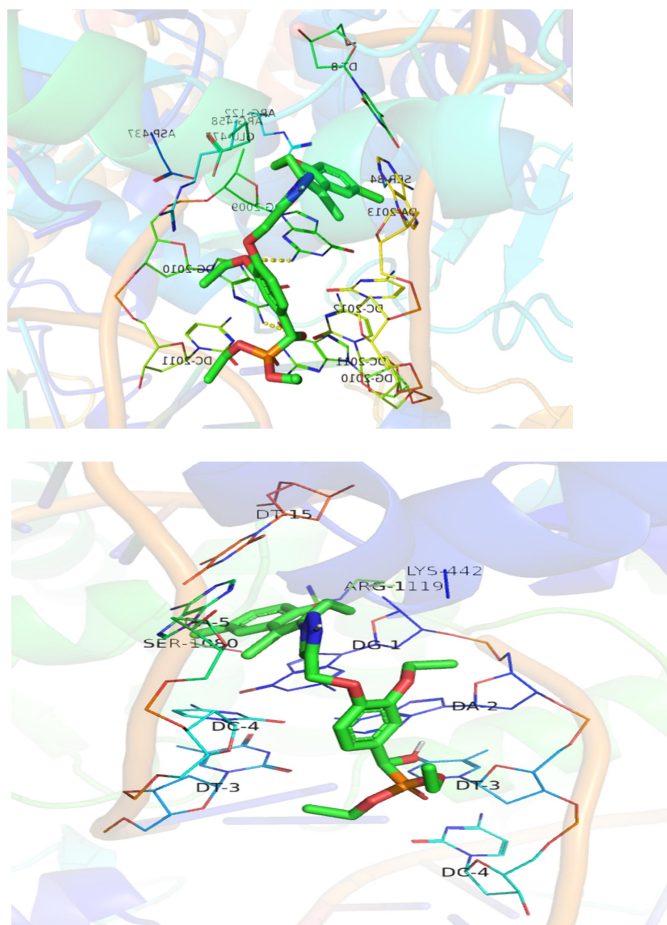


Fig 5 . Molecule **3g** docked in the active site of the DNA- active site of the topoisomerase cleavage complex of *S. aureus* (PDB_ID:5CDQ).

Fig 6. Molecule **3g** docked in the merage Top. IV of *K. pneumonia* (PDB_ID:5EIX).

Molecule **3g** was docked in the intercalation location of DNA-gyrase cleavage complex of *S. aureus* (PDB_ID:5CDQ). The ligand **3g** formed hydrogen bonding interactions between oxygen of C=O group DC2011 of chain E residue and OH group of ligand molecule. Other hydrogen bond formed with oxygen of ligand molecule and NH₂ group of DG2009 residue of chain F. This ligand benzene ring also stabilised by pi-pi interactions with chain F DG2009, chain E DA2013 and chain F DT8 residues. The interaction of DNA bases and the amino acid side-chains proteins are also shown in **Fig-5**.

The 5EIX crystal structure contains an inhibitor Levofloxacin intercalation with the E, F and I chains of DNA. The DNA binding proteins are A and G chains stabilizing the binding of the DNA with the bound Levofloxacin. The molecule **3g** was docked in the intercalation location of DNA of the topoisomerase, Top. IV complex. The molecule bound to the DNA stabilized by mainly hydrogen bonding and Pi-Pi interactions. **3g** formed hydrogen bonds with LYS442 residue from chain A and DA5 residue from chain I. On the other hand, this ligand also formed

Pi-Pi interactions between aromatic ring and DG1 residue from F chain, DT15 residue from H chain. **Fig- 6** depicts the interactions of DNA bases and the amino acid side-chains proteins.

3.4. Molinspiration calculations and Druglikeness

All the derivatives 1-13 under study have numerous hydrogen bond acceptors (≤ 6) and numerous hydrogen bond donors (≤ 1) as shown in **Table 4**. Number of rotatable bonds is an important indicator for molecular flexibility and conformational change for binding to the receptor. It reveals that the criteria for rotatable bonds should be ≤ 10 . e. TPSA of phosphonate derivatives was observed in the range of 65.0 -114.19 \AA^0 and is good below the range of 160 \AA^0 . The percentages of absorption for the given compounds calculated from TPSA ranged between 65 % and 74.23% indicated good bioavailability.

Table-4: The molinspiration values of structural analogue (**3a-3m**) compounds

S. No	Code of molecules	miLog P	TPSA	natoms	M.Wt	HBA	HBD	nviolations	nrotb	volume
1	3a	0.76	65.00	18	270.22	5	1	0	6	236.37
2	3b	0.74	65.00	18	270.22	5	1	0	6	236.37
3	3c	1.21	65.00	19	284.25	5	1	0	6	252.61
4	3d	0.35	74.23	20	300.25	6	1	0	7	261.92
5	3e	3.23	104.95	35	519.92	9	1	1	9	440.05
6	3f	3.87	114.19	39	598.42	10	1	1	12	496.17
7	3g	4.02	114.19	40	592.03	10	1	1	13	516.00
8	3h	3.50	114.19	38	584.39	10	1	1	11	479.37
9	3i	3.28	104.95	35	519.92	9	1	1	9	440.05
10	3j	3.46	104.95	35	540.34	9	1	1	9	437.02
11	3k	2.47	114.19	36	535.92	10	1	1	10	449.03
12	3l	3.64	114.19	39	578.00	10	1	1	12	499.20
13	3m	4.28	114.19	40	612.45	10	1	1	13	512.97

Note: mi LogP: logarithm of compound partition coefficient between n-octanol and water; %Abs: percentage of absorption; TPSA: topological polar surface area; MW: molecular weight; HBA: number of hydrogen bond acceptors; HBD: number of hydrogen bond donors; Nrotb: number of rotatable bonds

3.5. Insilico bioactivity study and Osiris Toxicity Study

The bioactivity scores of given compounds for drug targets were also predicted by Molinspiration and are represented in **Table 5**. Bioactivity of all selected antibacterial agents was evaluated against three different bacterial strains. Biological activity is measured by bioactivity score that are categorized under three different ranges; A molecule having bioactivity score more

than 0.00 is most likely to exhibit considerable biological activities, while values 0.50 to 0.00 are expected to be moderately active and if score is less than 0.50 it is presumed to be inactive. The results clearly reveal that the physiological actions of phosphonate derivatives might involve multiple mechanisms due to the interactions with GPCR ligands, nuclear receptor ligands, and inhibit protease and other enzymes. The bioactivity score of compounds is suggestive of moderate interaction with all drug targets Compounds **3a-3m** showed good bioactivities as enzyme inhibition (0.07-0.23 respectively). The result of this study was found that the selected agents are biologically active and the bioactivity score profile of the all selected agents is given in **Table-5**.

Table 5. Bioactivity score of the synthesized compounds (3a-3m) according to Molinspiration cheminformatics software.

S.No	Code of molecules	GPCR	ICM	KI	NRL	PI	EI
1	3a	-0.48	0.05	-0.49	-0.49	-0.24	0.22
2	3b	-0.48	0.03	-0.59	-0.49	-0.25	0.22
3	3c	-0.23	-0.09	-0.47	-0.23	0.00	0.19
4	3d	-0.38	-0.01	-0.36	-0.42	0.20	0.20
5	3e	-0.12	-0.12	-0.24	-0.18	-0.08	0.22
6	3f	-0.15	-0.29	-0.25	-0.27	-0.15	0.10
7	3g	-0.17	-0.39	-0.29	-0.29	-0.16	0.15
8	3h	-0.16	-0.23	-0.31	-0.29	-0.16	0.12
9	3i	-0.16	-0.15	-0.26	-0.22	-0.10	0.19
10	3j	-0.13	-0.10	-0.28	-0.20	-0.10	0.23
11	3k	-0.14	-0.15	-0.26	-0.28	-0.12	0.19
12	3l	-0.17	-0.34	-0.26	-0.27	-0.16	0.09
13	3m	-0.15	-0.34	-0.29	-0.30	-0.15	0.07

Note: GPCR: GPCR ligand; ICM: ion channel modulator; KI: kinase inhibitor; NRL: nuclear receptor ligand; PI: protease inhibitor; EI: enzyme inhibitor

Osiris property calculator I used mainly in drug discovery to determine the tumorigenic and mutagenic potentials of new chemical structural analogues. The toxicity risk values were predicted using the software Data warrior (Osiris) are shown as none, low and high for its mutagenic, tumorigenic, irritant, reproductive effective properties. The high risks of undesired effects like mutagenicity, tumorigenic, irritant, reproductive effective properties. Drug likeness may be defined as a complex balance of various molecular properties and structural features which determine whether a particular molecule is similar to the known drugs. The Osiris calculations for (**3a-3m**) compounds are represented in **Table-6**.

Table-6: Osiris calculations of toxicity risks and drug score of the selected compounds

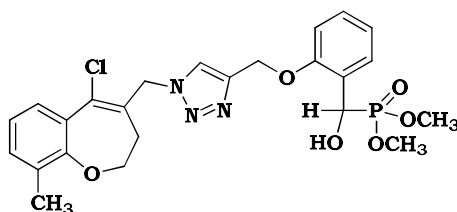
S.No	Code of molecules	Toxicity risks				Physico Chemical Properties			
		Mut	Tum	Ir	Re	cLogP	S	DL	DS
1	3a	G	G	R	R	0.74	-2.13	-28.73	0.17
2	3b	G	G	R	R	0.74	-2.13	-28.73	0.17
3	3c	G	G	R	R	0.74	-2.13	-27.03	0.17
4	3d	G	G	R	R	1.23	-3.26	-27.66	0.17
5	3e	R	G	R	R	1.23	-2.91	-27.52	0.07
6	3f	R	G	R	R	3.97	-3.92	-35.08	0.13
7	3g	R	G	G	O	4.12	-3.84	-36.78	0.13
8	3h	R	G	R	R	3.57	-3.62	-29.21	0.06
9	3i	R	G	R	R	2.97	-2.91	-27.49	0.07
10	3j	R	G	R	R	3.23	-3.30	-27.49	0.07
11	3k	R	G	R	R	2.55	-2.58	-26.60	0.07
12	3l	R	G	R	O	3.71	-3.53	-36.48	0.14
13	3m	R	G	R	O	4.38	-4.22	-35.37	0.12

MUT: mutagenic; TUM: tumourigenic; IRRIT: irritant; RE: reproductive effect. b CLP: c (logP); S: Solubility; DL: drug likeness; DS: drug score.

4. Analytical data of synthesized compounds 3e-3m.

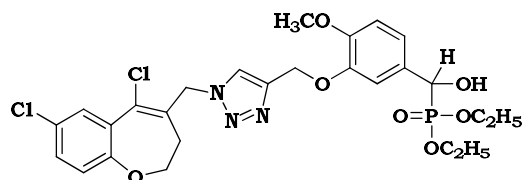
3a-3d Analytical data available on [10]

4.1 Dimethyl ((2-((1-((5-chloro-9-methyl-2,3-dihydrobenzo[b]oxepin-4-yl)methyl)-1H-1,2,3-triazol-4-yl)methoxy)phenyl)(hydroxy)methyl)phosphonate (**3e**)



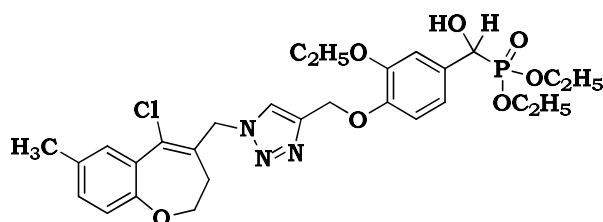
White solid; mp 124-126^oC; Rf: 0.34 (3:1 Ethyl acetate:Petroleum ether); MS m/z 520.0 (M + 1, 100%); **FTIR (KBr, ν in cm^{-1})**: 3260, 3070, 2956, 1050, 838, 729; **¹H NMR (400 MHz, CDCl₃)**: δ 7.83 (s, 1H), 7.45 (m, 2H), 7.22 (m, 1H), 7.13 (t, 1H, $J=7.78$ Hz), 7.01 (m, 3H), 5.45 (s, 2H), 5.21 (s, 2H), 4.50 (dd, 1H, $J=11.0, 4.75$ Hz), 4.27 (t, 2H, $J=6.52$ Hz), 3.74 (d, 3H, $J=10.3$ Hz), 3.65 (d, 3H, $J=10.3$ Hz), 3.21 (dd, 1H, $J=12.0, 5.30$ Hz), 2.32 (t, 2H, $J=6.30$ Hz), 2.25 (s, 3H); **¹³C NMR (CDCl₃, 100 MHz)**: δ 158.3, 153.6, 144.5, 132.4, 132.3, 130.5, 129.2, 129.3, 129.4, 129.5, 128.7, 128.7, 128.3, 123.2, 122.1, 114.8, 78.6, 70.7, 69.3, 53.8, 53.4, 52.6, 30.4, 17.3; **³¹P NMR (DMSO-d₆, 400 MHz)**: δ 23.3.

4.2 Diethyl ((3-((1-((5,7-dichloro-2,3-dihydrobenzo[b]oxepin-4-yl)methyl)-1H-1,2,3-triazol-4-yl)methoxy)-4-methoxyphenyl)(hydroxy)methyl)phosphonate (3f)



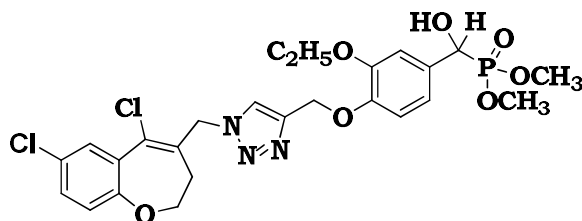
Pale yellow solid; mp 118-120⁰ C; Rf: 0.42 (3:1 Ethyl acetate:Petroleum ether); MS m/z 598.0 (M + 1, 100%); FTIR (KBr, ν in cm^{-1}): 3275, 3075, 2960, 1068, 845, 735; ¹H NMR (400 MHz, CDCl₃): δ 8.30 (s, 1H), 7.61 (d, 1H, $J=2.70$ Hz), 7.42 (dd, 1H, $J=8.52, 2.70$ Hz), 7.10 (d, 1H, $J=2.25$ Hz), 7.07 (d, 1H, $J=8.03$ Hz), 7.03 (d, 1H, $J=8.52$ Hz), 6.94 (dd, 1H, $J=8.03, 2.25$ Hz), 5.51 (s, 2H), 5.16 (s, 2H) 4.88 (dd, 1H, $J=13.0, 6.27$ Hz), 4.30 (t, 2H, $J=6.27$ Hz) 4.02-3.82 (m, 4H) 3.80 (s, 3H), 3.35 (dd, 1H, $J=12.0, 6.27$ Hz), 2.25 (t, 2H, $J=6.27$ Hz), 1.31 (t, 3H, $J=7.03$ Hz), 1.19 (t, 3H, $J=7.03$ Hz); ¹³C NMR (CDCl₃, 100 MHz): δ 153.7, 148.7, 146.6, 142.8, 134.2, 132.1, 130.5, 130.3, 128.7, 127.8, 125.9, 125.3, 124.1, 120.5, 113.4, 111.4, 78.4, 69.7, 68.1, 62.1, 62.0, 61.7, 55.4, 51.9, 30.3, 16.3; ³¹P NMR (DMSO-d₆, 400 MHz): δ 24.3.

4.3 Diethyl ((4-((1-((5-chloro-7-methyl-2,3-dihydrobenzo[b]oxepin-4-yl)methyl)-1H-1,2,3-triazol-4-yl)methoxy)-ethoxyphenyl)(hydroxy)methyl)phosphonate (3g)



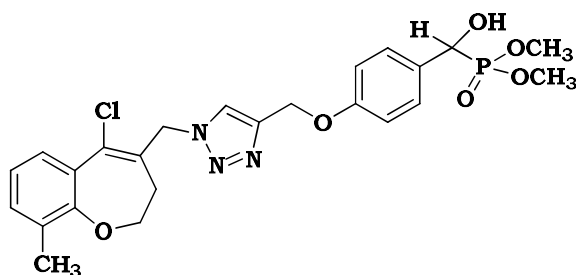
White solid; mp 118-120⁰C; Rf: 0.34 (3:1 Ethyl acetate:Petroleum ether); MS m/z 592.0 (M + 1, 100%); FTIR (KBr, ν in cm^{-1}): 3280, 3080, 2958, 1072, 846, 736; ¹H NMR (400 MHz, CDCl₃): δ 8.30 (s, 1H), 7.61 (d, 1H, $J=2.70$ Hz), 7.42 (dd, 1H, $J=8.52, 2.51$ Hz), 7.10 (d, 1H, $J=8.52$ Hz), 7.07 (d, 1H, $J=8.03$ Hz), 7.03 (t, 1H, $J=2.00$ Hz), 6.94 (dt, 1H, $J=6.52, 2.25$ Hz), 6.11 (dd, 1H, $J=15.5, 6.03$ Hz), 5.51 (s, 2H), 5.16 (s, 2H) 4.88 (dd, 1H, $J=13.0, 6.27$ Hz), 4.30 (t, 2H, $J=6.27$ Hz) 4.02-3.82 (m, 4H) 3.35 (s, 2H), 2.25 (t, 2H, $J=6.27$ Hz), 2.00 (s, 3H), 1.31 (t, 3H, $J=7.03$ Hz), 1.19 (t, 3H, $J=7.03$ Hz), 1.12 (t, 3H, $J=7.03$ Hz); ¹³C NMR (CDCl₃, 100 MHz): δ 153.6, 148.7, 146.5, 142.6, 134.5, 132.3, 130.4, 130.5, 128.6, 127.7, 125.8, 125.2, 124.3, 120.4, 113.3, 111.5, 78.3, 69.6, 68.3, 62.1, 61.5, 55.3, 51.8, 30.5, 17.7, 16.8, 16.3, 15.3; ³¹P NMR (DMSO-d₆, 400 MHz): δ 24.5.

4.4 Dimethyl ((4-((1-((5,7-dichloro-2,3-dihydrobenzo[b]oxepin-4-yl)methyl)-1H-1,2,3-triazol-4-yl)methoxy)-3-ethoxyphenyl)(hydroxy)methyl) (3h)



White solid; mp 134-136⁰ C; Rf: 0.44(3:1 Ethyl acetate:Petroleum ether); MS m/z 584.0 (M + 1, 100%); **FTIR (KBr, ν in cm^{-1}):** 3278, 3072, 2946, 1084, 848, 739 **¹H NMR (400 MHz, CDCl₃):** δ 8.31(s, 1H), 7.60 (d, 1H, $J=2.76$ Hz), 7.44 (dd, 1H, $J=8.53, 2.51$ Hz), 7.11 (d, 1H, $J= 8.53$ Hz), 7.08 (d, 1H, $J=8.03$ Hz), 7.04 (t, 1H, $J=2.00$ Hz), 6.92 (dt, 1H, $J=6.52, 2.25$ Hz), 6.10 (dd, 1H, $J=15.5, 6.03$ Hz), 5.50 (s, 2H), 5.15 (s, 2H), 4.84 (dd, 1H, $J=13.0, 6.27$ Hz), 4.29 (t, 2H, $J=6.27$ Hz) 3.62 (d, 3H, $J=10.2$ Hz), 3.54 (d, 3H, $J=10.2$ Hz), 3.34 (s, 2H), 2.25 (t, 2H, $J=6.27$ Hz), 1.31 (t, 3H, $J=7.03$ Hz). **¹³C NMR (CDCl₃, 100 MHz):** δ 153.4, 148.7, 147.3, 145.1, 132.4, 132.3, 130.3, 130.2, 129.1, 129.3, 128.3, 123.5, 123.1, 119.5, 114.6, 112.2, 78.5, 71.3, 69.3, 67.7, 64.5, 63.3, 52.5, 30.5, 16.3; **³¹P NMR (DMSO-d₆, 400 MHz):** δ 23.6.

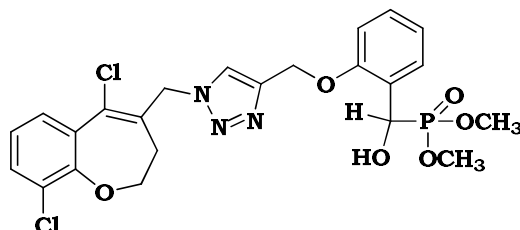
4.5 Dimethyl ((4-((1-((5-chloro-9-methyl-2,3-dihydrobenzo[b]oxepin-4-yl)methyl)-1H-1,2,3-triazol-4-yl)methoxy)phenyl)(hydroxy)methyl)phosphonate (3i)



White solid; mp 126-128⁰C; Rf: 0.36(3:1 Ethyl acetate:Petroleum ether); MS m/z 520.0 (M + 1, 100%); **FTIR (KBr, ν in cm^{-1}):** 3265, 3078, 2968, 1078, 848, 742; **¹H NMR (400 MHz, CDCl₃):** δ 7.81(s, 1H), 7.43 (m, 3H), 7.21 (m, 1H), 7.10 (t, 1H, $J=7.78$ Hz), 7.01 (d, 2H, $J=9.54$ Hz), 5.46 (s, 2H), 5.22 (s, 2H) 4.99 (dd, 1H, $J=11.0, 4.76$ Hz), 4.26 (t, 2H, $J=6.52$ Hz), 3.72 (d, 3H, $J=10.29$ Hz), 3.66 (d, 3H, $J=10.29$ Hz), 3.20 (dd, 1H, $J=12.0, 5.27$ Hz), 2.30 (t, 2H, $J=6.27$ Hz), 2.26 (s, 3H); **¹³C NMR (CDCl₃, 100 MHz):** δ 158.1, 153.7, 144.8, 132.2, 132.1, 130.6, 129.5, 129.3, 129.2, 128.6, 128.5, 123.7,122.9, 114.8, 78.8, 70.9, 69.3, 53.8, 53.6, 52.8, 30.7. 15.5; **³¹P NMR (DMSO-d₆, 400 MHz):** δ 23.5.

4.6 Dimethyl ((2-((1-((5,9-dichloro-2,3-dihydrobenzo[b]oxepin-4-yl)methyl)-1H-1,2,3-triazol-4-

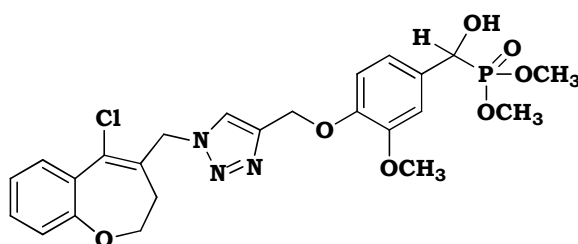
yl)methoxy)phenyl)(hydroxy)methyl)phosphonate (3j)



Off white solid; mp 130-132⁰C; Rf: 0.44(3:1 Ethyl acetate:Petroleum ether); MS m/z 540.0 (M + 1, 100%); FTIR (KBr, ν in cm^{-1}): 3255, 3069, 2962, 1076, 839, 756; ¹H NMR (400 MHz, CDCl₃): δ 7.83(s, 1H), 7.45 (m, 2H), 7.22 (m, 1H), 7.13 (t, 1H, $J=7.78$ Hz), 7.01 (m, 3H), 5.45 (s, 2H), 5.21 (s, 2H), 4.50 (dd, 1H, $J=11.0, 4.75$ Hz), 4.27(t, 2H, $J=6.52$ Hz), 3.74 (d, 3H, $J=10.3$ Hz), 3.65 (d, 3H, $J=10.3$ Hz), 3.21 (dd, 1H, $J=12.0, 5.30$ Hz), 2.32 (t, 2H, $J=6.30$ Hz); ¹³C NMR (CDCl₃, 100 MHz): δ 158.2, 153.5, 144.6, 132.3, 132.2, 130.4, 129.3, 129.4, 129.3, 129.4, 128.8, 128.6, 128.4, 123.5, 122.7, 114.9, 78.7, 70.8, 69.2, 53.7, 53.5, 52.7, 30.5; ³¹P NMR (DMSO-d₆, 400 MHz): δ 24.3.

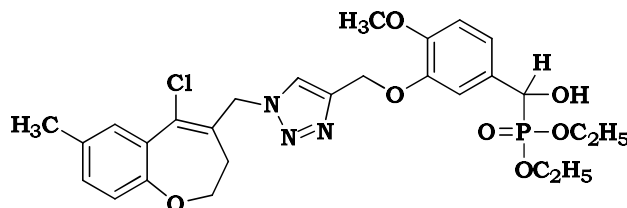
4.7 Dimethyl ((4-((1-((5-chloro-2,3-dihydrobenzo[b]oxepin-4-yl)methyl)-1H-1,2,3-triazol-4-yl)methoxy)-

3-methoxyphenyl)(hydroxy)methyl)phosphonate (3k)



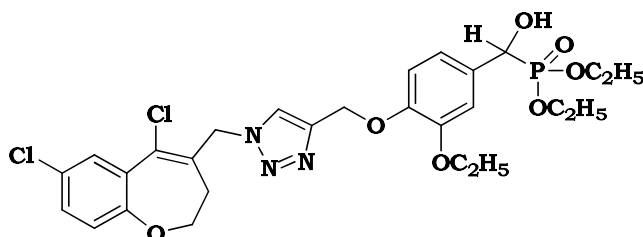
White solid; mp 132-134⁰C; Rf: 0.35(3:1 Ethyl acetate:Petroleum ether); MS m/z 536.0 (M + 1, 100%); FTIR (KBr, ν in cm^{-1}): 3270, 3050, 2969, 1074, 840, 729; ¹H NMR (400 MHz, CDCl₃): δ 8.35 (s, 1H), 7.60 (d, 1H, $J=2.76$ Hz), 7.44 (dd, 1H, $J=8.78, 2.76$), 7.35 (dd, 2H, $J=9.28, 2.51$), 7.11 (d, 1H, $J=8.78$), 7.01 (d, 2H, $J=9.28$), 6.17 (dd, 1H, $J=15.5, 6.52$), 5.49 (s, 2H), 5.16 (s, 2H), 4.93 (dd, 1H, $J=12.5, 6.27$ Hz), 4.29 (t, 2H, $J=6.42$ Hz), 3.62 (d, 3H, $J=10.2$ Hz), 3.54 (d, 3H, $J=10.2$ Hz), 3.34 (s, 3H), 2.25 (t, 2H, $J=6.27$ Hz); ¹³C NMR (CDCl₃, 100 MHz): δ 158.1, 153.7, 144.8, 132.2, 132.1, 130.6, 129.5, 129.3, 129.2, 129.1, 128.63, 128.59, 128.52, 123.7, 122.9, 114.8, 78.8, 70.9, 69.3, 61.9, 53.8, 53.6, 52.8, 30.7; ³¹P NMR (DMSO-d₆, 400 MHz): δ 26.1.

4.8 Diethyl ((3-((1-((5-chloro-7-methyl-2,3-dihydrobenzo[b]oxepin-4-yl)methyl)-1H-1,2,3-triazol-4-yl)methoxy)-4-methoxyphenyl)(hydroxy)methyl)phosphonate (3l)



White solid; mp 126-128⁰ C; Rf: 0.34(3:1 Ethyl acetate:Petroleum ether); MS m/z 578.0 (M+1, 100%); **FTIR (KBr, ν in cm^{-1}):** 3285, 3082, 2956, 1069, 843, 736; **¹H NMR (400 MHz, CDCl_3):** δ 8.37 (s, 1H), 7.60 (d, 1H, $J=2.76$ Hz), 7.44 (dd, 1H, $J=9.03, 2.76$ Hz), 7.20 (s, 1H), 7.11 (d, 1H, $J=9.03$ Hz), 7.00 (d, 1H, $J=10.29$ Hz), 6.94 (d, 1H, $J=8.78$ Hz), 6.11 (dd, 1H, $J=15.8, 6.52$ Hz), 5.49 (s, 2H), 5.11 (s, 2H), 4.85 (dd, 1H, $J=12.9, 6.27$ Hz), 4.31 (t, 2H, $J=6.27$ Hz), 4.02-3.79 (m, 4H), 3.73 (s, 3H), 2.26 (t, 2H, $J=6.27$ Hz), 2.12 (s, 3H), 1.19 (d, 3H, $J=7.27$ Hz), 1.13 (t, 3H, $J=7.27$ Hz); **¹³C NMR ($\text{CDCl}_3, 100$ MHz):** δ 153.7, 148.7, 146.6, 142.8, 134.2, 132.1, 130.5, 130.3, 128.7, 127.8, 125.9, 125.3, 124.1, 120.5, 113.4, 111.4, 78.4, 69.7, 68.1, 62.0, 61.6, 55.4, 51.9, 30.3, 17.5, 16.3, 15.1; **³¹P NMR ($\text{DMSO-d}_6, 400$ MHz):** δ 25.6.

4.9 Diethyl ((4-((1-((5,7-dichloro-2,3-dihydrobenzo[b]oxepin-4-yl)methyl)-1H-1,2,3-triazol-4-yl)methoxy)-3-ethoxyphenyl)(hydroxy)methyl)phosphonate (3m)



Off white solid; mp 128-130⁰ C; Rf: 0.45 (3:1 Ethyl acetate:Petroleum ether); MS m/z 612.0 (M + 1, 100%); **FTIR (KBr, ν in cm^{-1}):** 3288, 3074, 2954, 1052, 829, 738; **¹H NMR (400 MHz, CDCl_3):** δ 8.31(s, 1H), 7.60 (d, 1H, $J=2.76$ Hz), 7.44 (dd, 1H, $J=8.53, 2.51$ Hz), 7.11 (d, 1H, $J=8.53$ Hz), 7.08 (d, 1H, $J=8.03$ Hz), 7.04 (t, 1H, $J=2.00$ Hz), 6.92 (dt, 1H, $J=6.52, 2.25$ Hz), 6.10 (dd, 1H, $J=15.5, 6.03$ Hz), 5.50 (s, 2H), 5.15 (s, 2H), 4.84 (dd, 1H, $J=13.0, 6.27$ Hz), 4.29 (t, 2H, $J=6.27$ Hz), 4.01-3.81 (m, 4H), 3.34 (s, 2H), 2.25 (t, 2H, $J=6.27$ Hz), 1.31 (t, 3H, $J=7.03$ Hz), 1.18 (t, 3H, $J=7.03$ Hz), 1.13 (t, 3H, $J=7.03$ Hz); **¹³C NMR ($\text{CDCl}_3, 100$ MHz):** δ 153.7, 148.9, 147.6, 145.3, 132.2, 132.1, 130.6, 130.4, 129.4, 129.2, 128.5, 123.7, 123.0, 119.6, 114.7, 112.4, 78.7, 71.2, 69.6, 64.3, 63.5, 63.2, 52.8, 30.6, 16.5, 16.3, 14.8; **³¹P NMR ($\text{DMSO-d}_6, 400$ MHz):** δ 26.3.

5. Conclusion

In conclusion, the functionalized organo phosphonate derivatives can easily be prepared which are good yields, further tested their antibacterial properties and toxicity profiles. The positive results we have recorded, while encouraging for purposes of new structural analogue compounds design, confirm that most of these compounds could be used without great risk of toxicity in diverse antibacterial activity. All the synthesized derivatives showed moderate to reasonable activities against all the bacterial strains. Compound **3g** showed best antibacterial activity followed by **3f** and **3i**. Molecule **3g** was docked in the intercalation location of DNA-gyrase cleavage complex of *S. aureus* (PDB_ID:5CDQ) and the topoisomerase Top. IV of *K. pneumonia* (PDB_ID:5EIX). The synthesized structural analogues displayed drug like properties and exhibited excellent antibacterial activity. Based on their structural properties of all the compounds acts as novel structural analogues may acts as good antibacterial agents.

Acknowledgements

Jhonsee Rani Telu thanks DST-INSPIRE, New Delhi, India, for Research Fellowship. The authors also thank CFRD, Osmania University India for Recording spectra and CCST, IST, JNTU Hyderabad India for providing research facility.

Conflict of interest

The authors declare that they have no known competing financial interests or personal relationships that could have appeared to influence the work reported in this paper.

References

- [1] A Tripolszky, E Tóth, P T Szabo, L Hackler Jr, Laszlo Hackler Jr, B Kari, L G Puskás and E Bálint, *Molecules* **25** 2643 (2020)
- [2] Z Rezaei, S Khabnadideh, K Zomorodian, K Pakshir, S Nadali, N Mohtashami, and E F Mirzaei, *International Journal of Medicinal Chemistry* 678101 (2011)
- [3] D Xie, A Zhang, D Liu, L Yin, J Wan, S Zeng, and D Hu, *Phosphorus, Sulfur, and Silicon* **9** 192 (2017)
- [4] M K Awad, M F Abdel-Aal, F M Atlam and H A Hekal, *Journal of Molecular Structure* **1173** 128 (2018)
- [5] P A Turhanen, K D Demadis and P Kafarski, *Front. Chem* 695128 (2021)
- [6] J Guin, Q Wang, M V Gemmeren and Benjamin Angew. *Chem. Int. Ed.* **53** 1 (2014)
- [7] M. Tajbakhsh, S. Khaksar, Z. Tafazoli, A. Bekhradnia, *Chin. J. Chem.* **30** 827 (2012)
- [8] X Ma, Q Xu, H Li, C Su, C Lei Yu, X Zhang, H Caob and L B Han, *The Royal Society of Chemistry* 15 (2018)
- [9] B Hari Babu, G Syam Prasad, C Naga Raju and MV Basaveswara Rao 14 883 (2017)
- [10] J R Telu, N Kuntala, K Kankanala, V Banothu S Pal and J S Anireddy, *Heterocyclic Chem* **1** (2021)
- [11] H B Abdllha, A I. Mohamed, K A. Almoniem, N I Adam, W Alhaadi, A A Elshikh, A J Ali, I G. Makuar, A M. Elnazeer, N A Elrofaei, S F. Abdoelftah, M N Hemidan, *Advances in Microbiology* 6 9 (2016)
- [12] V. Singh, D. Katiyar, *Bioorg. Chem* **71** 120 (2017)
- [13] O Trott, A. J Olson, *Comput. Chem* **31** 455 (2010)
- [14] G M Morris, R Huey, W Lindstrom, M F Sanner, R K Belew D S Goodsell, and A J Olson, *J. Comp. Chemput* **16** 2785 (2009)
- [15] <http://www.molinspiration.com>. 2021
- [16] C A Lipinski, F Lombardo, B W Dominy and P J FeeneyLipinski, *Adv Drug Deliv Rev* **3** 26 (2001)
- [17] S K Lakavath *J. Drug Deliv. Ther.* **10** 139-144 (2020)
- [18] F Tsopeles, C Giaginis and AT Kakoulidou, *Opin Drug Discov* **9** 885 (2017)

[19] <http://www.organic-chemistry.org/prog/peo> (2021)

Using Fly Ash Bricks as a Sustainable Building Material

Priyanjana Saha^{1*} and Piyush Raj²

¹Department of Computer Science and Engineering, Institute of Engineering & Management, Kolkata-700091

²Department of Civil Engineering, Indian Institute of Technology Bombay, Mumbai, Mumbai-400076

Abstract

This review paper will focus on the potential of using fly ash bricks in place of the generic clay bricks in terms of sustainability, properties, chemical composition and in terms of availability. Wastes produced daily in refineries and furnaces contain toxic elements. This paper will explore the possibility of reducing the waste and a step towards a sustainable building. Fly ash bricks are environment friendly, manufactured by hydraulic pressure machines, are 28% lighter than normal clay bricks and have a compressive strength greater than 40 MPa than normal bricks[1]. Due to its advantages over other building materials, the demand is constantly increasing in India, China and the other Asian Pacific regions, which in turn has created a global traction in the creation of fly ash bricks[2]. The construction industry is also one of the highest contributors to the country's CO₂ emissions, accounting for 22% of the country's total annual CO₂ emissions. The climate-friendly fly ash brick technology produces bricks without using coal. It has the potential to eliminate carbon emissions from the brick-making industry, which burns huge amounts of coal and emits millions of tons of carbon dioxide each year. In practice, the construction material uses a lot of virgin materials[3]. But the fly ash building material uses very minimal amounts of the same, 49% less, thus reducing the energy requirement to make these. This paper will focus on how fly ash incorporation (Massive volume fly ash concrete) is a sustainable option for building material, as well as a durable material for the same, absorption capacity, methods of making fly ash bricks, its carbon footprint, how can they be made less toxic, the chemical composition compared to the generic clay bricks and how eco friendly it is. This paper studies the hazards in clay brick and advantages in fly ash brick extending with a comparative study on material properties of clay brick and fly ash brick.

Keywords: Fly ash bricks, carbon footprint, sustainable, greenhouse

Introduction

Usage of the general cement and bricks have a lot of adverse effects on the climate. Firstly, they use up a lot of virgin products. Secondly, the primary binder in any construction material is portland cement which is actually very harmful for the climate as its production causes emissions of a lot of greenhouse gases. And thirdly, concrete structure lacks durability which is unappreciated, which causes the production of construction materials to be more, thus creating more greenhouse gases. Incorporation of fly ash in construction materials such as bricks, as in this paper, will take care of the above mentioned issues and its adoption in the construction fields will enable the concrete industry to become more sustainable.

Fly Ash is the industrial waste that remains after burning out the substances in a pyre or a furnace. These are generally the coal combustion residuals that are composed of particulates that are driven out of the coal fired boilers together with fuel gas. It primarily contains oxides of silicon, aluminium, iron and calcium. More than 100 million tons of coal combustion ash is generated annually, of which 60 million tons are fly ash. Only about 27% of the fly ash produced is reused or recycled, and the rest is land filled.

In today's world, where sustainability is of a great concern and so is the fact that construction and the wastes produced go hand in hand. Climate change: over the years, global warming has increased to a great height with a lot of CO₂ emissions which have given rise to global warming. Also, the environmental

concentrations have increased from 280 to 370 ppm in the industrial age, and approximately 7% of the world's CO₂ is[5] contributed by the transportation and making of portland cement[4,5].The resource productivity, when taken into account, for regular cement, uses up approximately 1.6 billion metric tonnes of virgin materials including portland cement, gravel, crushed rocks, water and so on- that too every year. Also it has pretty intensive energy considerations. Fly ash can reduce the use of virgin materials and energy by upto 90%. Reportedly, over 1 billion tons of production and demolition waste is generated each year.[6] Cost-effective technology is available to recycle maximum of the waste as a partial substitute for the coarse aggregate in sparkling concrete combinations. Similarly, commercial wastewaters and non-potable waters can replace municipal water for blending concrete except tested dangerous with the aid of testing. Blended portland cements containing fly ash from coal-fired energy flora, and floor-granulated slag from the blast-furnace iron industry offer notable examples of industrial ecology because they provide a holistic answer for reducing the environmental impact of several industries.[7]

Mixture Composition

The chemical or the mixing composition's variation will bring differences in the final product's strength and flexibility. The amount of water is very essential in this due to the fact the quantity of water is varied inside a slim variety between 100-130 kg/m³ by the use of a combination of 1 or extra gear including a super plasticizing admixture, a high quality fly ash, and well-graded mixture. Depending on the favored energy degrees, the content material and the fly ash/cement ratio of the binder can be varied. As the water content between the unique electricity degrees does not range plenty, it's far vital to grow the cementitious substances notably to obtain higher energy. [8]

Cement: ordinary good grade portland cement-10%

Fine aggregate: fineness modulus 2.88-7%

Coarse aggregate: Qualified 5-20-mm broken gravel, broken stone being 51%-53%, broken index being 7.7%-8.0%

Superplasticizer: Naphthalene sulfonic acid-based superplasticizer

Ultra-fine fly ash: Collected by electro-static precipitators and airflow classing technology-60%[9]

Table1.Chemical composition of the Fly Ash (wt%)

Sample Fly Ash	SiO ₂	Al ₂ O ₃	Fe ₂ O ₃	CaO	MgO	K ₂ O	Na ₂ O	SO ₃	Cl
-	51.7	26.8	4.39	3.4	0.95	1.28	0.65	0.31	0.009

Table 2 Composition of Fly Ash bricks (kg/m³)

Mix Proportions	Composition
water	115-125
cement	150-160
fly ash	180-200
coarse aggregate	1100-1200
fine aggregate	800-900

Sustainability of Fly Ash Bricks

ISSN 2689-6389 (Print)

ISSN 2687-7939 (Online)

Fly ash brick is made from the burned coal ash. It is a green material having very little impact on the environment. If we burn coal for making fly ash bricks there is a big environmental issue but we don't do that. We use the ash made by burning coal for power generation. Fly ash is a by-product of thermal power generation. Due to the higher surface area compared to cement, fly ash is used as a substitution to the cement. Further, fly ash is used to reduce the heat of hydration in the higher grade of concrete[3]. Some of the most effective ways that fly ash bricks are sustainable.

Cooling nature of these bricks.

Lesser water absorption

Protects the groundwater from getting polluted

Protects the agricultural lands from getting polluted.

Protects the fly ash from transmitting into the air.

Eco-brick does not demand the use of local agricultural soil, which in case of clay bricks is very often extracted from the farms leading to loss of fertile soil.

Water conservation

Too much blending - water is probably the most essential purpose for many issues which can be encountered with concrete mixtures. There are two reasons why common concrete combos contain too much blending-water. Firstly, the water demand and workability are encouraged greatly by using particle size distribution, particle packing effect, and voids present within the strong structure. Typical concrete combos no longer have a desirable particle length distribution, and this accounts for the undesirably excessive water requirement to reap certain workability. Secondly, to plasticize a cement paste for attaining a first-class consistency, much large amounts of water than necessary for the hydration of cement should be used due to the fact that portland cement particles, due to the presence of electric statics on the floor, generally tend to form flocs that trap volumes of the integration water. It is typically determined that a partial substitution of Portland cement by fly ash in a mortar or concrete combination reduces that water requirement for acquiring a given consistency.[5] Depending on the amount of fly ash and the amount of cement changed, up to 20% reduction in water necessities can be performed. This method is excellent since fly ash can act as a super plasticizing admixture while being utilized in excessive-volume. The phenomenon is attributable to three mechanisms. First, quality particles of fly ash get absorbed on the oppositely charged surfaces of cement particles and save you from flocculation. The cement particles are for this reason successfully dispersed and will trap large quantities of water, meaning that the machine can have a discounted water requirement to attain a given consistency. Secondly, the spherical shape and the easy floor of fly ash particles assist to reduce the interparticle friction and as a consequence facilitates mobility. Thirdly, the "particle packing effect" is likewise answerable for the reduced water demand in plasticizing the gadget. It may be referred to that both portland cement and fly ash make a contribution to debris which can be mainly within the 1 to 45 μm size variety, and consequently serve as brilliant fillers for the void area inside the combination. In truth, because of its lower density and better quantity consistent with unit mass, fly ash is a more efficient void-filler than Portland cement.[4]

Dry cracking

Perhaps the greatest disadvantage related to the usage of neat portland-cement concrete is cracking due to drying shrinkage. The drying shrinkage of concrete is caused by the amount of the cement paste present[7]. It increases with a growth in the cement paste-to-combination ratio inside the concrete combination, and additionally will increase with the water content of the paste. Clearly, the water-reducing belongings of fly ash may be advantageously used for accomplishing a massive discount in the drying shrinkage of concrete combinations. Due to a widespread discount within the water requirement, the full quantity of the cement paste in everyday concrete is 25% in comparison to 29.6% for the conventional portland-cement concrete which represents a 30% reduction in the cement paste-to combination quantity ratio[6].

Thermal damage

Thermal cracking is of serious concern in huge concrete structures. It is commonly assumed that this isn't always a problem with reinforced-concrete systems of mild thickness, e.g. 50-cm thick or much less. However, because of the high reactivity of modern cements, instances of thermal cracking are said even from slight-length structures made with concrete combinations of excessive-cement content material that have a tendency to expand immoderate heat at some stage in curing. The physical-chemical traits of everyday portland cements nowadays are such that very high heat-of-hydration is produced at an early age in comparison with that of everyday portland cements available. Also, high early energy necessities in contemporary production exercise are usually satisfied via a growth within the cement content of the concrete mixture. Further, there's extensive creation interest now inside the warm-arid regions of the sector wherein concrete temperatures in excess of 60°C aren't unusual inside some days of concrete placement. For unreinforced mass-concrete production, several strategies are hired to save you from thermal cracking, and some of these techniques may be efficiently used for mitigation of thermal cracks in large strengthened-concrete structures. For instance, a 40-MPa concrete aggregate containing 350 kg/m^3 portland cement can boost the temperature of concrete by about $55\text{-}60^{\circ}\text{C}$ within per week if there is no heat loss to the environment. However, with concrete combination containing 50% cement replacement with a Class F fly ash, the adiabatic temperature upward thrust is expected to be $30\text{-}35^{\circ}\text{C}$. As a thumb rule, the most temperature differences between the interior and exterior concrete should now not exceed 25°C to keep away from thermal cracking. This is because better temperature differentials are finished by means of rapid cooling rates that typically bring about cracking. Evidently, within the case of conventional concrete it's far simpler to resolve the hassle either by using maintaining the concrete insulated and heat for an extended time within the bureaucracy till the temperature differential drops underneath 25°C or with the aid of reducing the proportion of portland cement within the binder through a extensive amount. The latter option may be exercised if the structural designer is willing to simply accept a slightly slower fee of power development during the primary 28 days, and the concrete electricity specification is primarily based on ninety-day in preference to 28-day electricity.

Properties of Fly Ash Bricks as compared to Clay Bricks:

It is considered green or eco-friendly as it can help curb the various forms of pollution.

It is denser and stronger than the generic red bricks.

It requires lesser mortar and plastering- almost 40% to 50% less usage of mortar.

A compressive strength of $9\text{-}10\text{N/mm}^2$ gives the building extra strength to withstand the sudden shocks or any damage.

They absorb less heat and thus keep the building cool. The pozzolanic reaction between the fly ash and the lime produces less heat.

These are highly durable which again is beneficial for the environment as it requires lesser attention or care compared to the red bricks.

It is highly sound and fire resistant.

They absorb less water compared to clay bricks.

Properties of Fly Ash Bricks

The conventional clay bricks are manufactured in relatively polluting brick kilns that emit fairly poisonous gases while burnt and for that reason are environmentally unsustainable. The Fly Ash Bricks on the contrary are synthetic with either the help of fully automatic machines or hand-operated machines. Both those procedures are completely easy and motivate minimum pollution if the fly ash loading and unloading is treated well.

1. Strength – Hundreds of laboratory brick tests conducted over a period of time have shown that Fly Ash Bricks which might be dried within the sun for 28 or more days are stronger than the traditional red bricks which might be heated in brick kilns for several minutes.
2. Precise Dimensions – Fly Ash bricks are required in smaller numbers as compared to the crimson bricks as they are larger in size and for this reason store value. The shape of the fly bricks is also greater regular making sure a smooth construction, which needs less plastering fabric, again saving on value.
3. Reasonable Priced – Although the rate of the fly ash bricks varies from one geographical place to every other depending on the proximity to the electricity flora and refineries. The common rate of this brick is much like that of the clay bricks if no longer lower.
4. Clean Technology – The largest benefit of this generation is that it causes minimum pollution (land or air) while being produced. Not most effective, it also places a pollutant to a better use by means of preventing it from being dumped into landfill websites that could cause excessive land, water and air pollutants seriously affecting public health.
5. No Agricultural Loss – This eco brick does not demand the usage of neighborhood agricultural soil, which in case of clay bricks could be very often extracted from the farms, leading to loss of fertile soil and losses to farmers.
6. Optimum use of water – In opinion of many creation employees and supervisors, the fly ash brick constructing calls for much less water all through production. This is a totally widespread benefit in a village that faces water shortages almost each 12 months.

Comparison of Carbon Footprint of Fly Ash Bricks and Clay Bricks:

The manufacturing of building materials contributes to the huge amount of CO₂ emission, specially in the cement industry and in the brick burning process. The cement industry is responsible for 5% of global world's energy use is in the form of electricity; the rest is used for heating and manufacturing. And atleast 40% of the world's electricity comes from coal which leads to huge CO₂ emission. For regular red bricks

CFP is 169 gCO₂/kg of fired brick excluding emissions due to biofuel combustion.

CFP is 195 gCO₂/kg of fired brick including emissions due to biofuel combustion.

For fly ash bricks

Fly ash is currently widely used for various applications in civil engineering. Due to their waste origins, the CO₂ emissions resulting from their use are almost zero.

Traditional clay brick manufacturing compared to fly ash brick manufacturing processes resulting in 40% recycled content and 85% energy reduction.

Table 3. Comparison of CO₂ emission between clay & fly ash bricks[9]

Item	Number of bricks	Equivalent CO ₂ emission
Clay Brick	20,760	10.38 tonnes
Fly Ash Brick	2,966	1,038 tonnes

Comparison of Fly Ash Bricks and Clay Bricks:

Fly ash is a waste material obtained from the combustion of coal. Fly ash brick consists of cement, water and fly ash (fly ash averagely 60%) which is stronger than clay bricks. The properties of a typical fly ash brick are presented in Table3.

Table 4. Properties comparison between clay bricks and fly ash bricks[9]

Properties	Clay brick	Fly ash brick
Drying time	7 days	3 days
Length of firing time	1-7 days	Few hours
strength Compressive	12-40 M Pa	43 M Pa
Average density	1800-2000 kg/m ³	1450 kg/m ³
Absorption capacity	5-20%	10%
Modulus of rupture	1 M Pa	10.3 M Pa

Conclusion

Fly ash brick is also eco-friendly as it reduces CO₂ emissions to a great extent. The fly ashes studied were collected by electro-static precipitators and airflow classing technology. Due to their spherical shape and smooth surface features, the fly ashes demonstrated improved water reduction effect with increased fineness. The concrete construction industry has realized that coal fly ash is a relatively inexpensive and widely available by-product that can be used for partial cement replacement to achieve excellent workability in fresh concrete mixtures. Consequently, in the modern construction practice 15%-20% of fly ash by mass of the cementitious material is now commonly used in North America. Higher amounts of fly ash on the order of 25%-30% are recommended when there is a concern for thermal cracking, alkali-silica expansion, or sulfate attack. Such high proportions of fly ash are not readily accepted by the construction industry due to a slower rate of strength development at an early age.

In conclusion, fly ash bricks offer a holistic solution to the problem of meeting the increasing demands for bricks in the future in a sustainable manner at the same time reducing the environmental impact of two industries that are vital to economic development namely the cement industry and the coal-fired power industry.

References

- [1]Mona Ghorbani, Behnaz Dahrazma, Seyed Fazlolah Saghravani, Ghazaleh Yousofizinsaz,A comparative study on physicochemical properties of environmentally-friendly lightweight bricks.276, 121937(2020)
- [2]Md Mainuddin,Stresses in Fly Ash Brick using different proportion of Lime, Cement, Gypsum, Sand and Stone Dust. (2014)
- [3]Felipe Rivera, Patricia Martinez, Javier Castro, Mauricio Lopez,Massive volume fly-ash concrete: A more sustainable material with fly ash replacing cement and aggregates., 63(4):104-112 (2015)

- [4]Mehta, P.K. “Concrete Technology for Sustainable Development.” Concrete International 21(11), (1999), pp. 47-52.
- [5]Mehta, P.K. “Durability: Critical Issues for the Future.” Concrete International 19(7), (1997), pp. 69-76.
- [6]Hawken, P., E. Lovins, and H. Lovins. Natural Capitalism: Creating the Next Industrial Revolution. Little Brown and Co.,(1999), 369 pp.
- [7]Aitcin, P.C. “The Art and Science of Durable High-Performance Concrete.” Proceedings of the Nelu Spiratos Symposium. Committee for the Organization of CANMET/ACI Conferences, (2003), pp. 69-88.
- [8]P. Kumar Mehta, High-Performance, High-Volume Fly Ash Concrete for Sustainable Development (2012)
- [9]Surendra P. Shah and Kejin Wang, Development of “Green” Cement for Sustainable Concrete Using Cement Kiln Dust and Fly Ash.(2014)